



Martin O'Malley, *Governor*
Anthony G. Brown, *Lt. Governor*

Beverley K. Swaim-Staley, *Secretary*
Neil J. Pedersen, *Administrator*

Maryland Department of Transportation

STATE HIGHWAY ADMINISTRATION

RESEARCH REPORT

AN INTEGRATED COMPUTER SYSTEM FOR ANALYSIS, SELECTION, AND EVALUATION OF UNCONVENTIONAL INTERSECTIONS

**XIANFENG YANG AND YANG LU
GANG-LEN CHANG**

**DEPARTMENT OF CIVIL AND ENVIRONMENTAL ENGINEERING
UNIVERSITY OF MARYLAND
COLLEGE PARK, MD 20742**

**SP909B4H
FINAL REPORT**

MARCH 2011

The contents of this report reflect the views of the author who is responsible for the facts and the accuracy of the data presented herein. The contents do not necessarily reflect the official views or policies of the Maryland State Highway Administration. This report does not constitute a standard, specification, or regulation.

Technical Report Documentation Page

1. Report No. MD-11- SP909B4H	2. Government Accession No.	3. Recipient's Catalog No.	
4. Title and Subtitle An Integrated Computer System for Analysis, Selection, and Evaluation of Unconventional Intersections		5. Report Date March 2011	
		6. Performing Organization Code	
7. Author/s Gang-Len Chang, Yang Lu, and Xiangfeng Yang		8. Performing Organization Report No.	
9. Performing Organization Name and Address University of Maryland, Department of Civil and Environmental Engineering, Maryland, College Park, MD 20742		10. Work Unit No. (TRAVIS)	
		11. Contract or Grant No. SP909B4H	
12. Sponsoring Organization Name and Address Maryland State Highway Administration Office of Policy & Research 707 North Calvert Street Baltimore, MD 21202		13. Type of Report and Period Covered Final Report	
		14. Sponsoring Agency Code (7120) STMD - MDOT/SHA	
15. Supplementary Notes			
16. Abstract The emergence of unconventional intersections in the traffic community has been motivated by the notion of improving service quality with innovative control strategies, such as rerouting the turning movements or flipping the paths of two traffic streams to facilitate the high-volume flows, thus increasing an intersection's overall capacity. The continuous flow intersection (CFI) and diverging diamond interchange (DDI) are the two most popular designs. This study, responding to the need, has produced a beta version of software for planning and analyzing the CFI family and the DDI designs. Building on the results of extensive simulation statistical experiments, this software comprises 16 well-calibrated queue estimation models and four equations for computing total delay. Its user-friendly interface can facilitate the efficient performance of a preliminary evaluation of any CFI or DDI design. To create a foundation for the future development of its operational modules for the final design stage, this study also investigated several critical issues that may affect the precise estimate of a design's effectiveness, including the complex interrelationships between the spatial distribution of queue lengths at different bays; the effects of time-varying demand patterns on the resulting queues and delays; and the effects of intersection spacing, as well as signal control strategies, on the overall performance of a CFI or DDI design.			
17. Key Words simulator, CFI, DDI, Unconventional intersection		18. Distribution Statement: No restrictions This document is available from the Research Division upon request.	
19. Security Classification (of this report) None	20. Security Classification (of this page) None	21. No. Of Pages 108	22. Price

Form DOT F 1700.7 (8-72) Reproduction of form and completed page is authorized.

Table of Contents

CHAPTER 1: INTRODUCTION	1
1.1 Research Background.....	1
1.2 Research Objective and Scope	2
1.3 Report Organization	2
CHAPTER 2: EVALUATION MODELS FOR CONTINUOUS FLOW INTERSECTIONS AT THE PLANNING STAGE.....	5
2.1 Introduction	5
2.2 Operational Advantages and Deficiencies	10
2.3 Summary of Previous CFI Studies	14
2.4 Experimental design for developing queue and delay models.....	17
2.5 Queue and Delay Models for the CFI-T design	21
2.6 Queue and Delay Models for the two-leg CFI design.....	30
2.7 Queue and Delay Models for a full CFI design	38
CHAPTER 3: EVALUATION MODELS FOR DIVERGING DIAMOND INTERCHANGES AT THE PLANNING STAGE.....	47
3.1 Introduction	47
3.2 Experimental Design for DDI Model Development	53
3.3 Development of Queue Models.....	55
3.4 Delay Model for DDI Design.....	61
CHAPTER 4: DEVELOPMENT OF DYNAMIC QUEUE MODELS FOR OPERATIONAL ANALYSIS	65
4.1 Introduction	65
4.2 Development of Operational Models	69
4.3 Delay Analysis	76
4.4 CFI Applications	79
4.5 Operational Analysis of DDI.....	87
4.6 Closure	89
CHAPTER 5: SOFTWARE DEVELOPMENT FOR CFI AND DDI DESIGNS	91
5.1 Software Structure.....	91
5.2 Illustrative Example	100
CHAPTER 6: CONCLUSION AND RECOMMENDATIONS	102
6.1 Conclusion.....	102
6.2 Recommendations for Future Extension.....	104
REFERENCES	106

CHAPTER 1: INTRODUCTION

1.1 Research Background

Unconventional intersections, in a variety of designs to accommodate differing resource constraints and traffic demands, have emerged as one of the most popular strategies for contending with both recurrent and nonrecurrent arterial congestion. Over the past several years, researchers from both the Maryland State Highway Administration (SHA) and The University of Maryland College Park (UMCP) have devoted tremendous effort to this vital subject. This work has yielded some research results well received by the traffic community as one of the most informative sources for learning and referencing any work related to unconventional intersections. The SHA is also well respected as one of the highway agencies having the best experience in design and implementation of various unconventional intersections. However, to continue its leadership in this area and to further convert all of its research accomplishments into operational tools for daily applications, much remains to be done.

One priority task along this line involves producing a convenient and reliable computer program to assist SHA engineers in efficiently identifying candidate designs for the given constraints, comparing the resulting costs and benefits, and assessing the designs' impacts on current traffic systems as well as on future development. Such an intelligent tool should also be able to provide users with a list of critical factors to consider in the selection process along with their relative weights, as well as to suggest the most effective designs for different selected MOEs (measures of effectiveness) and for the available budget. With such a tool, SHA can substantially reduce the design efforts given various constraints, yielding maximal benefits despite the diminishing resources. In addition, the developed design tool can also serve as a cost-effective system for training and educating highway engineers interested in this vital subject.

1.2 Research Objective and Scope

Since the continuous flow intersection (CFI) and the diverging diamond interchange (DDI) have emerged as the two most popular unconventional intersection designs (UID) for the traffic community, both in Maryland and nationwide, this study has set its primary objective as development of operational software for analyzing the properties of these two designs. Its scope of work includes:

- Development of well-calibrated CFI and DDI traffic simulators using VISSIM to comprehensively evaluate their operational properties under various constraints and traffic conditions;
- Construction of convenient yet reliable models to assist SHA engineers in identifying potential bottlenecks and approximating both queue lengths at each critical turning bay and the resulting delays for all potential CFI and DDI designs at the planning stage; and
- Integration of all developed models and analytical results regarding CFI and DDI properties as an interactive computer program for use by SHA engineers and other potential users.

Based on the scope of research, this study has produced the following products: (1) four simulators for CFI design (CFI-T, two-leg CFI-A, two-leg CFI-B, and full CFI) and one for DDI interchange; (2) four queue estimation models and one delay equation for different turning bays in each of those four CFI designs and in the DDI design; (3) a set of theoretical models to analyze the complex interactions between signal controls, spacing between intersections, and interdependence between queue patterns developed at different bays; and (4) user-friendly software that integrates all research results to assist potential users in evaluating the effectiveness of a preliminary CFI or DDI design.

1.3 Report Organization

Chapter 2 presents all of the research findings associated with CFIs, including a discussion of the operational strengths and deficiencies of different CFI designs, introduction of related literature and some CFI sites operated in recent years, and development of various queue and delay models for evaluation of the design quality at

the preliminary design or planning stage. Since the CFI family comprises the full four-leg CFI, two types of two-leg CFI, and the CFI T-intersection, this chapter details the simulator development process and its application to generate an extensive set of simulated traffic scenarios to serve as the basis for calibrating 16 queue estimation models and four equations for computing delays for the CFI family. This chapter also discusses the quasi-validation of calibrated models by comparing their predicted results with those generated from the simulators.

Chapter 3 details the model development process for the DDI, including the spatial distribution of its eight critical queue locations, the sampling process for simulation experiments, and the calibration results for four queue estimation models and one equation for computing delay. The chapter focuses on an extensive discussion of statistical analysis results and the identification of critical factors that may significantly affect the performance and operational capacity of a DDI design. Since DDIs are relatively new to the traffic community, this chapter also presents some well-known DDIs constructed over the past several years in both the United States and other countries.

Chapter 4 reports the research progress on the interrelationships between distribution of arrival and departure patterns among all subintersections in CFI or DDI designs. It provides a rigorous process for potential users to capture how signal control, intersection spacing, and levels of upstream congestion affect the formation of queues at the target bay. Estimating the spatial distribution of time-varying traffic demands among all subintersections and their interdependence on delay and queue developments are also part of the computing process. Unlike the simulation-based statistical models developed for use at the preliminary evaluation stage, the computational process presented in this chapter constitutes the theoretical basis for developing an operational model that can serve as an essential tool at the final stage of CFI and DDI design.

Chapter 5 illustrates the operational process of the developed software for the CFI family and DDI. It includes a brief discussion of the software configuration and its embedded modules, as well as their primary functions. This chapter also provides a step-by-step description of the procedures for computing the queue length at each potential

location and for estimating delays for CFIs or DDI given different demand distributions and congestion levels.

Chapter 6 summarizes the research findings associated with developing the software for evaluating DDI and CFI performance at the planning stage. It discusses the implications drawn from developed models that may serve as guidelines for best planning a target UAID, as well as critical issues that deserve special attention during the final design work. This chapter also outlines the further research needed to capture how both demand and geometric factors affect the final design of DDI or CFIs.

CHAPTER 2

EVALUATION MODELS FOR CONTINUOUS FLOW INTERSECTIONS AT THE PLANNING STAGE

2.1 Introduction

The continuous flow intersection (CFI) has been implemented in several locations across the US. The main feature of CFI is to eliminate the conflict between left turn and opposing through traffic by relocating the left turn bay several hundred feet upstream of the primary intersection, where they can cross the opposing through traffic. Such a control strategy has the advantage of allowing the through and left turn traffic to run concurrently at the primary intersection, reducing the number of signal phases. However, it creates four additional signalized crossover intersections to facilitate a left turn crossover along each leg of the intersection. These unique geometric features give CFI a larger footprint than a conventional intersection design.

Figure 2-1 illustrates a full CFI design, each of its four approaches containing a left turn crossover. The core design logic is to shift the through traffic lanes to the median so as to minimize the need for additional right-of-way. To accommodate a variety of traffic distribution patterns, traffic engineers often adopt a hybrid design that replace one or two legs in a conventional intersection with CFI design. Such hybrid intersection designs are referred as partial CFI hereafter in this report.

In practice, so far all existing CFI implementations belong to one of the following three partial CFI designs:

- CFI-T intersection: A T-intersection that contains one CFI leg (Figure 2-2).
- Two-leg CFI (Type A): An intersection containing displaced left turn legs in two opposite directions; the other two legs have the same geometry as a conventional intersection (Figure 2-3).
- Two-leg CFI (Type B): An intersection containing displaced left turn legs in two perpendicular directions; the other two legs have the same geometry as a conventional intersection (Figure 2-4).

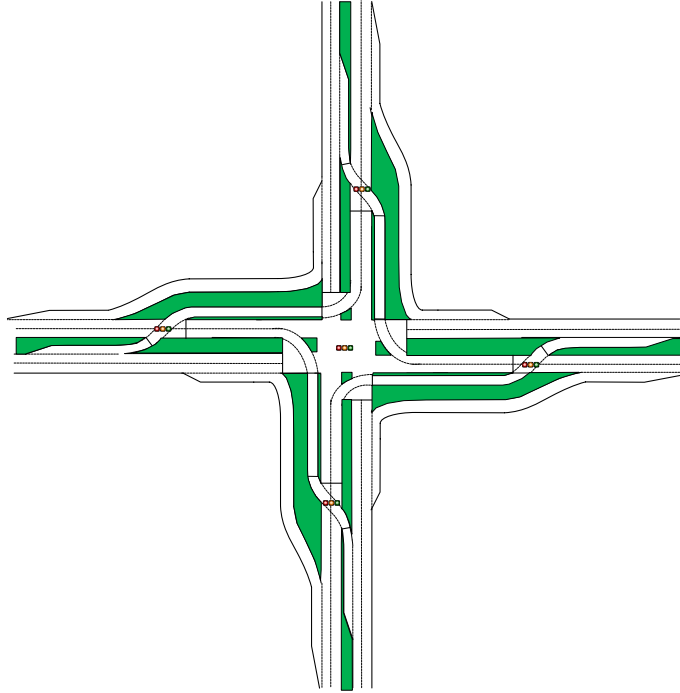


Figure 2-1: Graphical illustration of a full CFI design

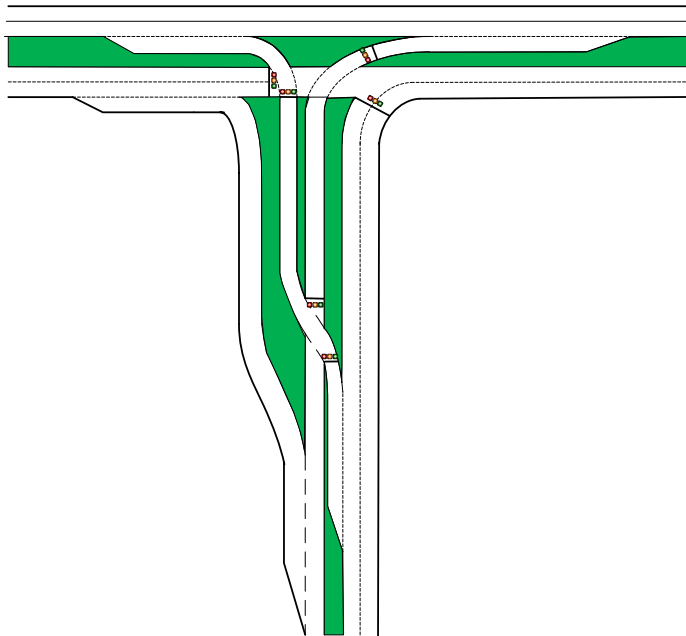


Figure 2-2: Graphical illustration of a CFI-T design

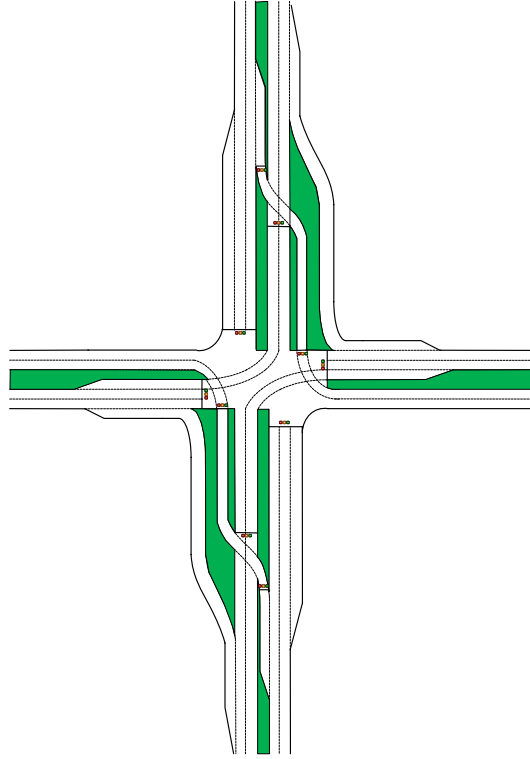


Figure 2-3: Graphical illustration of a two-leg CFI-A design

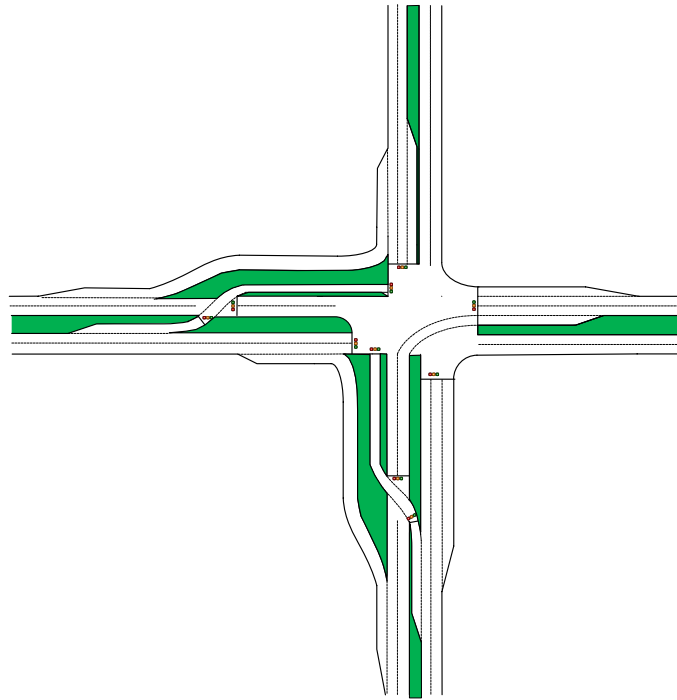


Figure 2-4: Graphical illustration of a two-leg CFI-B design

Over the past decade, highway agencies have successfully operated several CFI intersections; some of those most often referenced in the literature are listed below:

- A CFI-T prototype was constructed in 1995 at the intersection of William Floyd Parkway and the entrance of Dowling College National Aviation Technology (NAT) Center in Shirley, NY (Figure 2-5).
- Another CFI-T was constructed between MD 210 (Indian Head Highway) and MD 228 (Berry Road) in Accokeek, MD, in 2001. It uses signals to direct traffic movements, and the left turn movement occurs on the side street approach rather than on the major road approach, as with the above NY CFI intersection.
- A partial CFI design was implemented in 2006 at the four-leg intersection of U.S. 61 (Airline Highway) between Seigen Lane and South Sherwood Forest Road in Baton Rouge, LA.
- The intersection of 3500 South and Bangerter Highway in Salt Lake City, UT, was converted in September 2007 to a partial CFI with left turn crossovers on the approaches of Bangerter Highway.



Figure 2-5: Bird's eye view of CFI-T at Dowling College National Aviation Technology (NAT) Center in Shirley, NY



Figure 2-6: Bird's eye view of the CFI-T between MD 210 and MD 228



Figure 2-7: Bird's eye view of the CFI between Seigen Lane and South Sherwood Forest Road in Baton Rouge, LA



Figure 2-8: Bird's eye view of the CFI between 3500 South and Bangerter Highway in Salt Lake City, UT

2.2 Operational Advantages and Deficiencies

The full CFI is a symmetrical design which contains five small intersections (Figure 2-9). Its primary intersection (Figure 2-9, location 5), located at the center, serves all movements; a total of four subintersections (Figure 2-9), one on each of its four legs, accommodate left-turn movements. These subintersections, known as “left-turn crossovers” or “left-turn crossover intersections” function primarily to allocate the right-of-way between left turning and opposing through traffic. This left turn crossover design allows all intersections to operate with a two-phase signal control.

In designing the geometric layout for a CFI, one needs to take into account the following three factors:

- the distance between the primary intersection and its left-turn crossovers (Figure 2-9 at A, B, C, and D);
- the distance between each left-turn crossover and the beginning point of its left turn bay (Figure 2-9 at E, F, G, and H), called the left-turn bay length; and

- the distance from the stop-line of each through movement at the primary intersection to the beginning point of the left-turn bay (see those bays denoted as I, J, K, and L in Figure 2-9; also see Figure 2-10).

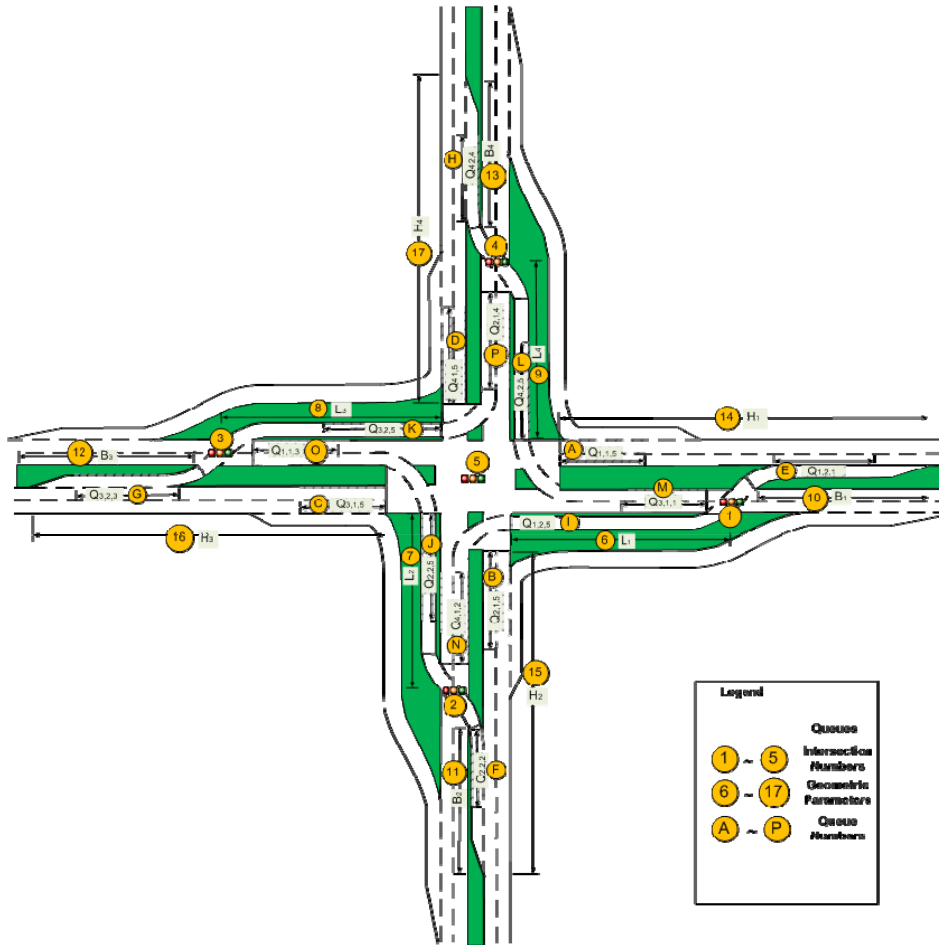


Figure 2-9: Key geometric parameters of a CFI design

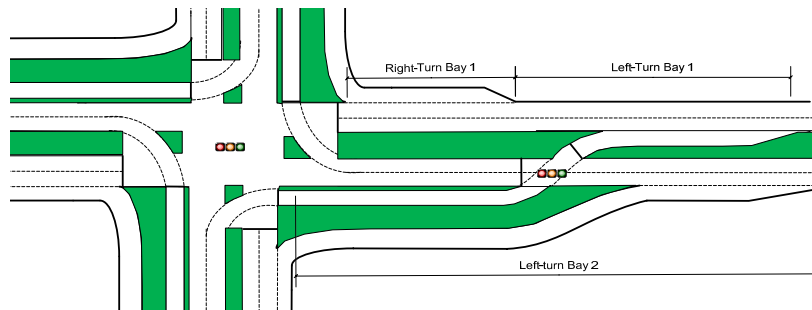


Figure 2-10: Turning bays along one approach of a CFI design

Note that converting a conventional intersection to a CFI generally can increase its capacity and decrease the delays experienced by through traffic. Moreover, CFIs cost

far less than a grade-separated interchange for the same functions. Rerouting the left turn traffic at CFI approaches shifts the conflicts between left turn and opposing through traffic from the primary intersection to its subintersections, significantly reducing the conflicting points at the primary intersection. Figure 2-11 and Figure 2-12 illustrate conflict points and their locations at a conventional intersection and a CFI design, respectively.

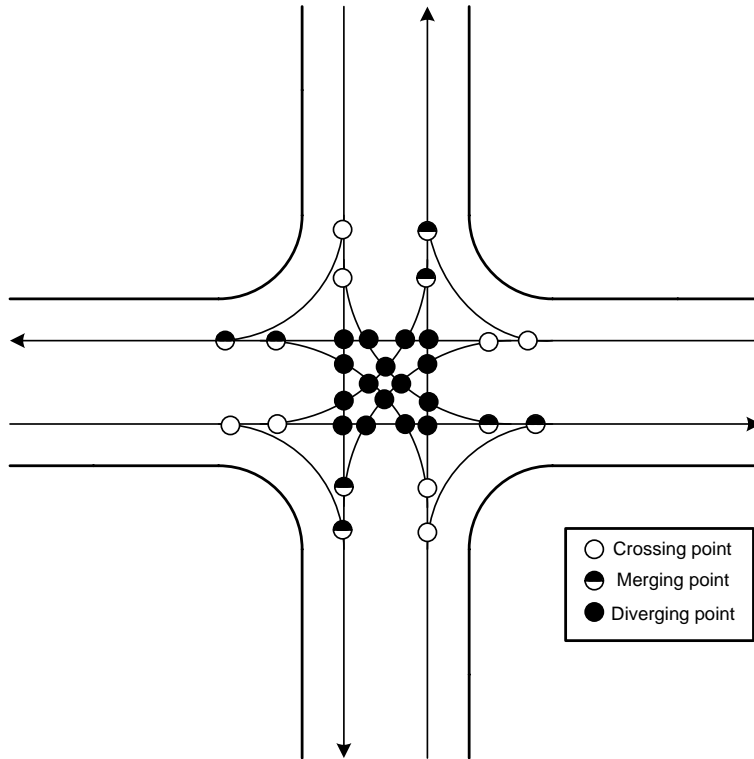


Figure 2-11: Conflict points of a conventional intersection

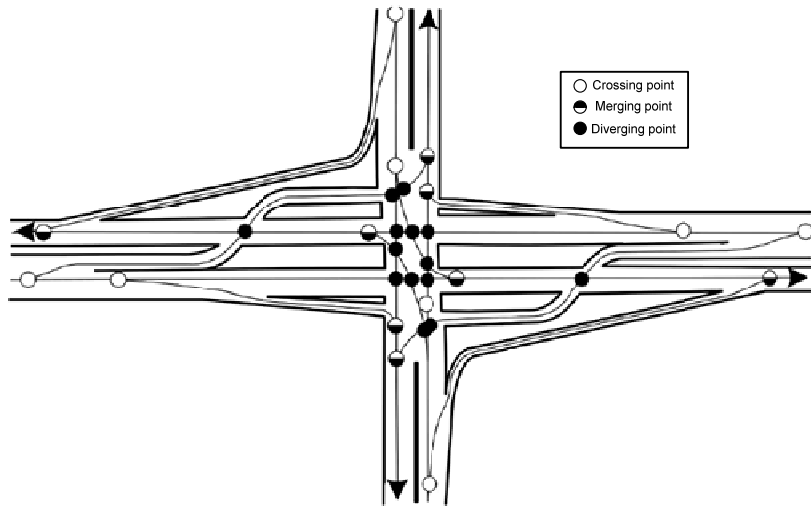


Figure 2-12: Conflict points of a partial CFI

Despite the lack of rigorous field studies, traffic engineers generally agree that the existence of a left turn bay between the primary intersection and its left turn crossover is the main factor contributing to the high capacity of a CFI design. The optimal distance between the primary intersection and the left turn crossover depends on both the traffic queue length at the main intersection and the additional cost involved in constructing the left-turn storage space.

Note that it is important to analyze the demand distribution when selecting a CFI design to ensure its cost-effectiveness. For instance, the CFI design tends to work best for intersections with heavy left turning and through traffic; thus, implementing a full CFI design at an intersection with a significant imbalanced distribution of traffic volume may not yield a desirable improvement of costs and benefits over a conventional intersection. Usually, partial CFI designs have proven more desirable for most circumstances, since traffic volumes from all four approaches are often not balanced. By constructing left turn crossovers on those approaches experiencing heavy demand, a partial-CFI design can concurrently attain both congestion alleviation and cost savings.

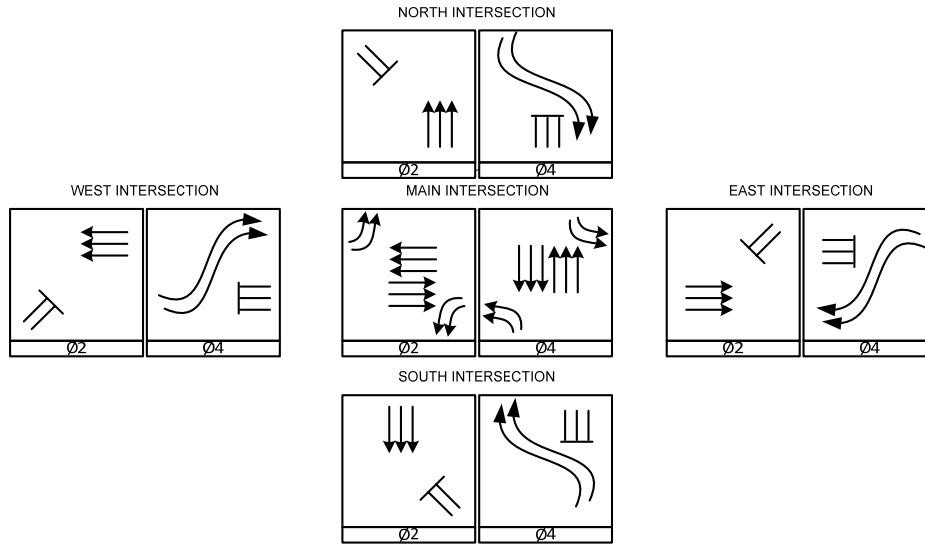


Figure 2-13: Signal phase diagram of a full CFI

Since all CFIs are designed to distribute conflict points between heavy through and left turn traffic movements, one can apply a simple two-phase control to regulate its intersection flows and to reduce delays due to the time loss between signal phase transitions. Figure 2-13 illustrates the signal configurations of a full CFI intersection.

2.3 Summary of Previous CFI Studies

Due to the increasing applications of CFI in practice over the past decade, some fundamental issues associated with its efficiency and capacity have emerged as priority research subjects for the traffic community. Some studies have employed either simulation or empirical observations to investigate the relationship between the capacity of a CFI design and its demand, as well as the resulting delay. For instance, Goldblatt and Mier (1994) showed that the benefits of CFIs are particularly pronounced when the volume at one or more of its approaches exceeds the capacity of a conventional intersection. Reid and Hummer (2000) used simulation experiments to compare the performance of seven unconventional intersection designs with an existing conventional intersection that had heavy left turn volume. They concluded that the CFI always outperformed all six other unconventional designs and the existing conventional design, using the moving-time-to-total-system-time ratio as the performance indicator.

Reid and Hummer (2001) also conducted several other studies on unconventional intersections between 1998 and 2000, and published a book summarizing their research findings (2003). Their studies consistently indicate the great potential of the CFI design in accommodating the traffic condition of having heavy demand and a high percentage of the left turn volume.

Jagannathan (2004) carried out a series of studies on the average delays and queues incurred at full CFIs, partial CFIs and CFI-Ts. Based on both the simulation results and regression analysis, he concluded that all three types of CFI design can substantially reduce intersection delays (50 to 85 percent for full CFIs, 60 to 70 percent for partial CFIs, and 20 to 90 percent for CFI-Ts) when compared with a conventional design. He also developed a real-time signal optimization model for CFIs using an integrated method based on the ANN and GA techniques, providing a quantitative tool to measure the effectiveness of CFI designs.

Another recent simulation-based study, conducted by Seonyeong, Saed, and Chang (2008), compared the performances of CFIs under balanced and unbalanced volume conditions. The results indicated that switching a conventional intersection to CFI can reduce the delay on average by 60 to 85 percent. Mohamed and Sayed (2007) reported similar conclusions, using VISSIM as the simulator and Synchro for signal optimization. They further argued that the capacity improvement from the CFI design is insensitive to increases in its left turn volume ratio and that the existence of a left turn bay between the primary intersection and the left turn crossover is the main contributing factor. A field study by Pitaksringkarn (2005) also confirmed that the CFI in Maryland reduced intersection delays and queues by 64 and 61 percent, respectively, during the PM hour.

The AIIR (Alternative Intersection/Interchanges: Informational Report), published by the FHWA (2010), discusses various aspects of six unconventional designs; the report reviews their geometric features, safety performance, operational efficiency, and construction cost. This report also includes a study concluding that a minimum of 19 and the maximum of 90 percent reduction in the average intersection delay, based on the simulation results of four CFIs with different geometry layouts under five demand levels

(from light to heavy) with a fixed left turn volume. The report points out that all signal timings adopted in the simulation were adjusted for the presence of pedestrians. The absence of pedestrians would allow the shortening of cycle lengths, further reducing the average delay.

The literature also contains another group of studies investigating the safety of different CFI designs from the point of view of either its geometric features or driver behaviors. In 1994, Dowling College sponsored a human factors study of the CFI in Shirley, NY, to assess the impact of the design on driving behaviors. The study found that 80 percent of first-time users expressed positive comments about the design and all daily commuters favored this new design.

Recently, Vaughan (2009) used a driving simulator to study driving behaviors in a CFI design with different navigation signs. He recruited 96 participants through the Internet and tested the scenarios of approaching a CFI from different directions. The results indicated that, even without prior experience, all participants managed to enter the crossover lanes when given appropriate navigation signs. The AIIR report also presented the five-year crash data at the intersection of Airline Highway and Seigen Lane in Baton Rouge, based on a before-and-after analysis. It reported that the total crash rate and severe crash rate decreased by 24 and 22 percent, respectively.

In summary, a number of researchers have studied the advantages and deficiencies of the CFI; empirical evidences support its superior performance, if properly designed. Further, none of the existing studies reported any adverse impacts on safety, which implies that most drivers will not be confused by the routing changes introduced by the left turn crossover.

However, it should be noted that many issues connected with this new intersection design for contending with intersection congestion remain to be studied. For example, although many studies reported significantly reduced delays, traffic researchers have not been able to identify all critical contributing factors and their collective impacts on the performance of CFIs. The interrelationship between intersection delays and the CFI's geometric features, such as bay length, awaits further study. Rigorous investigations into the dynamics of queue evolution at its primary intersection and

subintersections also need to be conducted. In fact, a CFI can be viewed as a small network comprising five intersection nodes and several interconnected links. Hence, the delays to different traffic movements are affected not only by the volume-to-capacity ratio at each node (intersection), but also by the queue lengths along all associated links.

The design of signal control strategies is another major research issue on promoting the CFI application. Without proper signal coordination between the primary intersection and its five subintersections, the traffic queue at each intersection could spill back to its upstream and neighboring links, thereby causing gridlock for the entire CFI. This critical issue of optimizing the signal design and coordination has long been neglected in the CFI research literature.

2.4 Experimental design for developing queue and delay models

This section first presents the set of models developed for estimating the queue length for each critical movement for different types of CFI design. The estimated queue length, along with the resulting delays at the primary and the four subintersections, will serve as the basis for engineers to identify potential bottlenecks in the preliminary design and to make necessary revisions to the safety and capacity of the final design.

Due to the lack of sufficient field data, the research team first employed VISSIM (simulation software) to build a simulator for each type of CFI design and then executed simulation experiments using extensive volume and geometric data. All experimental CFI scenarios included in the simulation analysis shared the following common features:

- All experimental intersections had two through-only lanes, one left turn lane, and one right turn lane;
- All right turn lanes were channelized and considered as free right-turn lanes; and
- Every subintersection in a full or partial CFI was independently controlled by a two-phase signal controller.

Table 2-1 presents the set of geometric parameters used to investigate the impact of intersection bay length on the resulting queues at a full CFI and at two types of partial CFIs under various demand distribution patterns. Note that, for convenience of experimental analysis, the research team set the turning bays for all conventional

intersection legs in the partial CFI designs to 300 feet. Figures 2-14 to 2-16 further illustrate those geometric parameters in CFI-T and two-leg CFI designs.

Table 2-1: Geometric parameters used in simulation experiments

Geometric parameters/case	A	B	C	D
Left turn crossover spacing (feet)	200	300	400	500
Left turn bay (feet)	250	350	450	550
Right-turn bay (feet)	300	300	300	300

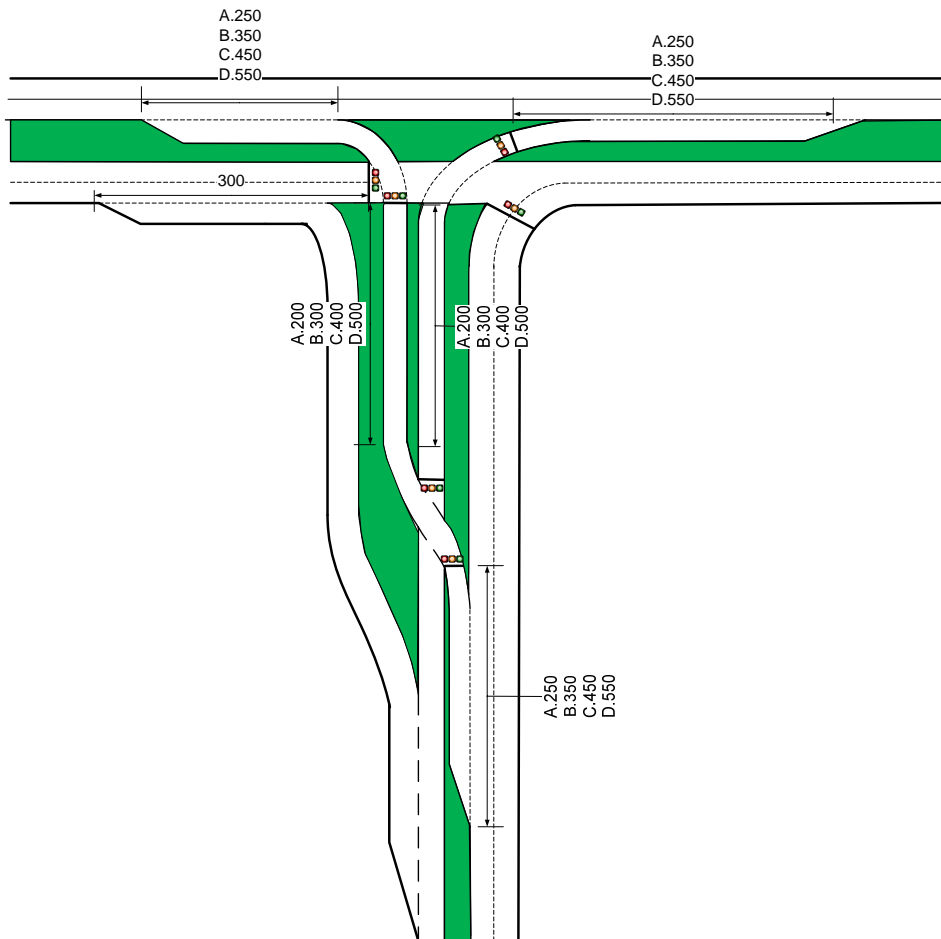


Figure 2-14: Geometric parameters of CFI-T for simulation scenarios A, B, C, D

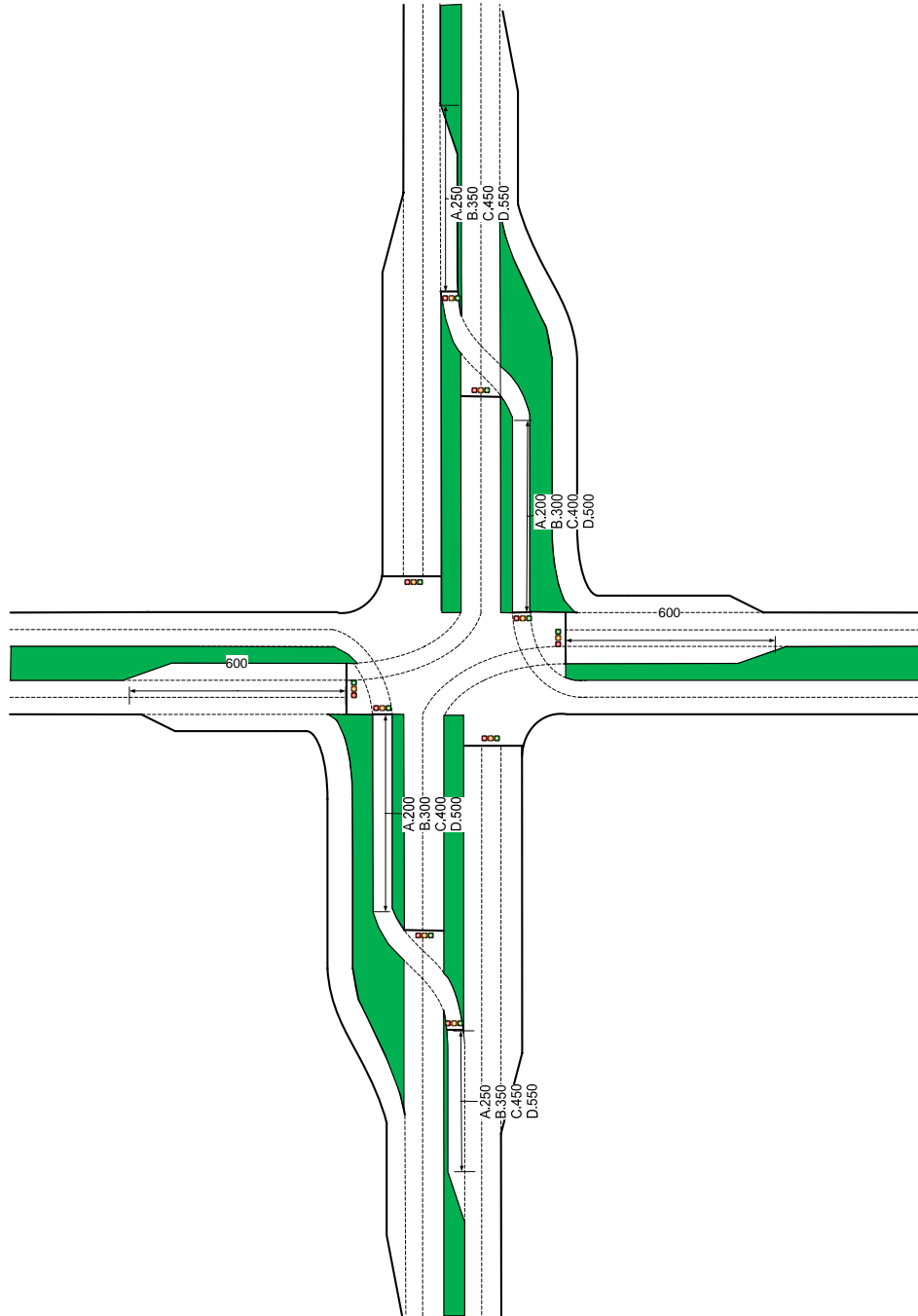


Figure 2-15: Geometric parameters of two-leg CFI-A for simulation scenarios A, B, C, D

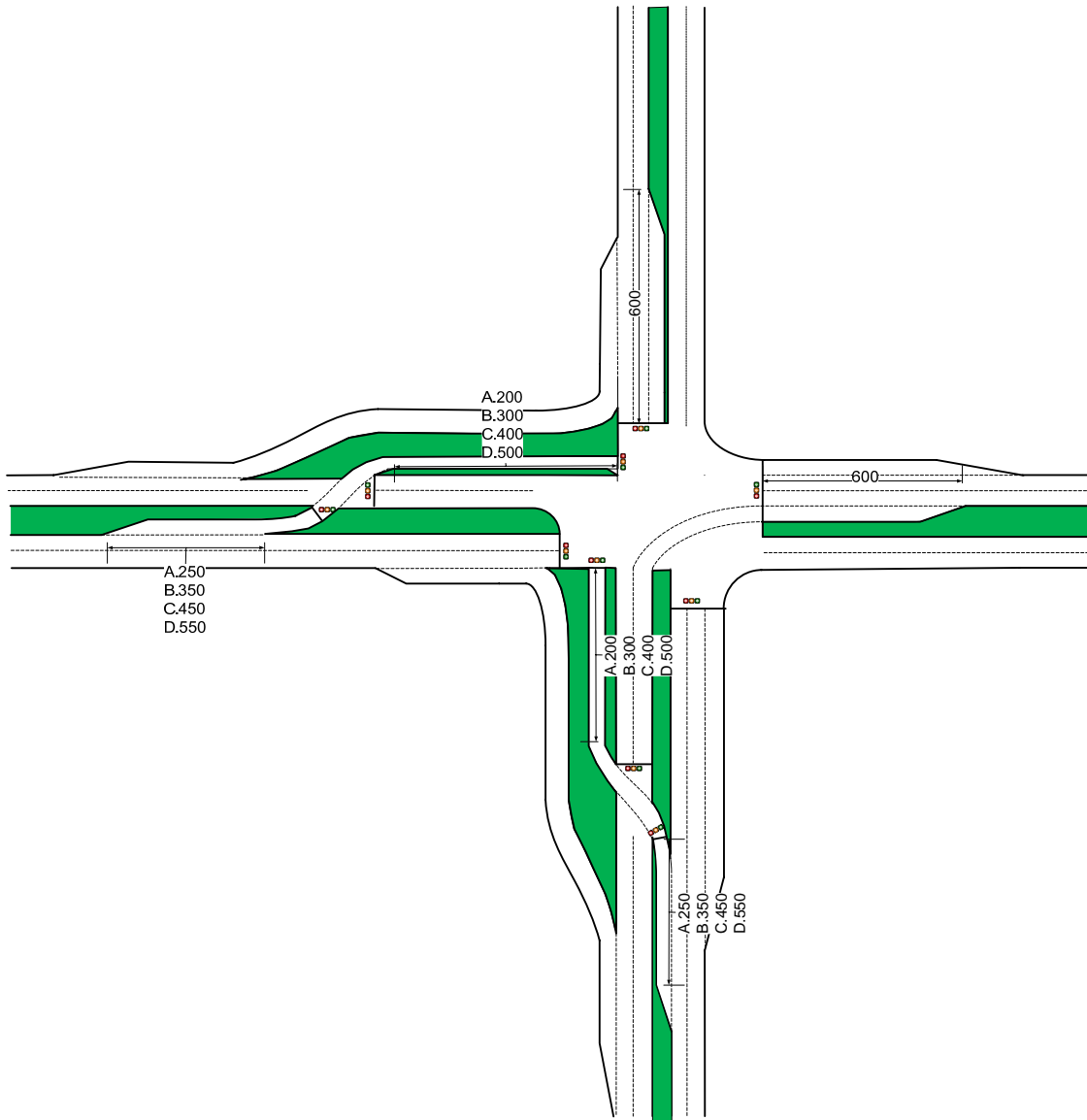


Figure 2-16: Geometric parameters of two-leg CFI-B for simulation scenarios A, B, C, D

Table 2-2 summarizes the distribution of traffic demand data and distribution used in the simulation experiments, including the sample size, range of volume, balance factor, and left turn ratio. Note that the balance factor, β , is defined as the total volume of two legs in the opposite directions divided by the total volume of the other pair of legs. To keep the balance factor between “0” and “1,” the pair of legs having the higher total volume was used as the denominator. The left turn ratio is defined as the ratio between the left turn volume and the total approach volume.

The simulation randomly generated a total demand of between 4,000 and 12,000 vehicles per hour for four approaches for a full CFI, and a demand of between 4,000 and 9,000 vehicles/hour for three types of partial CFI designs. For convenience of output analysis, all demand patterns were divided into the following three categories: low traffic scenario (from 1,800 to 2,500 vehicles/hour), medium traffic scenario (from 2,500 to 4500 vehicles/hour), and high traffic scenario (from 4,500 to 6,000 vehicles/hour).

Table 2-2: Summary of traffic demand generation plan for simulation experiments

CFI Type	Sample size	Total demand range for all four approaches (vph)	Balance factor β	Left turn volume ratio
Full CFI	800	4000 ~ 12000	0.0 ~ 0.3	0.15 ~ 0.35
CFI-T	800	4000 ~ 9000	N/A	0.15 ~ 0.35
Two leg CFI (A,B)	800	4000 ~ 9000	0.3 ~ 0.7	0.15 ~ 0.35

For all simulated experimental scenarios, the research team used the most popular signal optimization program, TRANSYT-7F, to optimize the signal settings for each full CFI (comprising five independent signal controllers) and for partial CFI designs, with three subintersections. The research team also specified all experimental scenarios with the set of default parameters in VISSIM to simulate the behavior of various driving populations. For convenience, and without loss of generality, this study employed an all-red interval of two seconds and a yellow phase of three seconds for all simulated scenarios.

2.5 Queue and Delay Models for the CFI-T design

Among the CFI design family, the CFI-T intersection has a simpler form than the other more sophisticated CFIs. It can be viewed as a modified form of a conventional T intersection, in which a left turn crossover is installed along one approach. This CFI design comprises two intersections, referred as the major and minor intersections, based on the number of intersection conflict points. Figure 2-17 shows the eight locations in a CFI-T intersection where queues may occur, due either to a traffic signal control or to merging maneuvers of traffic flows. The notations for these eight queue locations are defined below:

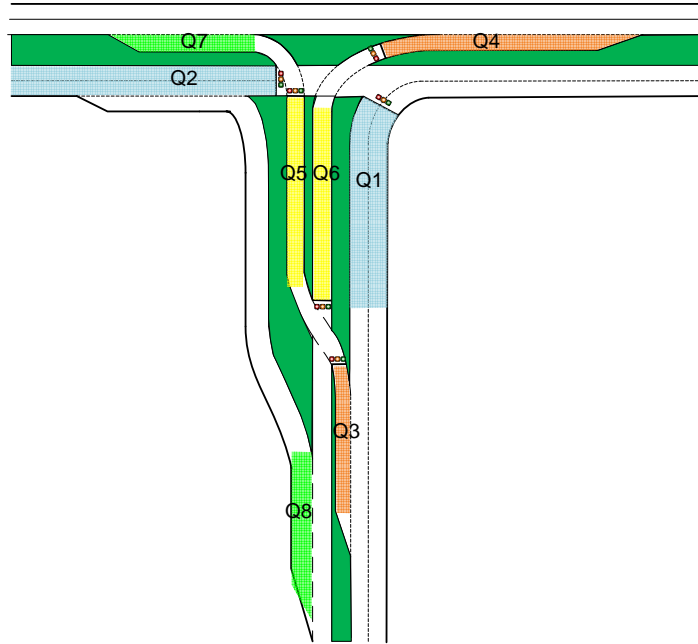


Figure 2-17: Classification of queue locations in a CFI-T design

Q₁: Northbound right-turn queue at the major intersection;

Q₂: Eastbound through queue at the minor intersection;

Q₃: Northbound left-turn queue at the minor intersection;

Q₄: Westbound left-turn queue at the major intersection;

Q₅: Northbound left-turn queue at the major intersection;

Q₆: Southbound left-turn queue at the minor intersection;

Q₇: Northbound left-turn queue before the merging point; and

Q₈: Eastbound right-turn queue before the merging point.

Depending on locations and contributing factors, the research team has divided those eight queue patterns into four types. A Type 1 queue, present at the signal stop line, is caused by the through and/or right-turning traffic volume (Q₁, Q₂). A Type 2 queue is caused by left turning vehicles (Q₃, Q₄). Those vehicles filtered by the upstream signal, and thus forming the queue at the stop line of the downstream signal, are denoted as a Type 3 queue (Q₅, Q₆). This type of traffic queues usually occurs when left turning flows from a CFI leg must consecutively pass two signals to reach their destination. The Type 4

queue is commonly observed in a merging area where approaching flows exceed the merging capacity (Q_7, Q_8).

Type 1 Queue Model (Q_1, Q_2)

The results of extensive simulation experiments indicate that the following factors may significantly affect the formation and dissipation of a Type 1 queue: the incoming demand to the target approach, the green time ratio, and the intersection's level of congestion as measured by the critical lane volume (CLV). Hence, this study has employed these three factors to calibrate the following Type 1 queue estimation model:

$$\log(Q_{1,2}) = 0.49C_v + 1.52 \frac{D}{s-C_v} + 0.78 \frac{D}{C_v}$$

t value (35.04) (35.43) (16.49)

$$R^2 = 0.92, \quad \text{Sample size N: 800} \tag{2.1}$$

where,

C_v : The critical lane volume of the major intersection;

D : Incoming through or right-turn demand in veh per hour; and

s : Saturation flow rate, 1700 veh/hour.

Type 2 Queue Model (Q_3, Q_4)

Unlike the Type 1 queue, the formation of a Type 2 queue mostly occurs due to the left turn movement and is affected by the potential queue spillback at its downstream location. Thus, to explicitly take the possible queue spillback into account, the research team calibrated the following equation for Type 2 queue estimation:

$$\log(Q_{1,2}) = 1.153C_v + 1.356 \frac{D}{s-C_v} + 1.292 \frac{D}{C_v} + 0.145Q_d$$

t value (68.63) (28.57) (42.36) (9.958)

$$R^2 = 0.96, \quad \text{Sample size N: 800} \tag{2.2}$$

where,

Q_d : Maximum queue incurred on its downstream link.

Figures 2-18 and 2-19 show how the performance of Equations (2.1) and (2.2) compares with the simulated results. As revealed by their distribution patterns of

estimation errors and the goodness-of-fit indicator, the Type 1 and Type 2 queue models have sufficient accuracy for use in assessing the quality of a preliminary design.

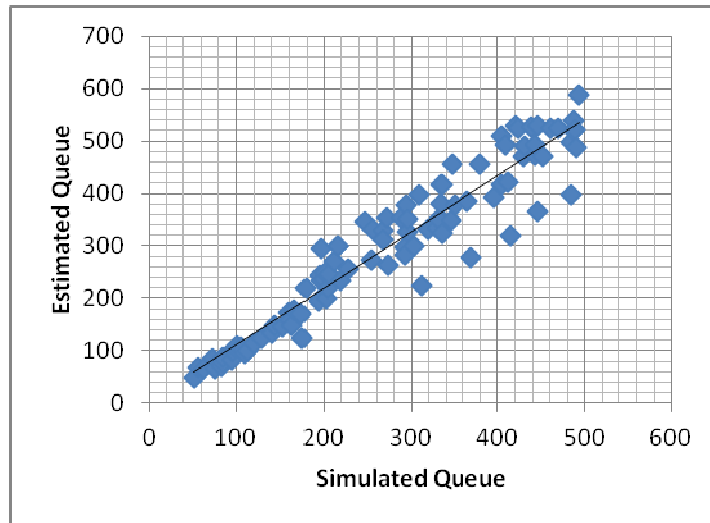


Figure 2-18: Evaluation results of Type 1 queue model for CFI-T design

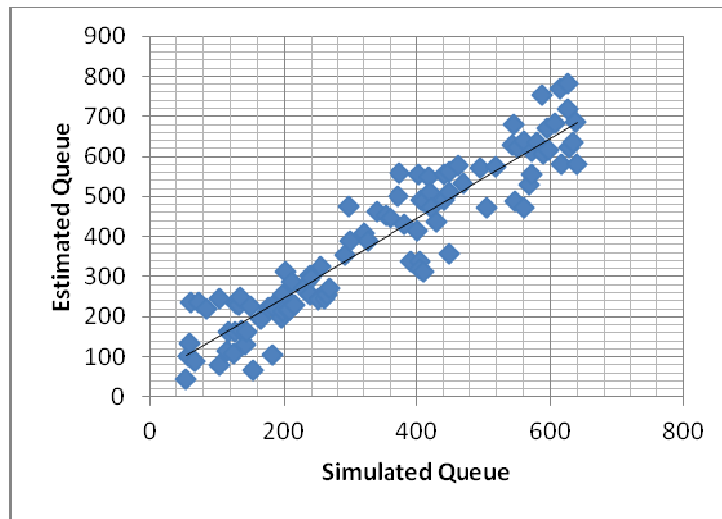


Figure 2-19: Evaluation results of the Type 2 queue model for CFI-T design

Type 3 Queue Model ()

The formation of a Type 3 queue varies with the congestion level at two signal intersections, because left turn traffic flows, after crossing the opposing through traffic at the crossover intersection, need to pass the second signal at the primary junction where they can move concurrently with the through (or right-turn) traffic stream. Hence, in addition to its left turn volume, the following empirical equation calibrated for Type 3 queue estimation also includes CLV at both the major and the crossover intersections:

$$\log(Q_{5,6}) = 0.6914D + 0.6745 \frac{D}{s-CV_1} + 0.3897 \frac{D}{CV_2}$$

t value (17.35) (5.415) (8.964)

$$R^2 = 0.92, \quad \text{Sample size } N: 800 \quad (2.3)$$

where,

CV_1 : The critical lane volume of the major intersection;

CV_2 : The critical lane volume of the crossover intersection; and

D : Incoming left-turn demand in vehicle per hour.

Type 4 Queue Model (Q_7, Q_8)

The Type 4 queue model is used to predict the queue length in a merging area. The merging flow tends to merge into the mainline during acceptable gaps. Such a relationship can be described with a classical M/G/1 model, which stands for random arrival/general service time distribution/single server. The service time, which is equivalent to the merge time, is assumed to be a general distribution (i.e., not the typical exponential distribution). Thus, the expected waiting time is:

$$E(S) = \frac{\lambda}{\mu} [e^{t_{nr}\mu} - (1 + t_{nr}\mu)] \quad (2.4)$$

where,

$E(S)$: The expected waiting time for a successful merging;

t_{nr} : The gap time required for a safe merge;

λ : The arrival rate of merging flow, in vehicle per hour; and

μ : The arrival rate of the mainline flow, in vehicle per hour.

According to Little's law, the average number of waiting vehicles is the product of the arrival rate and the expected waiting time, and can be expressed as follows:

$$\rho = \lambda E(S) \quad (2.5)$$

The results of the simulation experiments also confirmed the relationship between the maximum queue and the average number of waiting vehicles. Hence, based on

existing queuing theory and the simulation data, this research has produced the following equation for estimating a Type 4 queue:

$$(2.6)$$

where,

- The product of arrival rate and average service time;
- The arrival rate of merging flow, in vehicle per hour; and
- The arrival rate of the mainline flow, in vehicle per hour.

Note that we have proposed the second and third terms in Equation (2.4) to account for the impact of demand from both directions on the maximum queue length at the high demand level. Figures 2-20 and 2-21 show the evaluation results for Type 3 and Type 4 models, based on the comparison results between their estimated queues and the simulated queues generated from additional 100 cases for model validation. Overall, the uniform distribution of error terms along the 45 degree line indicates that these two models are well calibrated, reliable, and unbiased — and therefore suitable for use at the planning level.

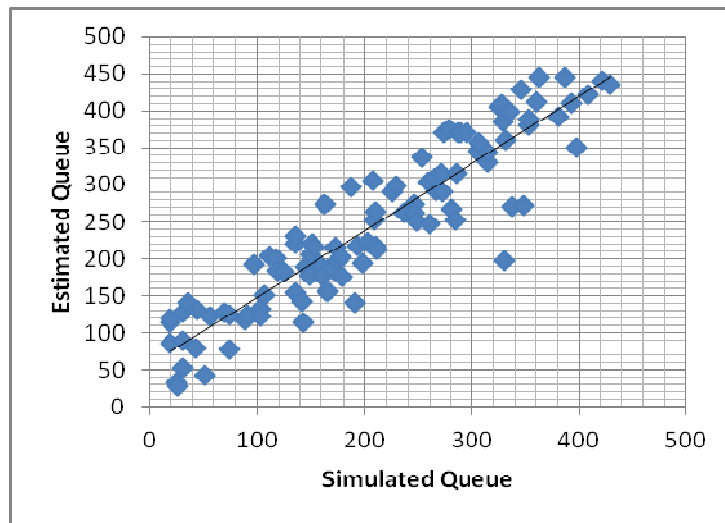


Figure 2-20: Evaluation results of the Type 3 queue model for CFI-T design

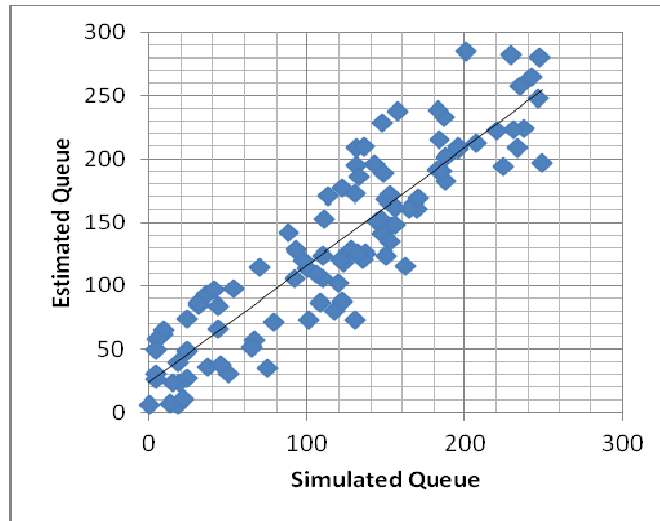


Figure 2-21: Evaluation results of the Type-4 queue model for CFI-T design

Development of Delay Models

Due to the unconventional structure of the CFI, both through and left turn traffic must pass more than one signal to get through the entire intersection. Hence, one cannot use existing classical delay models to estimate delays at CFIs. A reliable delay model for CFI design should take into account the impacts of various queue patterns, as well as the intersection’s geometric features. Otherwise, it may far underestimate delays, especially for the near-capacity condition.

This research estimated the potential maximum queue length for each CFI bay or link using queue models calibrated from extensive simulation experiments, where the maximum queue-to-bay length ratio is defined as a new measurement of the queue status. Figure 2-22 illustrates all factors that contribute to the delay at a CFI-T intersection, and Equation (2.7) presents the model reflecting the interrelationships between the intersection’s resulting delay and all contributing factors. The definition of each factor is also given below.

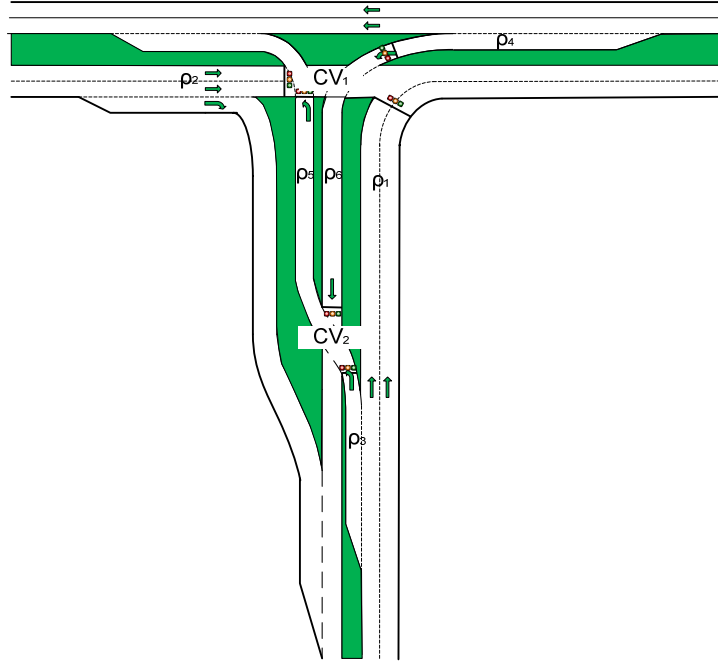


Figure 2-22: Graphical illustration of critical factors contributing to delays at a CFI-T

The queue-to-bay ratio for delay estimation is defined as follows:

$$\text{Queue to bay ratio} = \frac{\text{Maximum Queue length}}{\text{Bay length}}$$

$$\log(\text{Delay}) = 2.316 + 0.049 \frac{X_1}{1 - X_1} + 0.035 \frac{X_2}{1 - X_2} + 0.132\rho_1 + 0.151\rho_2$$

t value (7.12) (1.49) (24.3) (13.32) (53.2)

$$+ 0.213\rho_3 + 0.200\rho_4 + 0.514\rho_5 + 0.196\rho_6$$

(2.4) (6.7) (1.5) (7.41)

$$R^2 = 0.897, \quad \text{Sample size } N: 800 \quad (2.7)$$

where,

CV_1 : The critical lane volume of the primary intersection;

CV_2 : The critical lane volume of the crossover intersection;

X_1 : The degree of saturation of the primary intersection, $X_1 = CV_1/s$;

X_2 : The degree of saturation of the crossover intersection, $X_2 = CV_2/s$;

ρ_1 : Northbound right-turn queue to bay ratio at the major intersection;

Eastbound through queue to bay ratio at the minor intersection;
Northbound left-turn queue to bay ratio at the minor intersection;
Westbound left-turn queue to bay ratio at the major intersection;
Northbound left-turn queue to bay ratio at the major intersection; and
Southbound left-turn queue to bay ratio at the minor intersection.

Figure 2-23 compares the delay results of Equation (2.7) and the CFI-T simulator. The distribution and close correlation of these two sets of delays clearly indicate that the delay model would be useful at the planning level of evaluation.

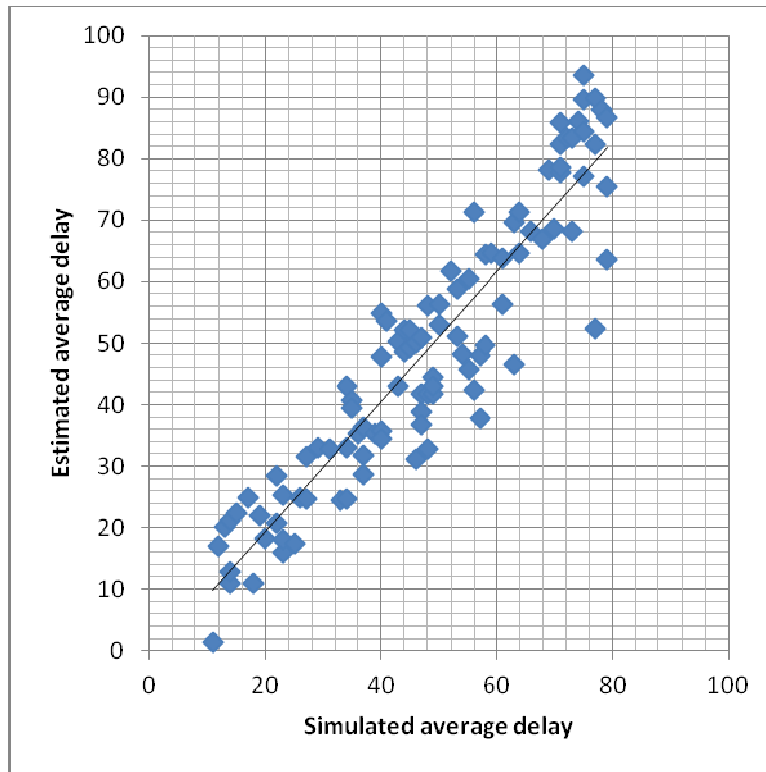


Figure 2-23: Comparison of estimated and simulated delays at a CFI-T

2.6 Queue and Delay Models for the two-leg CFI design

Two different designs exist for two-leg CFIs: a symmetrical partial CFI, with its two CFI legs running in opposite directions; and an asymmetrical partial CFI, with its two CFI legs running along two adjacent directions. Since these two designs have quite similar structures, the same set of queue formulations can be used to evaluate their performance. Figure 2-24 illustrates all potential queue locations in a symmetrical two-leg CFI, and the notation used for each queue location is defined below:

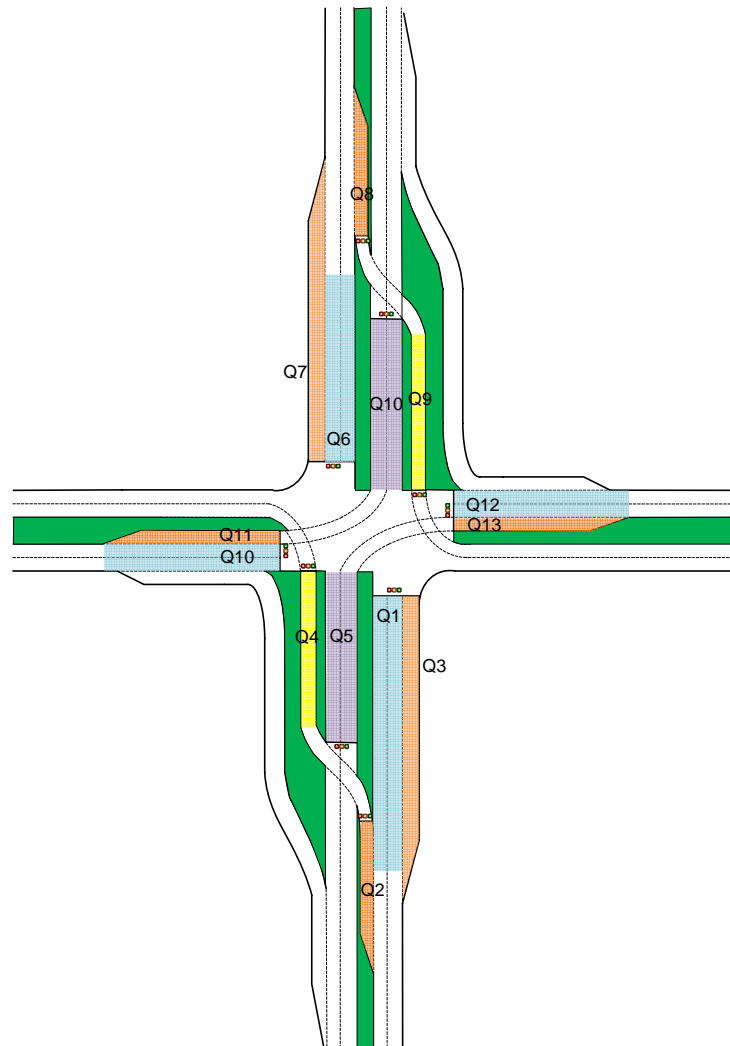


Figure 2-24: Potential queue locations at a two-leg CFI

Q₁: Northbound through queue at the major intersection;

Q₂: Northbound left-turn queue at the south crossover;

Q₃: Northbound right-turn queue at the major intersection;

- Q₄ : Northbound left-turn queue at the major intersection;
- Q₅ : Southbound through queue at the south crossover;
- Q₆ : Southbound through queue at the major intersection;
- Q₇ : Southbound right-turn queue at the north crossover;
- Q₈ : Southbound left-turn queue at the north crossover;
- Q₉ : Southbound left-turn queue at the major intersection;
- Q₁₀ : Eastbound through queue at the major intersection;
- Q₁₁ : Eastbound left-turn queue at the major intersection;
- Q₁₂ : Westbound through queue at the major intersection; and
- Q₁₃ : Westbound left-turn queue at the major intersection.

Based on the same definitions used to classify the CFI-T queue patterns and the same simulation experiment methods, this study calibrated the following four models to estimate the four types of queue patterns at a two-leg CFI:

Type 1 Queue Model (Q₁, Q₆, Q₁₀, Q₁₂)

$$\log(Q) = 0.839D + 0.322 \frac{D}{s - CV_m} + 0.064 \log(Q_d)$$

t value (24.238) (3.391) (2.583)

$$R^2 = 0.99, \quad \text{Sample size } N: 800 \tag{2.8}$$

where,

CV_m: The critical lane volume of the major intersection;

D : Incoming through volume (vehicle per hour);

s : Saturation flow rate, 1700 veh/hour; and

Q_d : Maximum queue reach of the downstream link.

Type 2 Queue Model (Q_2, Q_8, Q_{11}, Q_{13})

$$\log(Q) = 1.058D + 1.623 \frac{D}{s - CV_n} + 0.010 \log(Q_d)$$

$$t \text{ value } (155.49) \quad (16.64) \quad (2.18)$$

$$R^2 = 0.97, \quad \text{Sample size } N: 800 \quad (2.9)$$

where,

CV_n : The critical lane volume of the north or south crossover; and

D : Incoming left-turn volume (vehicle per hour).

Type 3 Queue Model (Q_4, Q_9)

$$\log(Q) = 0.679D + 0.789 \frac{D}{s - CV_m} + 0.454GC$$

$$t \text{ value } (14.651) \quad (5.873) \quad (9.303)$$

$$R^2 = 0.92, \quad \text{Sample size } N: 800 \quad (2.10)$$

where,

CV_m : The critical lane volume of the major intersection;

D : Incoming left-turn volume (vehicles per hour); and

GC : The estimated green time ratio at the crossover, $GC = D/CV_n$.

Type 4 Queue Model (Q_5, Q_{10})

$$\log(Q) = 0.8352D_t + 0.2376D_l + 0.1572 \frac{D_t + D_l}{s - CV_n}$$

$$t \text{ value } (10.707) \quad (3.811) \quad (5.435)$$

$$R^2 = 0.98, \quad \text{Sample size } N: 800 \quad (2.11)$$

where,

Incoming through volume (vehicles per hour);

Incoming left-turn volume (vehicles per hour); and

The critical lane volume of the south (north) crossover.

The research team evaluated the performance of the above four queue estimation models for two-leg CFI design in the same manner as with the CFI-T intersection, where the queue lengths estimated with each of the four models were compared with the results generated from a simulated scenario with VISSIM simulators.

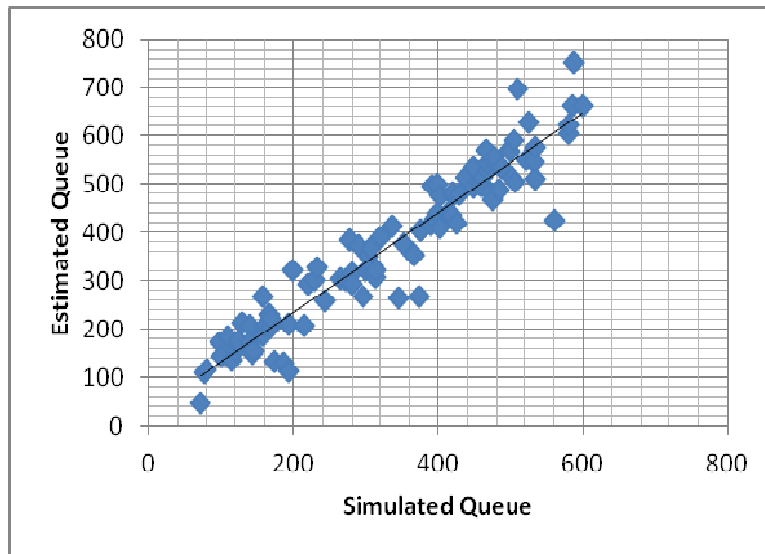


Figure 2-25: Comparison of estimated and simulated Type 1 queues at a two-leg CFI

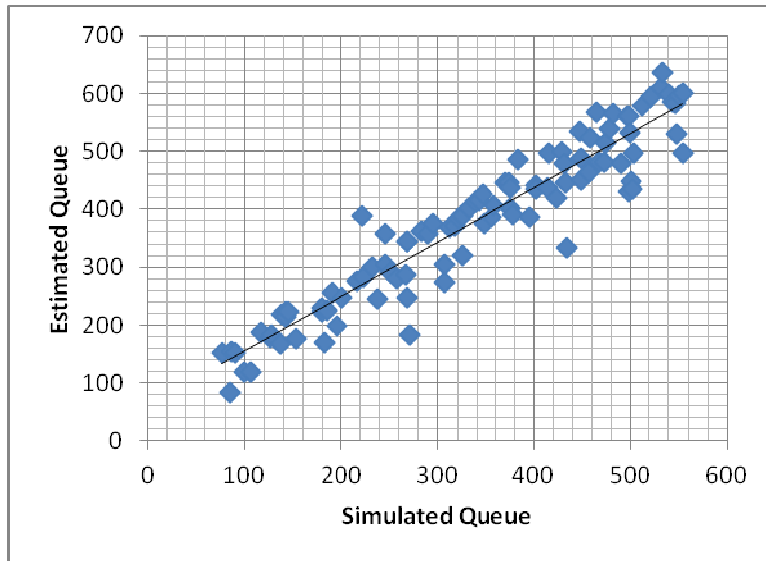


Figure 2-26: Comparison of estimated and simulated Type 2 queues at a two-leg CFI

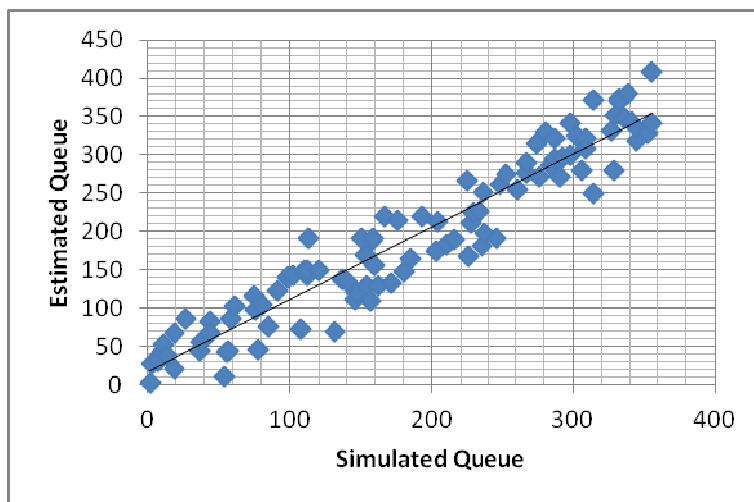


Figure 2-27: Comparison of estimated and simulated Type 3 queues at a two-leg CFI

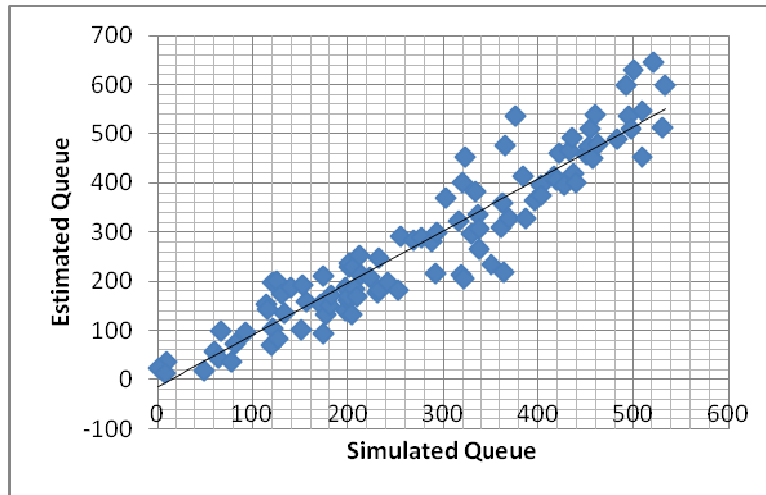


Figure 2-28: Comparison of estimated and simulated Type 4 queues at a two-leg CFI

The uniform distribution of the estimated and simulated queues over a wide range of intersection volumes and their close correlation allow one to comfortably conclude that all of the proposed models, although exploratory in nature, are sufficiently reliable to use in evaluating two-leg CFI designs at the planning stage.

Delay model for a two-leg CFI design

Figure 2-29 presents the spatial distribution of critical factors that contribute to the total delay at a two-leg CFI. The definition of each factor is defined below.

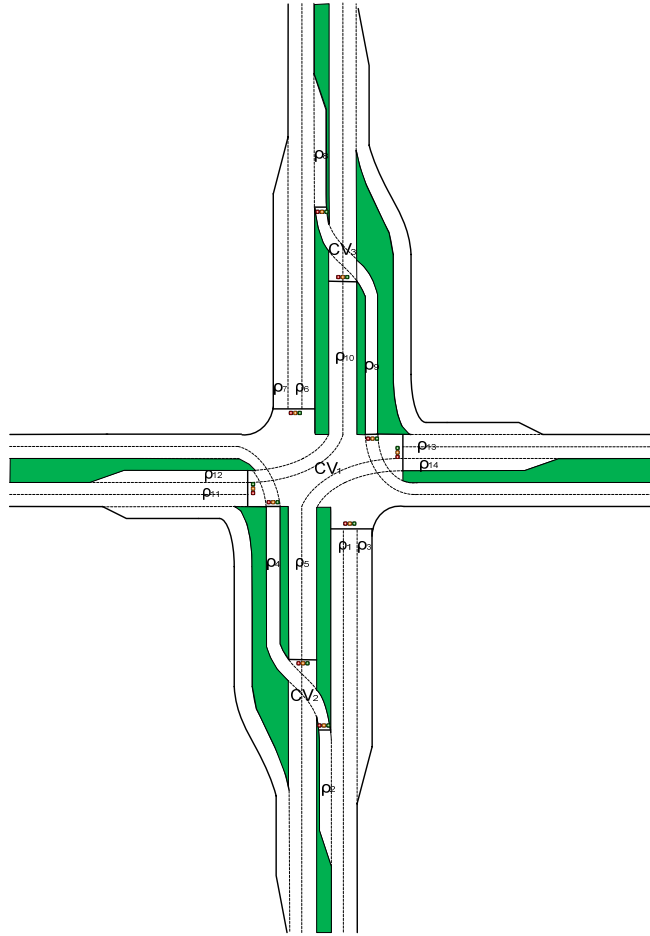


Figure 2-29: Distribution of factors contributing to delay at a two-leg CFI design

CV_1 : The critical lane volume of the central crossover intersection;

CV_2 : The critical lane volume of the south crossover intersection;

CV_3 : The critical lane volume of the north crossover intersection;

X_1 : Degree of saturation of the central crossover intersection, $X_1 = CV_1/s$;

X_2 : Degree of saturation of south crossover intersection, $X_2 = CV_2/s$;

X_3 : Degree of saturation of north crossover intersection, $X_3 = CV_3/s$;

ρ_1 : Northbound through queue to bay ratio at the major intersection;

ρ_2 : Northbound left-turn queue to bay ratio at the minor intersection;

ρ_3 : Northbound right-turn queue to bay ratio at the major intersection;

ρ_4 : Northbound left-turn queue to bay ratio at the major intersection;

ρ_5 : Southbound through queue to bay ratio at the crossover intersection;

- ρ_6 : Southbound through queue to bay ratio at the major intersection;
- ρ_7 : Southbound left-turn queue to bay ratio at the minor intersection;
- ρ_8 : Southbound right-turn queue to bay ratio at the major intersection;
- ρ_9 : Southbound left-turn queue to bay ratio at the major intersection;
- ρ_{10} : Northbound through queue to bay ratio at the crossover intersection;
- ρ_{11} : Eastbound through queue to bay ratio at the major intersection;
- ρ_{12} : Eastbound left-turn queue to bay ratio at the major intersection;
- ρ_{13} : Westbound through queue to bay ratio at the major intersection; and
- ρ_{14} : Westbound left-turn queue to bay ratio at the major intersection.

Using the same method as for the CFI-T design, this study calibrated the following equation for estimating the total delay at a two-leg intersection:

$$\begin{aligned}
 \log (D) = & 2.554 + 0.059 \frac{X_1}{1 - X_1} + 0.031 \frac{X_2}{1 - X_2} + 0.033 \frac{X_3}{1 - X_3} + 0.167\rho_1 + 0.072\rho_2 \\
 \text{t value} \quad & (8.32) \quad (13.85) \quad (23.4) \quad (23.4) \quad (23.60) \quad (3.13) \\
 & +0.178\rho_3 + 0.213\rho_4 + 0.182\rho_5 + 0.177\rho_6 + 0.082\rho_7 + 0.201\rho_8 \\
 & (20.94) \quad (97.93) \quad (30.17) \quad (27.65) \quad (3.85) \quad (29.13) \\
 & +0.245\rho_9 + 0.169\rho_{10} + 0.210\rho_{11} + 0.315\rho_{12} + 0.228\rho_{13} + 0.297\rho_{14} \\
 & (175) \quad (34.48) \quad (13.15) \quad (27.8) \quad (18.09) \quad (27.24) \\
 R^2 = & 0.98, \quad \text{Sample size N: 800} \quad (2.12)
 \end{aligned}$$

Note that the delay model includes two sets of factors. The first set consists of the CLVs at all three intersections (one primary and two subintersections), which reflect the overall congestion level at the target two-leg CFI, whereas the second set comprises the queue levels at all 14 potential queue locations, which captures the impact of spatial queue distributions on the overall intersection control delay.

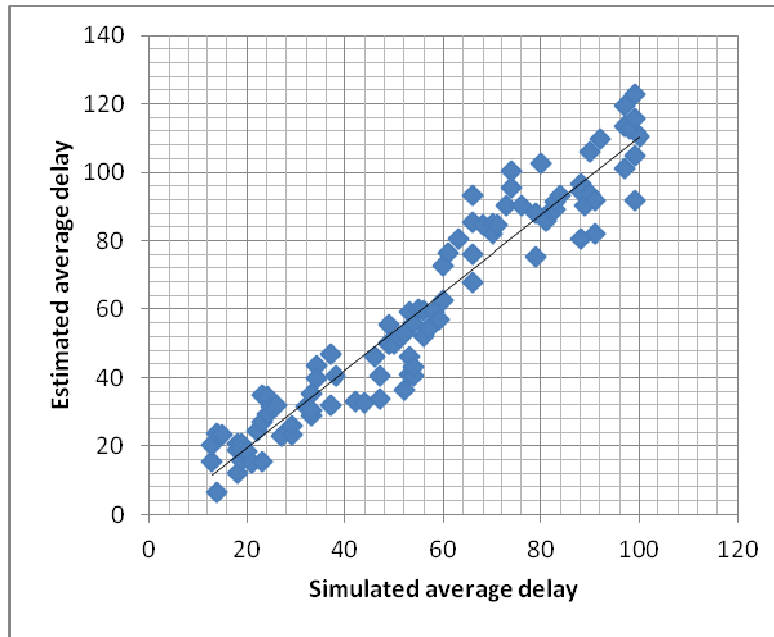


Figure 2-30: Comparison of estimated and simulated delays at a two-leg CFI

2.7 Queue and Delay Models for a full CFI design

A full CFI is the most complete and comprehensive design in the CFI family. Left turn crossovers, installed along all four legs, form a symmetrical design; left turning vehicles from all directions need to follow a displaced path to reach the primary intersection. Figure 2-31 shows all possible queue locations and their classifications, based on the same criteria used in the earlier CFI-T analysis. As with the models developed for CFI-T and for the two-leg CFI designs, this study also calibrated the following four equations for the four types of queue at a full CFI, based on the data generated from extensive simulation experiments:

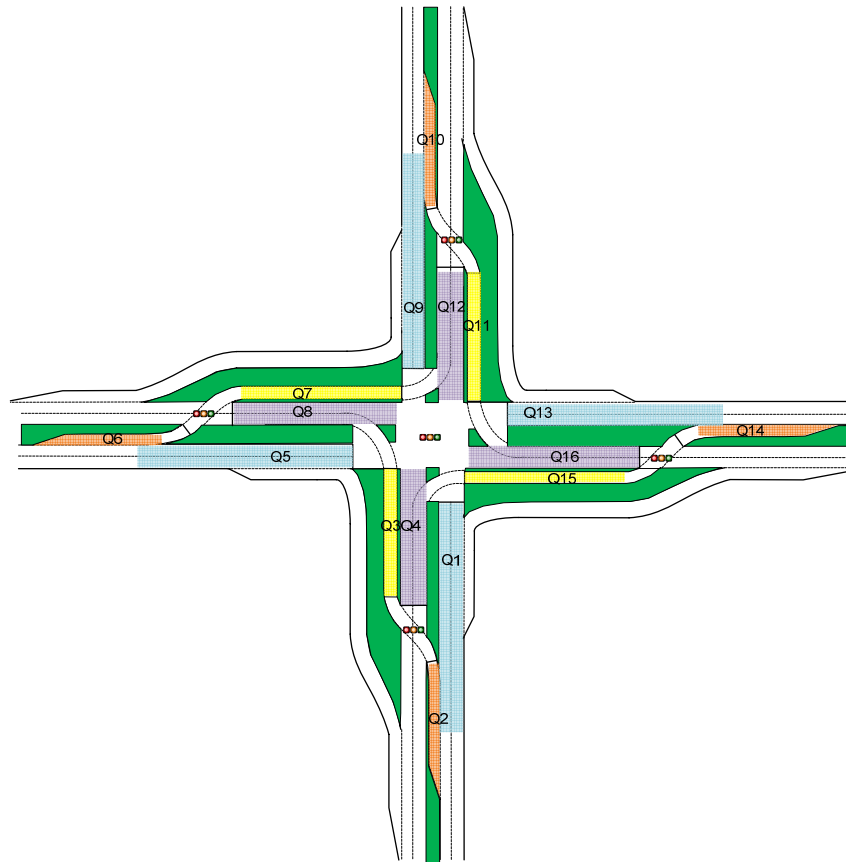


Figure 2-31: Spatial distribution of potential queue location at a full CFI

- Q₁: Northbound through queue at the major intersection;
- Q₂: Northbound left-turn queue at the south crossover intersection;
- Q₃: Northbound left-turn queue at the major intersection;
- Q₄: Southbound through queue at the south crossover intersection;
- Q₅: Eastbound through queue at the major intersection;
- Q₆: Eastbound through queue at west crossover intersection;
- Q₇: Eastbound left-turn queue at the major intersection;
- Q₈: Westbound through queue at the west crossover intersection;
- Q₉: Southbound through queue at the major intersection;
- Q₁₀: Southbound left-turn queue at the north crossover intersection;
- Q₁₁: Southbound left-turn queue at the major intersection;
- Q₁₂: Northbound through queue at the north crossover intersection;

- Q₁₃: Westbound through queue at the major intersection;
- Q₁₄: Westbound through queue at the east crossover intersection;
- Q₁₅: Westbound left-turn queue at the major intersection; and
- Q₁₆: Eastbound through queue at the east crossover intersection.

Type 1 Queue Model(Q₁, Q₅, Q₉, Q₁₃)

$$\log(Q) = 0.537D + 0.868 \frac{D}{s-CV_m} + 0.135 \log(Q_d)$$

t value (464.03) (146.31) (8.81)

$$R^2 = 0.9859, \quad \text{Sample size N: 800} \tag{2.13}$$

where,

- CV_m: The critical lane volume of the major intersection;
- D : Incoming through demand (vehicles per hour); and
- Q_d : Maximum queue at the downstream link.

Type 2 Queue Model (Q₂, Q₆, Q₁₀, Q₁₄)

$$\log(Q) = 0.679D + 0.967 \frac{D}{s-CV_n} + 0.157 \log(Q_d)$$

t value (155.49) (16.64) (2.18)

$$R^2 = 0.9723, \quad \text{Sample size N: 800} \tag{2.14}$$

where,

- CV_n: The critical lane volume of the north or south crossover intersection;
- D : Incoming left-turn demand (vehicles per hour); and
- Q_d : Maximum queue at the downstream link.

Type 3 Queue Model (Q₃, Q₇, Q₁₁, Q₁₅)

$$\log(Q) = 0.279D + 0.991 \frac{D}{s-CV_m} - 4.388W + 0.562GC$$

t value (25.33) (95.93) (-38.88) (18.88)

$$R^2 = 0.9723, \quad \text{Sample size } 00 \quad (2.15)$$

where,

CV_m: The critical lane volume of the major intersection;

D : Incoming left-turn demand (vehicles per hour);

W : Estimated green time ratio at the major intersection; and

GC : The estimated green time ratio at the crossover intersection, GC = D/CV_n.

Type 4 Queue (Q₄, Q₈, Q₁₂, Q₁₆)

$$\log(Q) = 0.1232D_t + 1.1332D_1 + 1.4953 \frac{D_t+D_1}{s-CV_n} - 2.8461W$$

t value (25.33) (95.93) (38.88) (-18.88)

$$R^2 = 0.9142, \quad \text{Sample size } N: 800 \quad (2.16)$$

where,

D_t : Incoming south (north) bound through volume (vehicles per hour);

D₁ : Incoming west (east) bound left-turn volume (vehicles per hour);

CV_n: The critical lane volume of the south (north) crossover intersection; and

W : Green time ratio for through movement at the primary intersection.

Figures 2-32 to 2-35 present the evaluation results for the performance of the above four queue models developed for the full CFI design. Clearly, from the distribution of the estimated and simulated queue patterns and their strong linear correlation, all four calibrated queue models seem sufficiently reliable for use in estimating the queue levels at each critical location during the planning stage of a full CFI design.

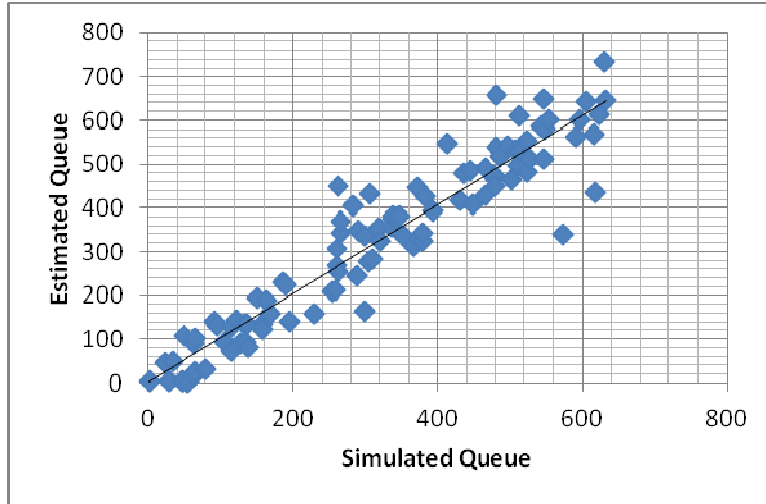


Figure 2-32: Performance evaluation of Type 1 queue model for a full CFI design with simulation results

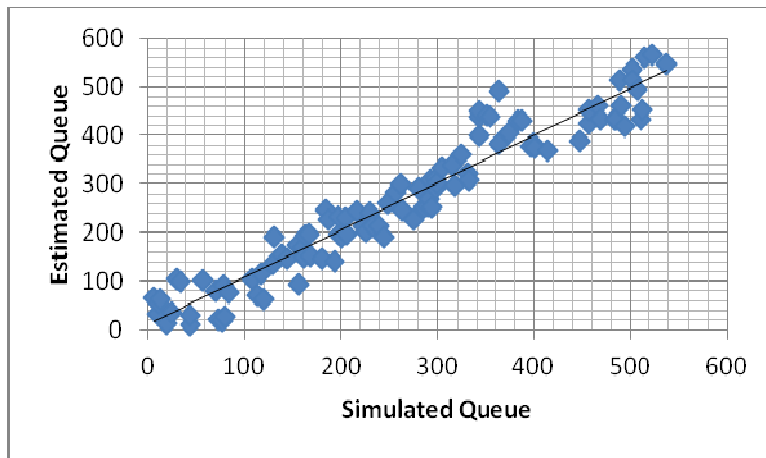


Figure 2-33: Performance evaluation of Type 2 queue model for a full CFI design with simulation results

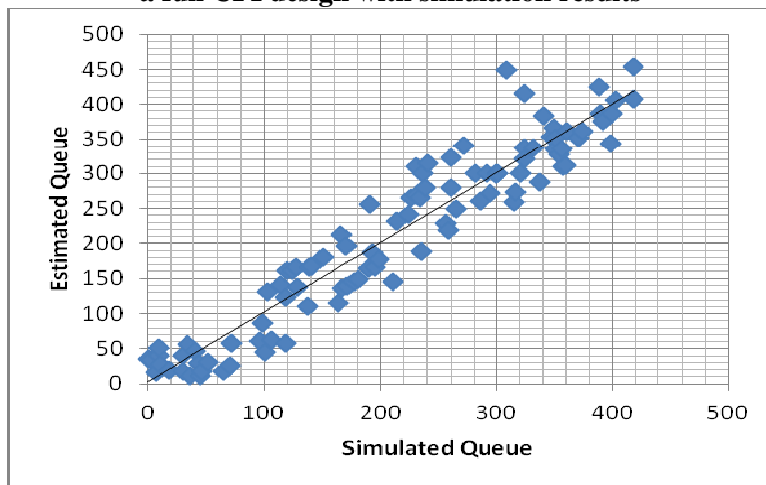


Figure 2-34: Performance evaluation of Type-3 queue model for a full CFI design with simulation results

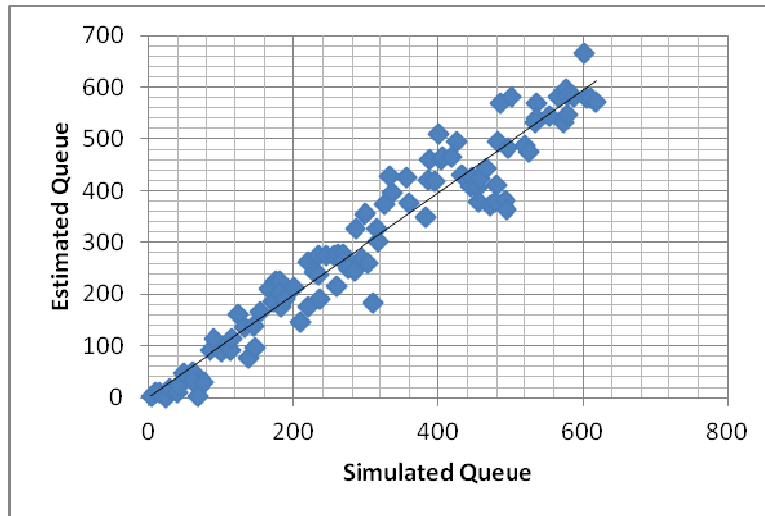


Figure 2-35: Performance evaluation of Type 4 queue model for a full CFI design with simulation results

Delay model for a full CFI

Following the same procedures used to develop the previous delay models, this study calibrated the full CFI delay models with two sets of variables: the CLV at each of the four intersections and the queue length at all critical locations. The former set captures the congestion levels at the primary and subintersections, whereas the latter reflects how spatial queue distributions at all critical locations affect the overall intersection delay. Figure 2-36 illustrates the spatial distribution of all critical factors that may contribute to the total delay at a full CFI. The definition of each factor is presented below, along with the calibrated overall delay model in Equation (2.17).

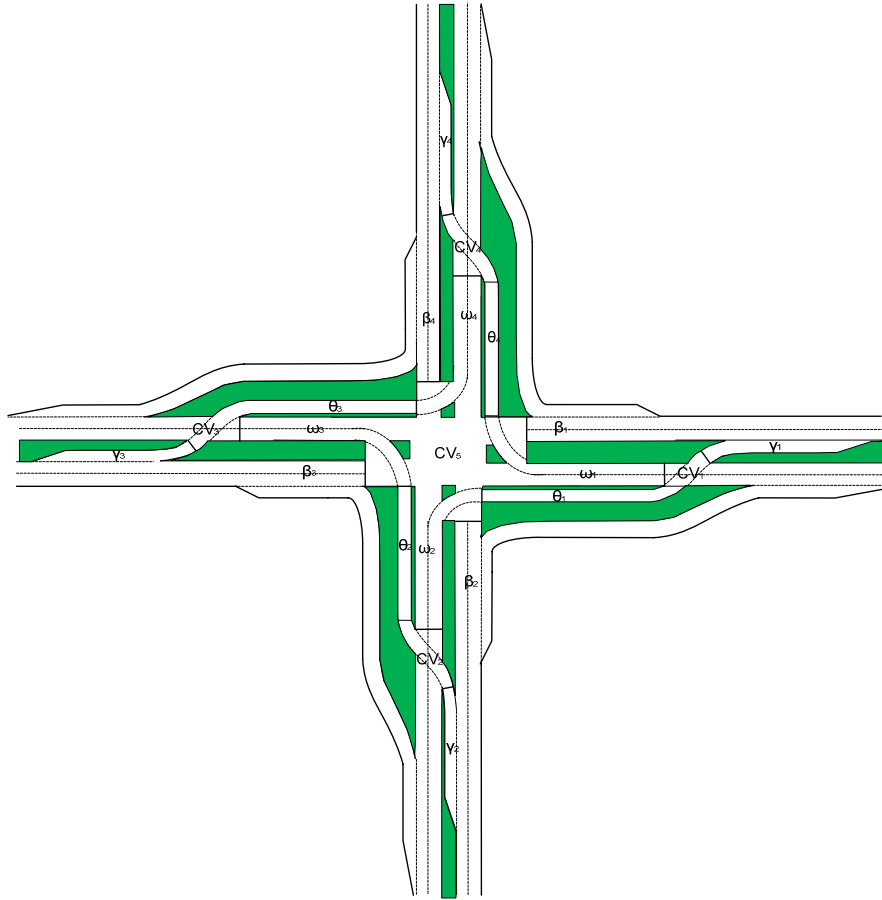


Figure 2-36: Spatial distribution of critical factors associated with the total delay at a full CFI design

CV_1 : The critical lane volume of the east crossover intersection;

CV_2 : The critical lane volume of the south crossover intersection;

CV_3 : The critical lane volume of the west crossover intersection;

CV_4 : The critical lane volume of the north crossover intersection;

CV_5 : The critical lane volume of the central intersection;

X_1 : The degree of saturation of the east crossover intersection, $X_1 = CV_1/s$;

X_2 : The degree of saturation of the south crossover intersection, $X_2 = CV_2/s$;

X_3 : The degree of saturation of the west crossover intersection, $X_3 = CV_3/s$;

X_4 : The degree of saturation of the north crossover intersection, $X_4 = CV_4/s$;

X_5 : The degree of saturation of the central intersection, $X_5 = CV_5/s$;

β_1 : Southbound through queue at the major intersection;

β_2 : Eastbound through queue at the major intersection;

- β_3 : Northbound through queue at the major intersection;
- β_4 : Westbound through queue at the major intersection;
- θ_1 : Southbound left-turn queue at the major intersection;
- θ_2 : Eastbound left-turn queue at the major intersection;
- θ_3 : Northbound left-turn queue at major intersection;
- θ_4 : Westbound left-turn queue at the major intersection;
- γ_1 : Southbound left-turn queue at the crossover intersection;
- γ_2 : Eastbound left-turn queue at the crossover intersection;
- γ_3 : Northbound left-turn queue at the crossover intersection;
- γ_4 : Eastbound left-turn queue at the crossover intersection;
- ω_1 : Southbound through queue after the major intersection;
- ω_2 : Westbound through queue after the major intersection;
- ω_3 : Northbound through queue after the major intersection; and
- ω_4 : Eastbound through queue after major intersection.

$$\log(D) = 2.583 + 0.047 \frac{X_1}{1 - X_1} + 0.028 \frac{X_2}{1 - X_2} + 0.025 \frac{X_3}{1 - X_3} + 0.033 \frac{X_4}{1 - X_4}$$

$$\text{t value } (237.9) \quad (46.69) \quad (20.116) \quad (18.86) \quad (4.66)$$

$$+ 0.062 \frac{X_5}{1 - X_5} + 0.167\beta_1 + 0.182\beta_2 + 0.192\beta_3 + 0.195\beta_4 + 0.23\theta_1$$

$$(5.49) \quad (7.27) \quad (8.368) \quad (11.8) \quad (12.27) \quad (4.37)$$

$$+ 0.196\theta_2 + 0.207\theta_3 + 0.219\theta_4 + 0.072\gamma_1 + 0.091\gamma_2 + 0.101\gamma_3$$

$$(11.697) \quad (8.042) \quad (13.233) \quad (5.126) \quad (7.462) \quad (9.609)$$

$$+ 0.049\gamma_4 + 0.213\omega_1 + 0.229\omega_2 + 0.187\omega_3 + 0.281\omega_4$$

$$(2.284) \quad (9.475) \quad (10.396) \quad (9.616) \quad (5.601)$$

$$R^2 = 0.9142, \quad \text{Sample size } N: 800 \quad (2.17)$$

Figure 2-37 presents the comparison results between the estimated and simulated delays for a full CFI at various traffic volumes.

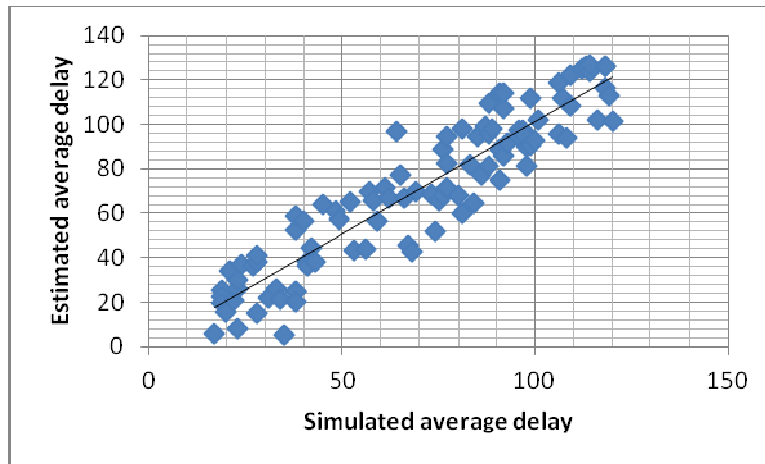


Figure 2-37: Comparison results of estimated and simulated delays for a full CFI

Note that the above delay model indicates that the average control delay becomes very large when either of the following two conditions occurs: (1) the CLV of the major or crossover intersection approaches its theoretical capacity, and (2) the queue-to-bay length ratio exceeds one which indicates the queue spillback at some location within the CFI. Also note that the relative weights of the different factors contributing to the overall intersection delay can be seen from their relative parameter values, since all variables have been standardized in the regression process. Thus, the congestion level of the central (primary) intersection, reflected in its CLV, clearly plays a more critical role than the other four crossover intersections in causing overall delay.

Similarly, how a traffic queue potentially affects the overall intersection delay, reflected in its parameter value, also varies with its location and associated geometric features. Therefore, one can use such information to rank the impacts of different bays on the total delay at the intersection and can determine the design or improvement priority under any given resource constraint.

CHAPTER 3

EVALUATION MODELS FOR DIVERGING DIAMOND INTERCHANGES AT THE PLANNING STAGE

3.1 Introduction

The Diverging Diamond Interchange (DDI), one of the new unconventional intersection designs, has received increasing attention in recent years due to its cost-effectiveness and its operational advantages over the traditional diamond interchange design. The DDI is designed mainly to allow efficient navigation for both left turn and through movements between highway ramps. Thus, its core design logic is to accommodate left turning movements onto the arterial and also to eliminate the need for a left turn bay.

As shown in Figure 3-1, the reverse operations of the through traffic between the two ramp terminals in a DDI design allow its left turn traffic flows from the freeway off-ramp to move concurrently with the opposing flows at each subintersection. Its right-turn movements from the cross street to the ramps take place at the ramp terminal intersections. With this assignment of different movement flows, the DDI design can significantly reduce the number of conflict points. Figure 3-2 illustrates the typical flow paths in a DDI design; the merged flows, comprising both through and left-turn traffic from the arterial and left-turn vehicles from the freeway off-ramp, split at the end of the bridge, and all of the reversed traffic flows return to their normal operational paths.

Note that the unique geometric features of DDI not only increase its overall capacity, but also reduce the total vehicle delay, as all of its intersections can be operated with a simple two-phase signal. In addition, all ramp intersections in a DDI design are relative small and thus cause less vehicle delay. However, calculating the optimal length for the DDI's bridge is a critical design issue, since the bridge serves as the queue storage area and may significantly affect the overall interchange capacity.

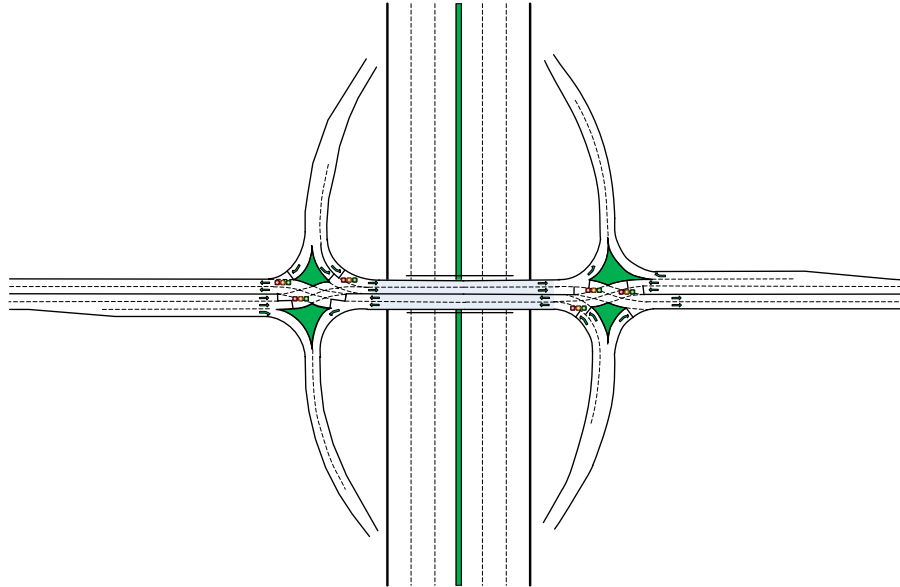


Figure 3-1: Bird's eye view of a typical DDI design

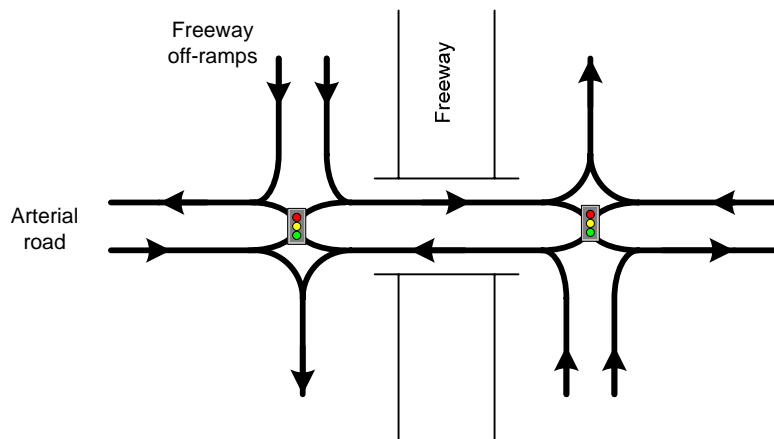


Figure 3-2: Graphical illustration of movement paths in a typical DDI design

Due to both the operational efficiency and potential safety improvements that DDIs offer, highway agencies are increasingly interested in constructing these interchanges. Some of those having successfully operated in recent years are listed below:

- The crossing of I-44 and US Route 13 in Springfield, MO (Figure 3-3).
- The crossing of Highway A13 and RD 182 (Boulevard de Jardy) in Versailles, France (Figure 3-4).
- The crossing of Highway A4 (Boulevard des Allies) and Boulevard de Stalingrad in Le Perreux-sur-Marne, France (Figure 3-5).
- The crossing of Highway A1 and Route d'Avelin in Seclin, France (Figure 3-6).



Figure 3-3: Bird's eye view of a DDI in Springfield, MO



Figure 3-4: Bird's eye view of a DDI in Versailles, France



Figure 3-5: Bird's eye view of DDI in Perreux-sur-Marne, France



Figure 3-6: Bird's eye view of DDI in Seclin, France

The main operational strength of above DDIs lies in its ability to reduce traffic conflict points and signal phases at ramp terminal intersections. The DDI should prove especially effective when both the left turning traffic from freeway off-ramps and the through traffic from the arterial experience high demand volumes. The DDI design allows the reduction of the signal phase by flipping the traffic flows between its two ramp

terminal intersections, creating fewer conflict points than a conventional diamond interchange.

Figure 3-7 shows the phase sequence for signal control at a DDI, and Figure 3-8 shows the distribution of merging, splitting, and conflict points of a DDI. The reduction in conflict points indicates that the DDI design will likely offer a safer driving environment than conventional diamond interchanges.

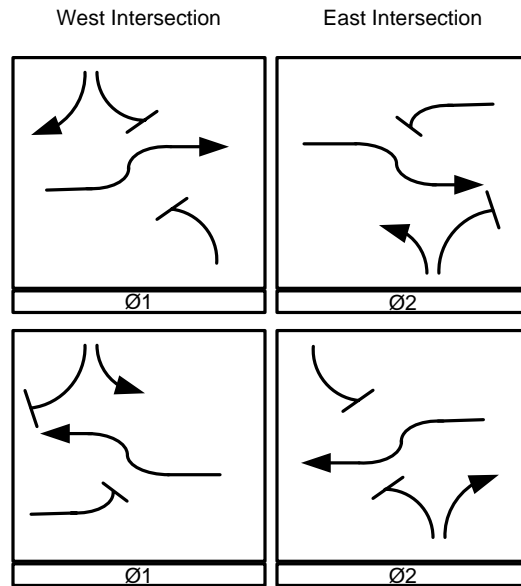


Figure 3-7: Signal phase diagram at a DDI

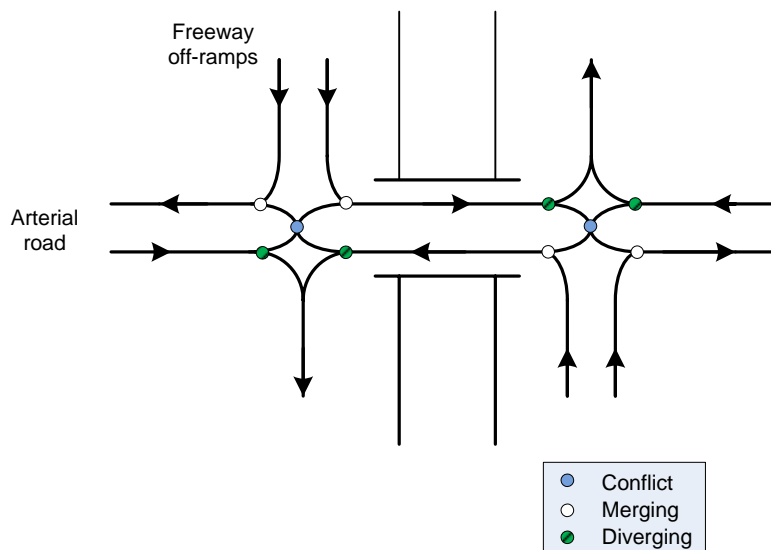


Figure 3-8: Conflict points of a DDI

Despite its potential efficiency and safety improvements, a DDI may increase driver discomfort or confusion, due to the use of reversed paths for through movements between the two ramp terminals. As driver confusion may compromise the safety performance of the interchange and increase delays, adding some countermeasures to assist drivers will be desirable during its initial operation period.

Although few DDIs have been implemented in the US, the traffic community has started to investigate its strengths and deficiencies over the past decade. For instance, Chlewicki (2003) used Synchro and SimTraffic to analyze the delays in a DDI design and compared its performance to that of the conventional interchange under various demand levels. Using the conventional diamond interchange as the basis for comparison, his study concluded that the DDI design can reduce about 60 percent of the total intersection delay and stop delay, and the total number of stops in a DDI can be reduced to the 50 percent level under most volume conditions. Applying the same simulation tools, Septh (2007) conducted a similar analysis of DDI and conventional diamond interchanges and also reached the same conclusions, especially regarding the average delay and average number of stops per vehicle.

Bared, Edara, and Jagannathan (2009) extensively investigated the performance of DDIs at five volume levels and under two geometric conditions. Their research results, based on simulation experiments, indicated that a DDI can outperform a conventional diamond interchange, particularly at high levels of volume. Regardless of the demand level, a DDI design generally can accommodate higher volumes for all movements, especially for left turn flows, than a conventional diamond interchange. They also concluded that converting an interchange into a six-lane DDI is economically more beneficial than widening the bridge using a traditional design.

Note that existing DDI studies are quite limited and focus mainly on exploring its benefits using microscopic traffic simulations. No researcher has yet published a rigorous theoretical study that quantifies the interrelation between all factors affecting the total delay and queue distribution in a DDI design. Some critical issues for DDI proponents to address include: (1) development of a convenient and effective planning stage tool for evaluating the performance of a DDI design, such as identifying potential queue spillback

locations and their impacts on the overall delay; (2) optimization of the geometric parameters based on different demand patterns; and (3) coordination of signal timings and offsets between multiple subintersections.

3.2 Experimental Design for DDI Model Development

As with the previous model developed for CFIs, this study employed simulation experiments to generate various DDI performance data for model calibration and delay analysis. All experimental scenarios for DDI development share the following common features:

- All interchange approaches had the same number of lanes for each movement, i.e., two through lanes, and left turn and through volumes shared the same lane.
- All right-turn lanes were channelized and considered as free right-turn lanes.
- Two DDI subintersections were controlled together using a signal controller.

Table 3-1 presents the four sets of geometric parameters designed to enable simulation experiments to test the impact of three critical bay/link lengths (denoted as A, B, and C locations in Figure 3-9) on the interchange delays and capacity.

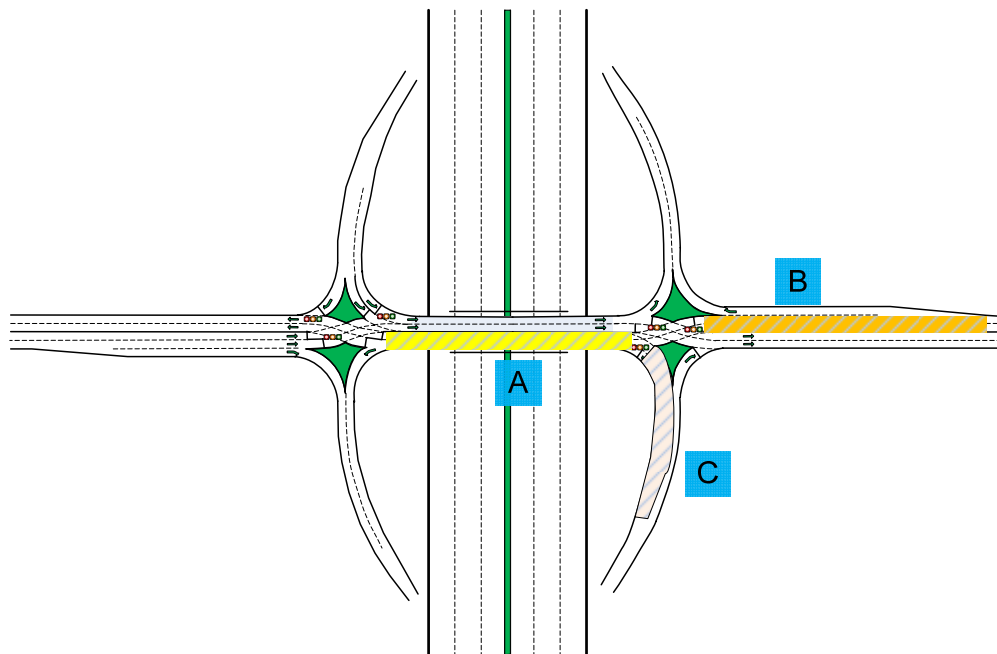


Figure 3-9: Spatial distribution of three critical bay lengths in a DDI design

Table 3-1: Geometric parameters used in simulating different DDI designs

Case	Length A	Length B	Length C
1	400 ft	360 ft	300 ft
2	600ft	550ft	450ft
3	800ft	700ft	600ft
4	1000ft	900ft	750ft

Note that the DDI is symmetrical and consists of two subintersections and eight potential queue locations. Figure 3-10 shows the spatial distribution of the potential queue areas. Due to the interdependent nature of traffic queues in those bays, any spillback at one location may propagate the congestion to the entire interchange and degrade the available interchange capacity. This makes understanding the relationship between the queue development in each bay and its contributing factors one of the most critical issues in evaluating the performance of a DDI design.

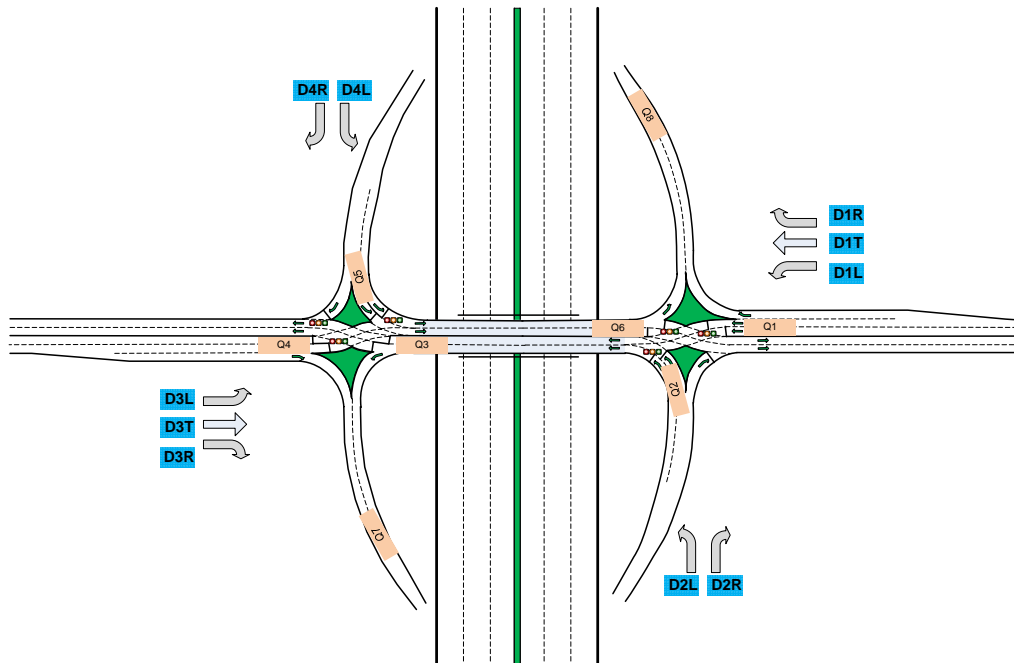


Figure 3-10: Spatial distribution of traffic queues in a DDI design

Note that, due to the symmetry of the DDI, one can classify the eight potential queues into four distinct types. The notation for each queue type is defined below:

Q_1 : Westbound through queue on the arterial;

Q_2 : Northbound queue on the freeway off ramp;

- Q₃: Westbound queue on the bridge;
- Q₄: Eastbound through queue on the arterial;
- Q₅: Southbound queue on the freeway off ramp;
- Q₆: Eastbound queue on the bridge;
- Q₇: Southbound merge queue on the freeway on ramp; and
- Q₈: Northbound merge queue on freeway on ramp.

The Type 1 queue (Q₁, Q₄) is generated by the through or left-turn flows at the intersection stop line, whereas the Type 2 queue (Q₃, Q₆) forms on the bridge between ramp terminals; the bridge is the most critical location in a DDI design. Those queues incurred at freeway off-ramps and merging areas are classified as the Type 3 queue (Q₂, Q₅) and the Type 4 queue (Q₇, Q₈), respectively.

3.3 Development of Queue Models

Type 1 Queue Model (Q₁, Q₄)

Since the Type 1 queue mainly occurs at signal control locations, the proposed model for capturing its development takes into account the impacts of the following contributing factors: the incoming demand level; the assigned green time ratio; and the overall congested level, as reflected by CLV (Figure 3-1). Equation 3-1 presents the model calibration results from extensive simulation experiments.

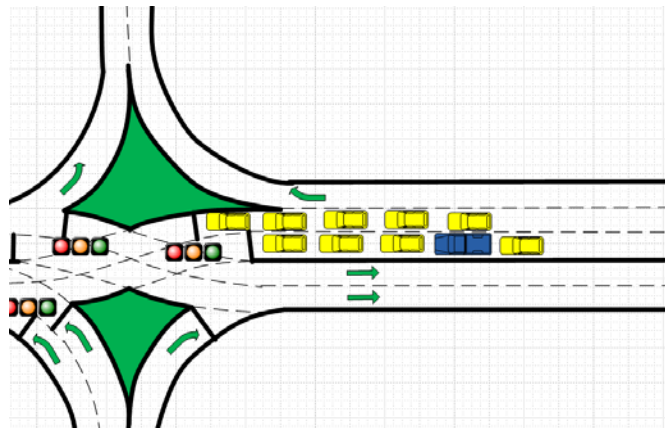


Figure 3-11: Graphical illustration of a Type 1 queue pattern

$$\text{Log}(Q) = 0.682\text{Log}(D_L + D_T) + 0.380 \frac{D_L + D_T}{s - CV} + 1.374\rho_3$$

t value (35.04) (6.93) (21.56)

$$R^2 = 0.9978, \quad \text{Sample size } N: 1200 \quad (3.1)$$

where,

D_L : Incoming left-turn demand in veh/hour;

D_T : Incoming through demand in veh/hour;

CV: The critical lane volume of the intersection; and

ρ_3 : Maximum queue to bay length ratio at the downstream link.

Type 2 Queue Model (Q_3, Q_6)

Unlike the Type 1 queue, traffic joining the Type-2 queue may come from three upstream traffic streams (see Figure 3-12) and may discharge in two possible directions (i.e., turning left onto the freeway on-ramp or onto the arterial). Therefore, this study has employed the following formulation to predict the Type 2 queue development:

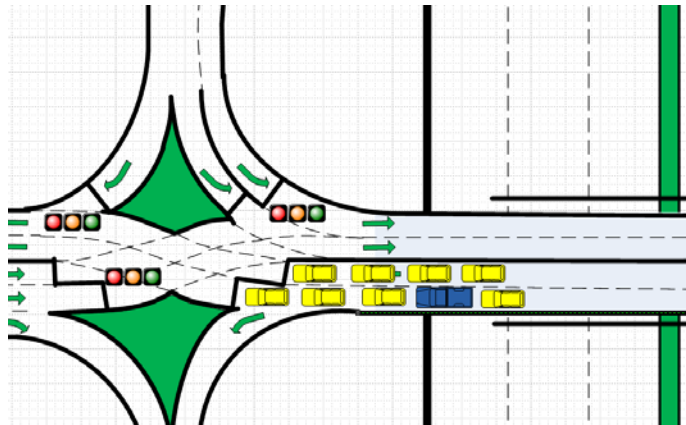


Figure 3-12: Illustration of a Type 2 queue pattern

$$\log(Q) = 0.208 \log(D_W) + 0.537 \log(D_{NL}) + 0.833 \frac{D_W + D_{NL}}{s - CLV}$$

t value	(35.04)	(6.93)	(13.69)
---------	---------	--------	---------

$$R^2 = 0.9942, \quad \text{Sample size } N: 1200 \quad (3.2)$$

where,

D_W : Westbound volume from the arterial upstream;

D_{NL} : Northbound left-turn volume from the freeway off ramp; and

CLV: The critical lane volume of the intersection.

Type 3 Queue Model (Q_5, Q_6)

Figure 3-13 illustrates the Type 3 queue pattern, which forms at the freeway off-ramps. Its main contributing factors include the freeway off-ramp left turn volume, the intersection congestion level, and the maximum queue-to-bay-length ratio. Equation 3-3 presents the calibration results for this prediction model.

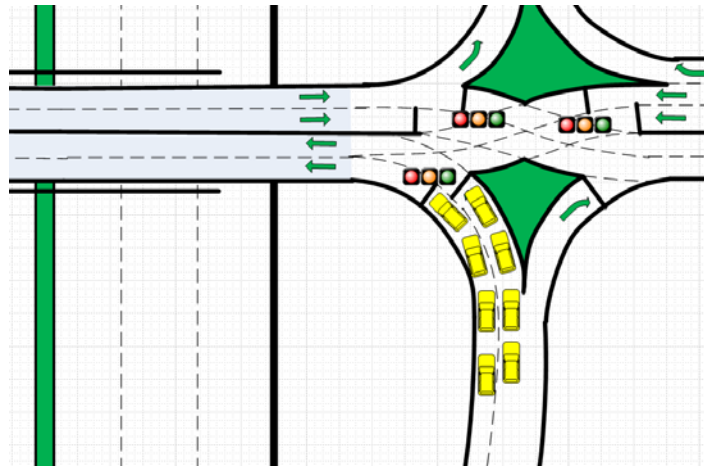


Figure 3-13: Illustration of a Type 3 queue pattern

$$\text{Log}(Q) = 0.6631 \text{Log}(D_L) + 0.6745 \frac{D_L}{s - CLV} + 0.3897 \rho$$

t value	(233.257)	(7.113)	(37.665)
---------	-----------	---------	----------

$$R^2 = 0.9965, \quad \text{Sample size } N: 1200 \quad (3.3)$$

where ,

D_L : Freeway off ramp left-turn demand in veh/hour; and

ρ : Maximum queue to bay length ratio at its downstream link.

Type 4 Queue Model (Q_7, Q_8)

The Type 4 queue model allows the estimation of the queue length in a merging area, where two traffic streams from different directions merge at the freeway on-ramp and then proceed to enter the freeway mainline. Since the queue length during the merging process is determined by not only the flow rate but also the distribution of available gaps for merging maneuvers. This process, discussed in Chapter 2, can best be captured with the classical M/G/1 model, which stands for random arrival/general service time distribution/single server. It assumes that the service time, which is equivalent to the merge time, is a general distribution (i.e., not the typical exponential distribution). Thus, one can calculate the expected waiting time as:

$$E(S) = \frac{\lambda}{\mu} [e^{t_{nr}\mu} - (1 + t_{nr}\mu)] \quad (3.4)$$

where,

$E(S)$: The expected waiting time for a successful merge;

t_{nr} : The gap time required for a safe merge;

λ : The arrival rate of merging flows in vehicles per hour; and

μ : The arrival rate of the mainline flow in vehicles per hour.

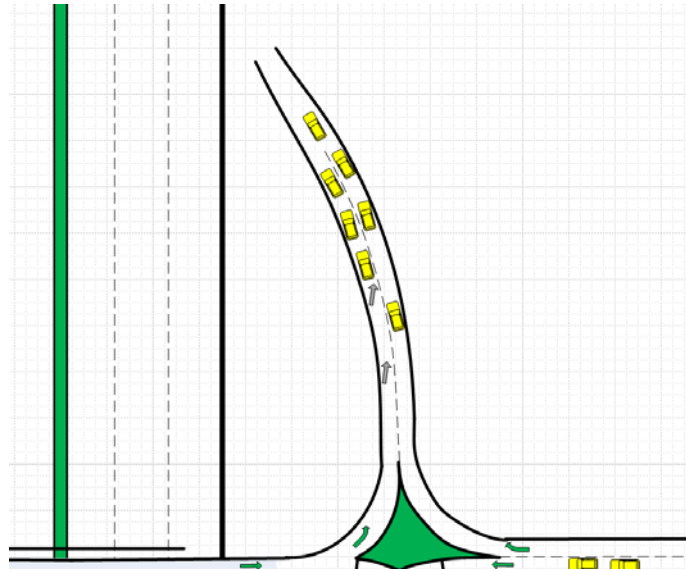


Figure 3-14: Illustration of a Type 4 queue pattern

Also, the average number of waiting vehicles is the product of arrival rate and the expected waiting time, as shown in Equation (3.5):

$$\rho = \lambda E(S) \quad (3.5)$$

Equation (3.6) shows the best calibrated model for Type 4 queue estimation, based on the above theoretical relationships and on results from simulation experiments.

$$Q_{\max} = 6.54 + 24.87\rho^2 + 896.56\lambda^2 + 289.75\mu^2$$

t value	(2.68)	(14.37)	(54.23)	(47.39)
---------	--------	---------	---------	---------

$$R^2 = 0.9133, \quad \text{Sample size } N: 1200 \quad (3.6)$$

Figures 3-15 to 3-18 show the comparison results between the queues estimated with the calibrated models and the simulated queues generated from each type of traffic simulator. As expected, the data are distributed uniformly along the diagonal line, indicating that all four calibrated queue models can yield unbiased prediction results, making them sufficiently reliable for use as evaluation tools at the planning stage.

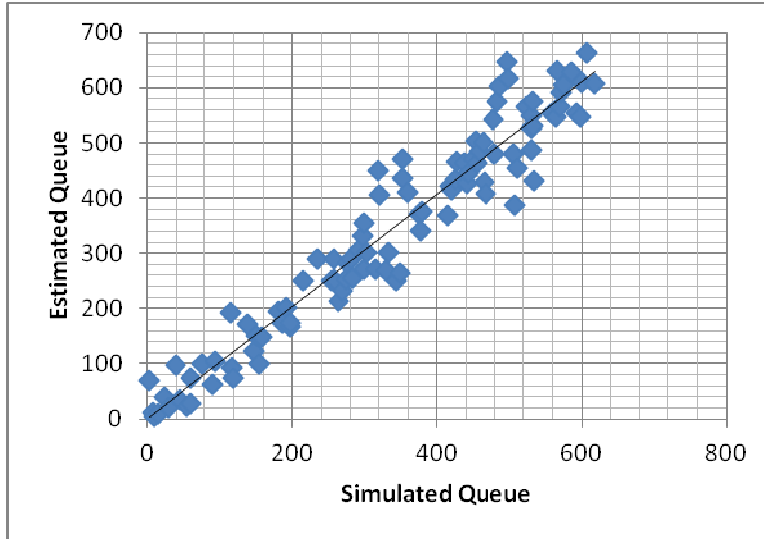


Figure 3-15: Comparison of the estimated and simulated Type 1 queue lengths in a DDI design

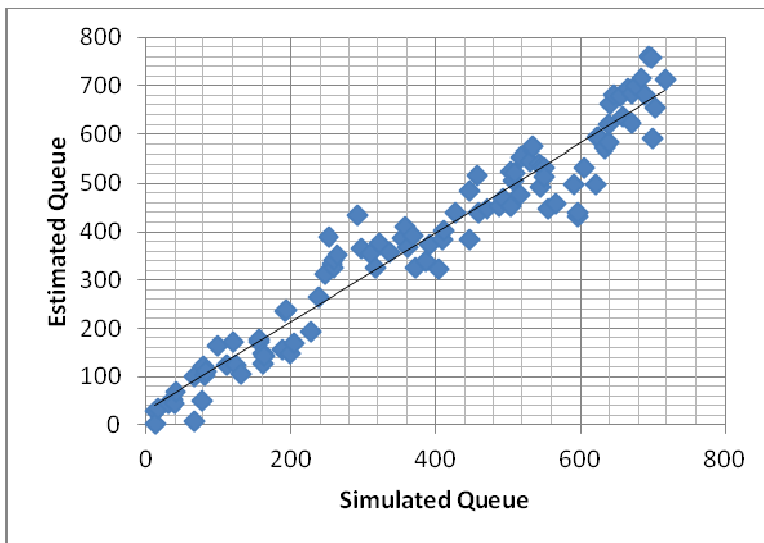


Figure 3-16: Comparison of the estimated and simulated Type 2 queue lengths in a DDI design

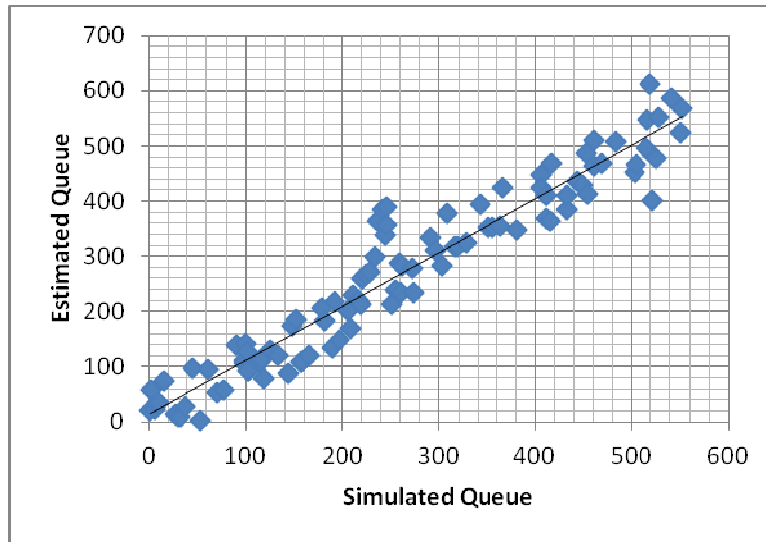


Figure 3-17: Comparison of the estimated and simulated Type 3 queue lengths in a DDI design

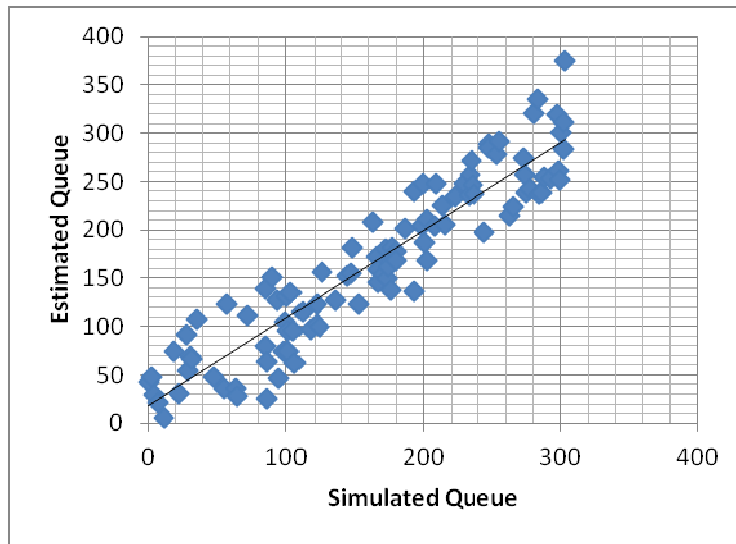


Figure 3-18: Comparison of the estimated and simulated Type 4 queue lengths in a DDI design

3.4 Delay Model for DDI Design

Unlike a conventional diamond interchange, DDI is designed to make it easier to navigate left turn and through movements between two ramp terminals and to accommodate vehicles turning left onto the arterials. On the cross street, all vehicles must move to the left side of the roadway between the ramp terminals. Such geometric features

make the DDI design quite different from all existing interchanges or intersections; thus, one cannot use any of the existing delay models to assess its operational capacity and efficiency. Therefore, this study developed a preliminary delay model for DDI evaluation, based on extensive simulation experiments and on the results of statistical calibration. Figure 3-19 illustrates the spatial distribution of all factors associated with the total delay at a DDI, and Equation (3.7) shows the calibrated delay model for use at the planning stage.

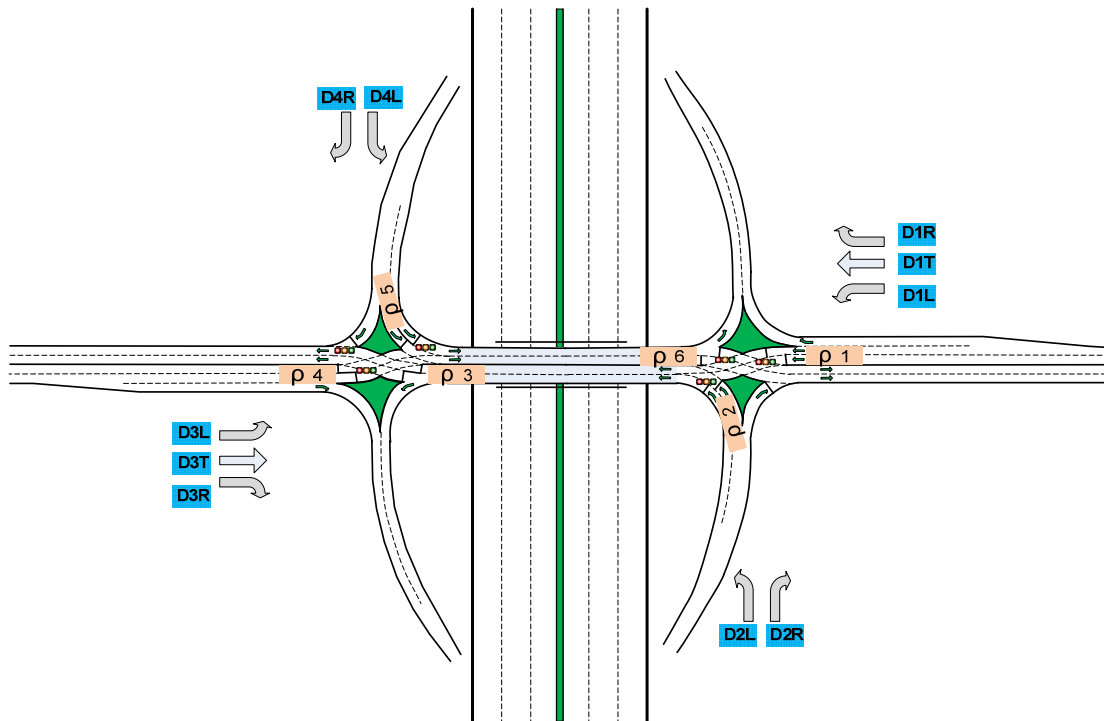


Figure 3-19: Spatial distribution of all factors associated with the total delay at a DDI

CV_1 : The critical lane volume of the west intersection;

CV_2 : The critical lane volume of east intersection;

X_1 : The degree of saturation of the west intersection, $X_1 = CV_1/s$;

X_2 : The degree of saturation of the east intersection, $X_2 = CV_2/s$;

ρ_1 : Maximum queue to bay length ratio on the arterial=Queue1/link length;

ρ_2 : Maximum queue to bay length ratio on off ramp=Queue2/ramp length;

ρ_3 : Maximum queue to bay length ratio on the bridge=Queue3/link length;

ρ_4 : Maximum queue to bay length ratio on the arterial=Queue4/link length;

ρ_5 : Maximum queue to bay length ratio on off ramp=Queue5/ramp length; and

ρ_6 : Maximum queue to bay length ratio on the bridge=Queue6/link length.

$$\text{Log(Delay)} = 2.549 + 0.154 \frac{X_1}{1 - X_1} + 0.149 \frac{X_2}{1 - X_2} + 0.206\rho_1 + 0.213\rho_2$$

t value (3.87) (13.98) (21.37) (16.58) (3.87)

$$+0.253\rho_3 + 0.212\rho_4 + 0.197\rho_5 + 0.251\rho_6$$

(5.78) (54.31) (42.64) (5.98)

$$R^2 = 0.947, \text{ sample size N: 1200} \tag{3.7}$$

Figure 3-20 shows the comparison results between delays predicted by the calibrated model and by the DDI simulator under different volume conditions. The approximately uniform distribution along the diagonal line suggests that Equation (3.7) offers an unbiased and reliable estimate of the total interchange delay suitable for assessing a DDI at its planning stage.

The analysis between the total delay and each of those contributing factors indicates that the ramp terminal intersection at a high congestion level (reflected in its CLV) has the most impact on the overall DDI delay. As shown by the denominators in Equation (3.7), the entire DDI will become gridlocked if the volume at either of its ramp terminal intersections exceeds its capacity (i.e., its maximum CLV). Hence, the level of service at one of the more congested ramp terminal intersections can reasonably reflect the overall performance level of the entire DDI, provided that the bridge length between two intersections is sufficient for queue storage.

A further comparison of the estimated parameters in Equation (3.7) also reveals that, among the three types of queue development locations, the one on the bridge link has the most significant impact on the overall DDI delay, confirming the general perception that determining the optimal length for the bridge link is one of the most critical tasks in designing a DDI.

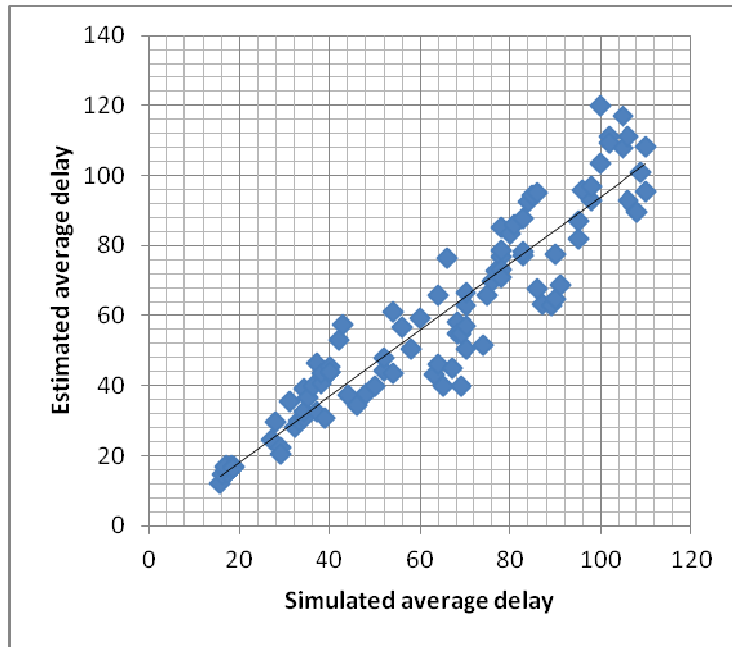


Figure 3-20: Comparison of the delays estimated by the model and simulation

CHAPTER 4: DEVELOPMENT OF DYNAMIC QUEUE MODELS FOR OPERATIONAL ANALYSIS

4.1 Introduction

This chapter presents the dynamic queue models developed for operational analysis of the CFI and DDI designs, including a discussion of critical factors associated with intersection queue evolution, presentation of the formulations for stochastic queue patterns, and illustration of the solution algorithm. Unlike those formulations calibrated for use at the planning stage, the dynamic models provide a precise estimate of the time-varying queue length, based on the following unique operational features of CFI and DDI:

- The design includes one primary and several mutually dependent subintersections to collectively determine the performance of the entire intersection;
- Most vehicles must go over multiple signals to pass through the entire intersection;
- The spacing between neighboring intersections is relative short, thus they are likely to experience link spillback during congestion periods;
- The queue length at each intersection depends not only on its approaching flow rates, but also the queue lengths at both its upstream and downstream intersections;
- All signals operate with a two-phase control due to the separation between the primary and turning movements; and
- A signal failure at any sub-intersection or the primary intersection will propagate the queues to all other intersections and cause gridlock.

Hence, any model developed for operational analysis of CFI or DDI shall have the capability to capture the stochastic nature of the arriving and discharging traffic patterns in a signalized network, and to estimate the impacts of intersection spacing, volume level, and signal timings on the evolution of intersection traffic queues. It shall also be able to account for the mutual dependence of traffic queues between neighboring signals under different congestion levels. A brief review of related delay and queue models reported in the traffic literature is presented below:

Deterministic Queuing Models

Deterministic queuing model offers a simplified process to estimate the intersection delay under uniform arrival and departure patterns. Based on the difference between the accumulative arrival and departure rates, one can approximate its delays from the queue length with Equations (4.1) and (4.2), respectively, for the under-saturated and over-saturated conditions, where the average delay is a function of arrival rate ν , saturation flow rate s , capacity c , and cycle length C :

$$d = \frac{r_e^2}{2C} \left(\frac{s}{s-\nu} \right) \quad (4.1)$$

$$d = \frac{3600T}{2} \left(\frac{\nu}{c} - 1 \right) \quad (4.2)$$

Note that the intersection delay in Equation (4.2) is a function of time, indicating that its residual queue will increase over time under over-saturated conditions.

Shockwave Queuing Models

Shockwave queuing model is one of the popular classic methods used by the researchers at the early stage of traffic flow theory development. For instance, Rorbeck (1968) investigated the intersection queue formation at the beginning of a red interval with the shockwave theory. Stephanopoulos (1979) further investigated the dynamics of queue formation and dissipation at an isolated intersection by taking into account the flow conservation principle. Michalopoulos (1980) studied the queue formation along an arterial and proved the existence of shockwave propagation from its downstream to upstream intersections. Michalopolos and Pisharody (1981) employed the same theoretical basis to further develop a signal optimization algorithm that can minimize the total delay of an isolated intersection under the maximum queue length constraint. Such models developed with the shockwave theory, despite its deterministic nature, can approximate the intersection queues at different volume levels.

Stochastic Steady-state Queuing Model

Unlike the deterministic models, most studies in this category attempt to account for the effects of time-varying traffic flow patterns on intersection delay. For example, Webster (1958) developed a formula to estimate the average delay experienced by drivers, based on the Poisson arrival assumption and simulation experimental results. McNeil (1968) derived a function for the average delay, using the average stationary queue length at the beginning of each green phase. Newell (1965) proposed an analytical method to approximate the queue with a continuous fluid model and the Central Limit theorem.

By applying the probability generation function, Meissl (1963) and Darroch (1964) independently formulated a creative but computationally cumbersome model to estimate the traffic queue distribution at different time intervals within a signal cycle. Ohno (1978) conducted a numerical evaluation of several models for average delay and queue estimation, including those by Webster (1958), Webster and Cobbe (1966), McNeill (1968), Miller (1963), and Newell (1965). He concluded that Newell's model outperforms all others. Along the same research line but employing a more realistic non-Poisson arrival process, Cowan (1981) derived a model for the average delay and queue at isolated intersections. Heidemann (1994) derived a closed form expression for the mean residual queues for traffic following Poisson distribution. Broek and Leeuwaarden (2006) presented a computing process for estimating the boundaries of the residual queue evolution that may exist during a green phase.

Note that the distribution of FCTL (Fixed Cycle Traffic Light) queue models developed independently by Meissl (1963) and Darroch (1964), using the probability generating function (PGF) and the equilibrium condition, was not considered useful in practice, despite its theoretical elegance. This is due to the fact that one needs to adopt complex computing procedures to find out the roots within the unit circle of their models' characteristic equations and to invert the PGF function to explicitly represent the stochastic queue properties. However, due to the ever-growing computing power of computers over the recent decades, those cumbersome computing tasks no longer pose any difficulty to the traffic researchers. Besides, Chaudhry, Marchal, and Harris (1900) offered a detailed procedure for identifying those roots and showed that the root locations

are obtainable under most arrival distributions. As for inversion of the PGF function, Abate and Whitt (1995) developed two numerical methods for inverting the Laplace transformation of the cumulative distribution function within an acceptable range of errors. Hence, the primary deficiency of Darroch's model due to its complex computing work becomes negligible, and its rigorous theoretical process for estimating the delay and queue distributions emerged as a promising method.

Stochastic Time-dependent Queuing Model

One primary limitation of steady-state stochastic queuing models lies in that the estimated queue length becomes extremely long when the approaching volume to capacity ratio equals one. To overcome this constraint, traffic researchers have developed various time-dependent queuing models over the past decades. For example, Roberson (1979) first introduced the time-dependent delay model, which was later enhanced by Kimber and Hollis (1979) with the coordinate transformation technique to transform the steady-state delay equation that can asymptotically produce the same overflow queues as with Equation (4.3). Although no one has provided a rigorous theoretical proof to validate their coordinate transform technique, some empirical evidences showed that such a model can indeed yield a reasonable delay estimation when the volume to capacity ratio exceeds one (Akcelik, 1988; Akcelik and Roupail, 1994; Olszewski, 1990).

$$Q_0(t) = \begin{cases} \frac{CT}{4} \left[(x - 1) + \sqrt{(x - 1)^2 + \frac{12(x-x_0)}{CT}} \right] & \text{when } x > x_0 \\ 0 & \text{o.w} \end{cases} \quad (4.3)$$

where, $x_0 = 0.67 + \frac{Sg}{600}$.

Other studies along the same line of developing time-dependent queue or delay models are available in the traffic literature (Brilon and Wu, 1990; Akcelik, 1981; Akcelik and Roupail, 1993; Fambro and Roupail, 1997).

4.2 Development of Operational Models

Since the operational model presented in this chapter is based on Darroch's work, this section first illustrates its core logic of Probability Generation Function (PGF) which is a power series representation of the probability mass function of a random variable.

The mathematical definition of PGF is given by the following equation:

$$G(z) = E(z^X) = \sum_{x=0}^{\infty} p(x) z^x \quad (4.4)$$

where, X is a discrete random variable and its probability density function is denoted by $p(x)$. The analytical queue model developed by Darroch (1964) with PGF has the following properties:

Property 1: Given the PGF of a random variable X , denoted by $G(z)$, its probability mass function is the derivative of $G(z)$.

$$p(X = k) = \frac{G^{(k)}(0)}{k!}$$

Property 2: Given the PGF of a random variable X , denoted by $G(z)$, its expectation is the first order derivative of $G(z)$.

$$E(X) = G'(1)$$

Property 3: Given the PGF of two random variables X and Y , denoted by $G(z)$ and $F(z)$, the PGF of the sum of the two random variables, $H(z)$ is the product of their PGF functions.

$$H(z) = G(z)F(z)$$

In addition to using the above three statistical properties, Darroch (1964) also employed the following assumptions in deriving his model:

Assumptions:

- The continuous time period can be divided into consecutive intervals with equal length, and each interval is called a slot.
- The length of each slot equals the time needed for a delayed vehicle to discharge from the queue; and
- The cycle time (C), green duration (g), and red phase timing (r) of each signal can be expressed as a number of discrete time slots.

Based on the above assumptions, Darroch modeled the queue evolution at an intersection as follows:

$$Q_{k+1,n} = Q_{k,n} + A_k \quad k = 0, 1 \dots, r - 1 \quad (4.5)$$

$$Q_{k+1,n} = \begin{cases} Q_{k,n} + A_k - 1 \\ U_k \end{cases} \quad \text{for } k = r, r + 1 \dots, r + g - 1 \quad (4.6)$$

Note that $Q_{k,n}$ denotes the number of vehicles in the queue on its upstream link; A_k is the number of arrivals at time slot k in cycle n.

The above two recursive equations represent the queue evolution during a cycle, based on the assumptions of random arrivals and a fixed departure rate. Note that deriving the distribution of $Q_{k,n}$ is the most critical task of the entire model development because both the delay and the maximum queue can be indirectly computed from this distribution.

Also note that the arriving distribution of A_k in the above formulations is assumed to be given. Thus, the distributions of $A_{k,n}$ and $A_{k,n+1}$ are identical and one can thus remove their under script n to compress the presentation. The queue spillback indicator, $B_{k,n}$, is independent from both A_k and $Q_{k,n}$, and is determined by the downstream queue

distribution ($Y_{k,n}$), and the downstream link length L . $U_{k,n}$ is a random variable, and has the following relationship with $A_{k,n}$:

$$U_{k,n} = \begin{cases} A_{k,n} - 1 & \text{if } A_{k,n} > 1 \\ 0 & \text{otherwise} \end{cases} \quad (4.7)$$

Since the distributions of both $A_{k,n}$ and $U_{k,n}$ are to be determined prior to the queue estimation, one can use their PGF properties to replicate the evolution of queue distribution over consecutive signal cycles.

Let the PGFs of $Q_{k,n}$, A_k and $U_{k,n}$ be denoted as $\delta_{k,n}(z)$, $\mu_k(z)$ and $\varepsilon_k(z)$, respectively. By applying Property 3, one can derive the following recursive relationships for $\delta_{k+1,n}(z)$ and $\delta_{k,n}(z)$:

$$\delta_{k+1,n}(z) = \delta_{k,n}(z)\mu_k(z) \quad k = 0, 1 \dots r - 1 \quad (4.8)$$

$$\delta_{k+1,n}(z) = \frac{\mu_k(z)}{z} (\delta_{k,n}(z) - \delta_{k,n}(0)) + \varepsilon_k(z)\delta_{k,n}(0) \quad k = r, r + 1 \dots r + g - 1 \quad (4.9)$$

Note that Equations (4.8) and (4.9) represent the queue evolution during the red and green phases, respectively. Since the time-dependent arrival distribution, $A_{k,n}$, is given or pre-estimated, one can compute the queue distribution at different time slots by iteratively applying these two equations.

Note that through a complex mathematical manipulation, Darroch successfully derived the analytical solution for the stochastic traffic queue distribution under a steady-state condition. His model and solution are certainly mathematically elegant, but suffer from the following limitations:

- The distribution of random arrivals per time slot, $A_{k,n}$, must be identical during all time slots and cycles;
- The average arrival rate must be less than the intersection capacity to ensure the existence of a stationary distribution of $Q_{k,n}$;

- The maximum departure rate during the effective green time is fixed and independent from external conditions, such as the intersection geometric features or the downstream queue length; and
- The point queue concept cannot realistically reflect the impact of traffic queues on the intersection control delay.

Violating any of these assumptions will make the model unsolvable. Despite the aforementioned limitations existing in most CFI and DDI designs, Darroch's methodology for analyzing the queue distribution remains a uniquely promising way to estimate the intersection delay. Hence, the dynamic queue model developed in this study has taken advantage of his model's strengths but overcome its theoretical limitations with additional extensions. The principal extension tasks are presented below:

Upstream Signal Effect

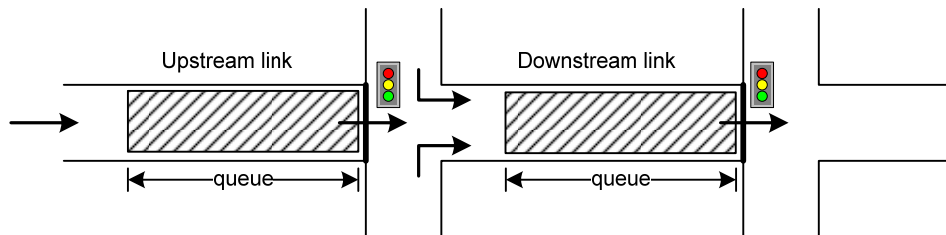


Figure 4-1: Two-signal arterial illustration

Consider a typical signalized arterial of two links, referred as the upstream link and downstream link, respectively (Figure 4-1). Any vehicle, traveling over the arterial, must pass two consecutive signals. Thus, the arriving flows to the downstream signal is likely to be affected by the signal and queue status of the upstream link as long as the distance between these two signals is relatively short to justify their dependent relationships. As reported in the aforementioned review, most traffic queue models, developed for isolated intersections, assume that the vehicle arriving distribution is time-invariant and follows the Monrovia process. Such assumptions are certainly not applicable to unconventional intersections such as CFI or DDI, as both comprise a cluster of mutually dependent signalized intersections with a relatively short spacing. Hence, to

realistically capture the delays and queues for unconventional intersections, one needs to first formulate the interdependence of the arriving flow distribution and the resulting queue length between neighboring intersections.

One popular method to model such an interdependent relationship is to formulate a platoon dispersion function, introduced first by Pacey (1956). Based on the assumptions of normally distributed speeds and unrestricted overtakings, Pacey derived the following distribution of travel times along a roadway segment:

$$f(\tau) = \frac{D}{\tau^2 \alpha \sqrt{2\pi}} e^{-\left[\frac{D}{\tau} - \frac{D}{\bar{\tau}}\right]^2 / 2\delta^2} \quad (4.10)$$

where,

D: Distance from the signal to the point where arriving flows are observed;

τ : Individual vehicle travel time along the distance D;

$\bar{\tau}$: Mean travel time; and

δ : Standard deviation of speeds.

One can then apply the above travel time distribution to transform a traffic flow profile along the roadway segment of distance, D, with the following integral equation.

$$q_2(t_2)dt_2 = \int_{t_1}^{t_2} q_1(t_1)f(t_2 - t_1)dt_1dt_2 \quad (4.11)$$

where,

$q_2(t_2)dt_2$: Total number of vehicles passing a downstream location of the signal at the interval (t, t+dt);

$q_1(t_1)dt_1$: Total number of vehicles passing the signal during the interval (t, t+dt) at the upstream intersection; and

$f(t_2 - t_1)$: Probability density function of travel times derived from Equation (4.10).

To substantiate the platoon diffusion effects, Hiller and Rothery (1967) conducted field observations and analyzed vehicle delays at pre-timed signals using the observed traffic profiles, and reached the following conclusions:

- The deterministic delay strongly depends on the offset between the upstream and downstream signals;
- The minimum delay, at the optimal offset, increases substantially with the distance between two neighboring signals; and
- The signal offset does not appear to have any significant effect on the overflow delay.

Note that the above platoon dispersion relationship is used in deriving the operational queue model presented in the remaining section, as it is essential for capturing the upstream signal effect on the distribution of traffic flows arriving at the downstream intersection.

Downstream Queue Spillback Effect

The interdependent relationship between two neighboring intersections also includes the impacts of the downstream intersection queues on the discharging flow rate of its upstream intersection. This is due to the fact that vehicles from the upstream intersection cannot either enter the target downstream links or need to slow down from the discharging process if traffic queues at the downstream intersection have been propagated to the entire link or observed by the approaching drivers.

The core modeling logic proposed to capture the downstream queue effect is to estimate the time-dependent blockage probability indicator, β_k , based on the Darroch's PGF method (1964). The blockage probability reflects the possible duration during which the vehicle discharging process may be blocked by its downstream link queue, given the traffic volumes and signal settings at both neighboring intersections.

More specifically, let $Q_{k,n}$ denote the number of queue vehicles in the upstream link and A_k be the number of arrivals at time slot k in cycle n . The recursive relation between $Q_{k+1,n}$ and $Q_{k,n}$ can be defined with equations (4.12) and (4.13) as follows:

$$Q_{k+1,n} = Q_{k,n} + A_k \quad k = 0, 1, \dots, r-1 \quad (4.12)$$

$$Q_{k+1,n} = \begin{cases} Q_{k,n} + A_k - 1 & \text{if } Q_{k,n} > 0 \text{ and } B_{k,n} = 0 \\ U_k & \text{if } Q_{k,n} = 0 \text{ and } B_{k,n} = 0 \\ Q_{k,n} + A_k & \text{if } B_{k,n} = 1 \end{cases}$$

for $k = r, r+1, \dots, r+g-1$

(4.13)

where $B_{k,n}$ is a binary variable to indicate the existence of downstream spillback at time slot k in cycle n .

$$B_{k,n} = \begin{cases} 1 & \text{if queue spillback occurs at downstream;} \\ 0 & \text{otherwise} \end{cases} \quad (4.14)$$

It should be mentioned that the arriving distribution, A_k , is assumed to be given in the above equations. Thus, the distributions of $A_{k,n}$ and $A_{k,n+1}$ are identical so that their under script n can be discarded to compress the notations. Besides, the queue spillback indicator, $B_{k,n}$ is independent from both A_k and $Q_{k,n}$, which is determined only by the distribution of downstream queue ($Y_{k,n}$), and the downstream link length (L); $U_{k,n}$ is a random variable, varying with $A_{k,n}$ based on the following relation:

$$U_{k,n} = \begin{cases} A_{k,n} - 1 & \text{if } A_{k,n} > 1 \\ 0 & \text{otherwise} \end{cases} \quad (4.15)$$

Let the PGFs of $Q_{k,n}$, A_k and $U_{k,n}$ be denoted as $\delta_{k,n}(z)$, $\mu_k(z)$ and $\varepsilon_k(z)$, respectively. Then, one can use the following two recursive equations to capture the relationship between $Q_{k+1,n}$ and $Q_{k,n}$.

$$\delta_{k+1,n}(z) = \delta_{k,n}(z)\mu_k(z) \quad k = 0, 1, \dots, r-1 \quad (4.16)$$

$$\delta_{k+1,n}(z) = \left[\frac{\mu_k(z)}{z} (\delta_{k,n}(z) - \delta_{k,n}(0)) + \varepsilon_k(z) \delta_{k,n}(0) \right] (1 - \beta_{k,n}) + \mu_k(z) \delta_{k,n}(z) \beta_{k,n} \quad k = r, r + 1, \dots, r + g - 1 \quad (4.17)$$

where, $\beta_{k,n} = E(B_{k,n})$.

By introducing the queue spillback factor, β , one can derive a new queue model based on the PGF concept. For an arterial consisting of multiple links, the computation should start from the furthest downstream link where its departure rate is not affected by the existence of any downstream queue.

4.3 Delay Analysis

The control delay, experienced by vehicle passing a signalized intersection, is defined as the difference between the actual travel time and the ideal travel time without signal control. When an incoming vehicle approaches an intersection, it may either travel through the intersection at the prevailing traffic speed or decelerate to join the queue. Most studies in the literature decomposed the control delay into three components: deceleration delay, stop delay, and acceleration delay. Figure 4.2 illustrates the process for an approaching vehicle to experience these three types of delay.

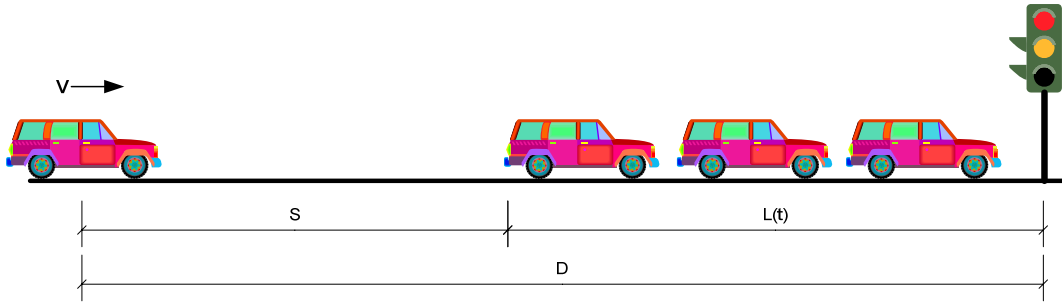


Figure 4-2: A graphical illustration of approaching vehicles and the control delay

Let $L_{t,n}$ be the queue length at time slot t of cycle n , which is determined by $Q_{t,n}$ and average vehicle length; S represents the safety stopping distance for the approaching vehicle to join the queue at the speed of v ; D is the required deceleration distance to the

intersection stop line. Let a_d and a_c denote the maximum deceleration and acceleration rates. One can then have the following relationships:

$$S = \frac{v^2}{2a_d}$$

$$T_{ff}(t) = \frac{L_{t,n} + S}{v} = \frac{v}{2a_d} + \frac{Q_{t,n}l}{v}$$

$$T_d(t) = \frac{v}{a_d} + w(t) + \frac{Q_{t,n}}{s} + \frac{v}{a_c}$$

$$\begin{aligned} d(t) &= T_d - T_{ff} = \frac{v}{a_d} + w(t) + \frac{Q_{t,n}}{s} + \frac{v}{a_c} - \left(\frac{v}{2a_d} + \frac{L_{t,n}}{v} \right) \\ &= \frac{v}{2a_d} + \frac{v}{a_c} + w(t) + \left(\frac{1}{s} - \frac{l}{v} \right) Q_{t,n} \end{aligned}$$

(4.18)

where,

$T_{ff}(t)$: Free flow travel time at time t ;

$T_d(t)$: Delay at time t when the approaching vehicle is caught by the queue or red signal;

$w(t)$: The time lag between the beginning of the next green phase and current time t ;

s : The saturation queue discharge rate; and

l : Average vehicle length.

Let the probability density function of $Q_{t,n}$ be denoted as $p_{t,n}(k)$, $k = 1, 2, \dots, n$. One can then compute the average delay with the following expression:

$$\bar{d}(t) = \begin{cases} \left(1 - p_{t,n}(0)\right) \left[\frac{v}{2a_d} + \frac{v}{a_c} + \left(\frac{1}{s} - \frac{l}{v}\right) \sum_{k=1}^{\infty} \frac{p_{t,n}(k)}{1 - p_{t,n}(0)} Q_{t,n} \right] & \text{if } t = 0, 1, \dots, g-1 \\ \frac{v}{2a_d} + \frac{v}{a_c} + w(t) + \left(\frac{1}{s} - \frac{l}{v}\right) \sum_{k=0}^{\infty} p_{t,n}(k) Q_{t,n} & \text{if } t = g, g+1, \dots, g+r-1 \end{cases} \quad (4.19)$$

Note that if without any residual queue at the intersection, one can rewrite Equation (4-19) into the following concise form:

$$\bar{d}(t) = \begin{cases} (1 - \varepsilon_{t,n})[\rho + \beta E(\widetilde{Q}_{t,n})] & \text{if } t = 0, 1, \dots, g-1 \\ \rho + w(t) + \beta E(Q_{t,n}) & \text{if } t = g, g+1, \dots, g+r-1 \end{cases} \quad (4.20)$$

where,

$$\varepsilon_{t,n} = p_{t,n}(0), \rho = \frac{v}{2a_d} + \frac{v}{a_c} \text{ and } \beta = \left(\frac{1}{s} - \frac{l}{v}\right)$$

$$E(\widetilde{Q}_{t,n}) = \sum_{k=1}^{\infty} \frac{p_{t,n}(k)}{1 - p_{t,n}(0)} Q_{t,n} \text{ and } E(Q_{t,n}) = \sum_{k=0}^{\infty} p_{t,n}(k) Q_{t,n}$$

One can further compute the average delay incurred between t_1 and t_2 by using the following weighted average method:

$$D(t_1, t_2) = \sum_{t=t_1}^{t_2} \mu(t) \bar{d}(t) \quad (4.21)$$

Note that $\mu(t)$ is the average arrival rate at time slot t . Based on the assumption of having a stationary distribution of $Q_{t,n}$, the following expression offers a straightforward way to compute the average intersection control delay:

$$D = \sum_{t=0}^{g+r-1} \mu(t) \bar{d}(t) \quad (4.22)$$

4.4 CFI Applications

This section illustrates how to apply the above models to estimate the queues and delays at a full CFI design as it has the most complex structure in the CFI family. One can apply the same procedures to analyze all other CFI designs.

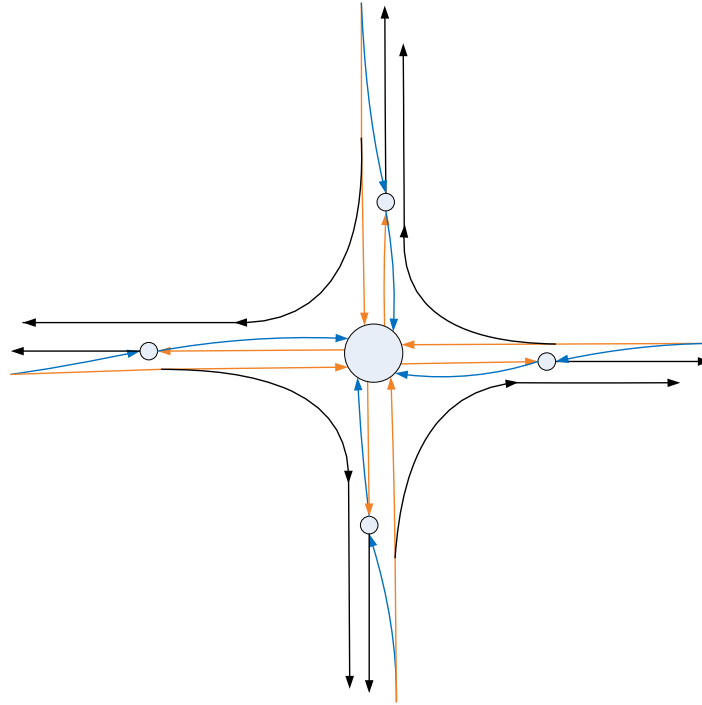


Figure 4-3: Graphical illustration of a full-CFI intersection

Figure 4.3 presents the link-node illustration of a CFI design, where nodes denote signalized intersections and links represent possible queues. Each movement follows a designated “path” to travel from its entry to exist. The entire queuing network contains two types of queue vehicles:

- Left turn traffic Queues: Left turning vehicles, traveling on an exclusive lane, must traverse over two signals to go through the entire intersection. Hence, one can apply the dynamic queue models presented in the previous section for a two-signal system to analyze the delays experienced by left turning vehicles.
- Through traffic Queues: Through traffic in a CFI also needs to cross over two consecutive signals, i.e., the primary intersection and one crossover intersection. Likewise, one can use the dynamic model for a two-signal system to capture the

interrelationships between volume, signal control, and the time-dependent through queues.

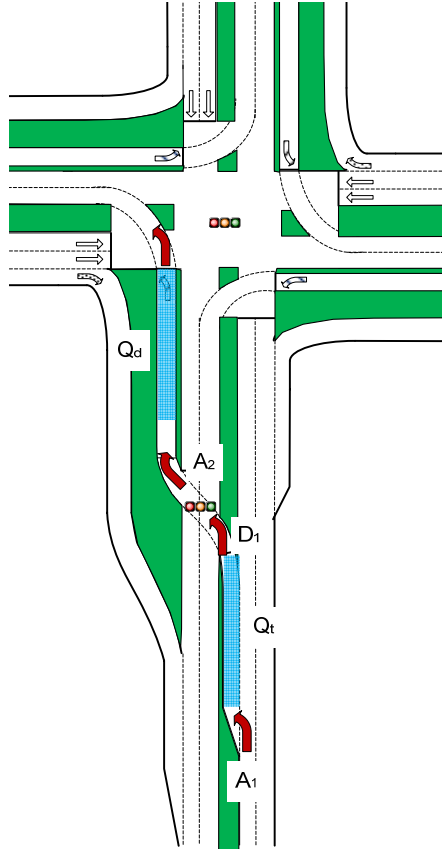


Figure 4-4: Left turn queue network in a full-CFI design

Left turn queue analysis

Let Q_t and Q_d denote the left turn queue preceding and after the crossover intersection, and let A_1 be the upstream arriving distribution. One can compute the time-varying vehicles (A_2) joining the downstream traffic queues (Q_d) directly from the upstream departure rate (D_1) and traffic queues (Q_t). Assuming that A_1 follows a Poisson distribution, one can formulate the following time-dependent queues based on the PGF model:

For Q_t

$$\begin{cases} \delta_{k+1,n}(z) = \delta_{k,n}(z)\mu_k(z) & k = 0, 1 \dots, r - 1 \\ \delta_{k+1,n}(z) = \left[\frac{\mu_k(z)}{z} (\delta_{k,n}(z) - \delta_{k,n}(0)) + \varepsilon_k(z)\delta_{k,n}(0) \right] (1 - \beta_{k,n}) \\ \quad + \mu_k(z)\delta_{k,n}(z)\beta_{k,n} & k = r, r + 1 \dots, g \end{cases} \quad (4.23)$$

For Q_d

$$\begin{cases} \theta_{k+1,n}(z) = \theta_{k,n}(z)\omega_k(z) & k = 0, 1 \dots, r - 1 \\ \theta_{k+1,n}(z) = \frac{\omega_k(z)}{z} (\theta_{k,n}(z) - \theta_{k,n}(0)) + \pi_k(z)\theta_{k,n}(0) \\ \quad & k = r, r + 1 \dots, r + g - 1 \end{cases} \quad (4.24)$$

where,

$\delta_{k,n}(z)$: The PGF of Q_t at time slot k of cycle n;

$\theta_{k,n}(z)$: The PGF of Q_d at time slot k of cycle n;

$\mu_k(z)$: The PGF of stochastic arriving distribution (A_1);

$\omega_k(z)$: The PGF of stochastic arriving distribution (A_2);

$\varepsilon_k(z)$: The PGF of the random variable determined by A_1 ;

$\pi_k(z)$: The PGF of the random variable determined by A_2 ; and

$\beta_{k,n}$: The probability of having a queue spillback at time slot k of cycle n.

Under the equilibrium condition, the queue distribution at both the upstream and downstream intersections should become stable, implying the existence of stationary (z) and $\theta_k(z)$ distributions.

Note that due to the non-linear nature of those derived equations, this study presents an efficient numerical procedure for approximating the queues and delays. Figure 4-5 shows the flowchart of the entire computing process.

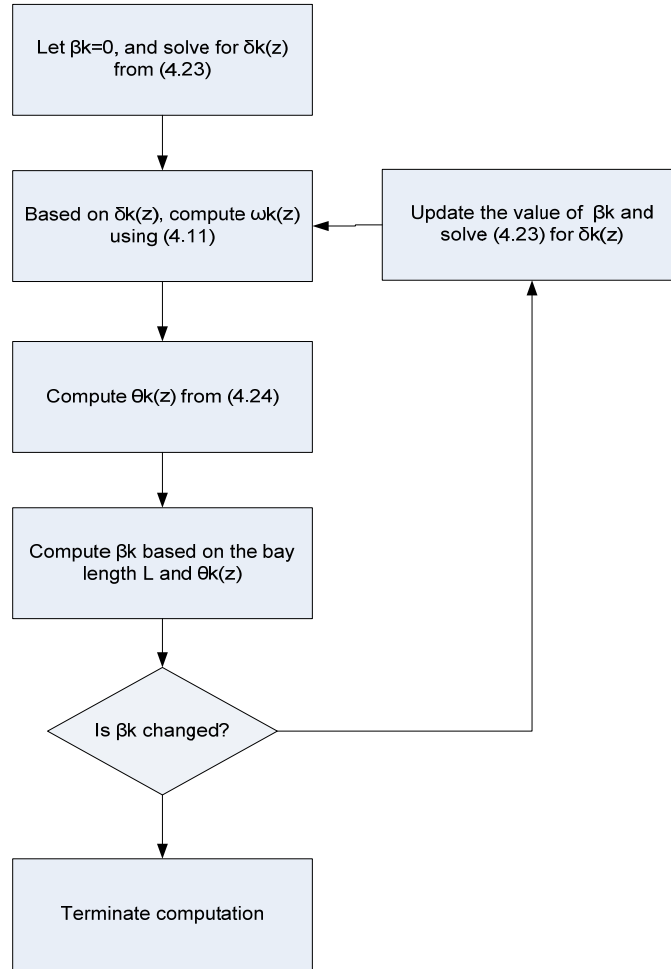


Figure 4-5: Flowchart for computing the stochastic left turning traffic queues

The proposed computing procedures comprise the following steps:

Step-1: Initialization. Set $\beta_{k,0} = 0$ for any k ;

Step-2: Solve Equation (4.23) for $\delta_{k,n}(z)$, based on $\beta_{k,0}$ and $\mu_k(z)$;

Step-3: Compute the time-dependent departure rate, $\omega_k(z)$, based on $\delta_{k,n}(z)$ and the platoon dispersion relation given by equation (4.11);

Step-4: Solve (4.24) for $\theta_{k,n}(z)$;

Step-5: Check the convergence based on the difference between $\beta_{k,n}^{(i-1)}$ and $\beta_{k,n}^{(i)}$, and

terminate the iteration if the difference between $\beta_{k,n}^{(i-1)}$ and $\beta_{k,n}^{(i)}$ is less than a

specified threshold (τ); Otherwise, proceed to Step 6.

Step-6: Adjust the spillback probability (β) by setting $\beta_{k,0}^{(i+1)} = \alpha\beta_{k,n}^{(i)} + (1 - \alpha)\beta_{k,n}^{(i-1)}$

and return to Step (2); α is a parameter between 0 and 1.

Through Queue Analysis

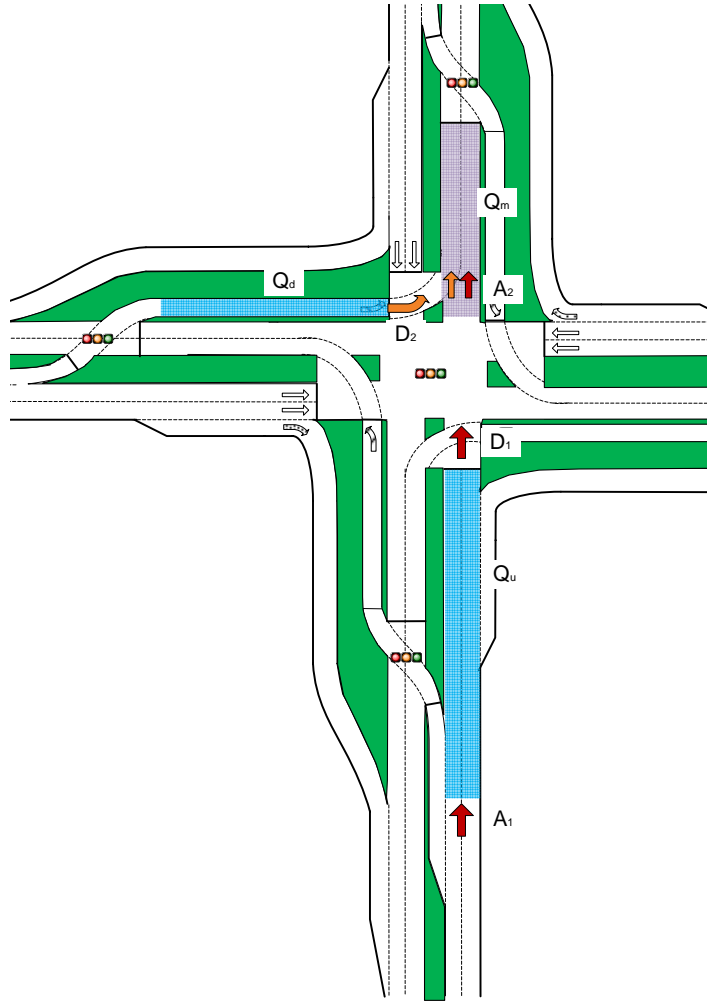


Figure 4-6: Through-queue distribution at a CFI design

Let Q_u and Q_m be the through queues preceding and after the primary intersection, and Q_d be the queues of left turning movement after the crossover intersection. The arrival and departure rates of Q_u is represented with A_1 and D_1 . The departure process of Q_d , denoted by D_2 , is assumed to be known because its PGF can be obtained by solving Equations (4.23) and (4.24). The arrival process of Q_m , denoted as

A_2 , is the flow rates of two merging traffic streams (D_1 and D_2). By the same token, one can estimate the time-dependent through queues by using the previously derived PGF queuing models as follows:

For Q_u

$$\begin{cases} \delta_{k+1,n}(z) = \delta_{k,n}(z)\mu_k(z) & k = 0,1 \dots, r-1 \\ \delta_{k+1,n}(z) = \left[\frac{\mu_k(z)}{z} (\delta_{k,n}(z) - \delta_{k,n}(0)) + \varepsilon_k(z)\delta_{k,n}(0) \right] (1 - \beta_{k,n}) \\ \quad + \mu_k(z)\delta_{k,n}(z) \beta_{k,n} & k = r, r+1 \dots, r+g \end{cases} \quad (4.25)$$

For Q_m

$$\begin{cases} \tau_{k+1,n}(z) = \tau_{k,n}(z)\gamma_k(z) & k = 0,1 \dots, r-1 \\ \tau_{k+1,n}(z) = \left[\frac{\gamma_k(z)}{z} (\tau_{k,n}(z) - \delta_{k,n}(0)) + \vartheta_k(z)\tau_{k,n}(0) \right] (1 - \beta_{k,n}) \\ \quad + \gamma_k(z)\tau_{k,n}(z) \beta_{k,n} & k = r, r+1 \dots, r+g \end{cases} \quad (4.26)$$

For Q_d

$$\begin{cases} \theta_{k+1,n}(z) = \theta_{k,n}(z)\omega_k(z) & k = 0,1 \dots, r-1 \\ \theta_{k+1,n}(z) = \frac{\omega_k(z)}{z} (\theta_{k,n}(z) - \theta_{k,n}(0)) + \pi_k(z)\theta_{k,n}(0) & k = r, \dots, r+g-1 \end{cases} \quad (4.27)$$

where,

$\delta_{k,n}(z)$:The PGF of Q_u at time slot k of cycle n;

$\tau_{k,n}(z)$:The PGF of Q_m at time slot k of cycle n;

$\theta_{k,n}(z)$:The PGF of Q_d at time slot k of cycle n;

$\mu_k(z)$:The PGF of the stochastic arriving distribution (A_1);

$\gamma_k(z)$: The PGF of the stochastic arriving distribution (A_2);

$\omega_k(z)$:The PGF of the stochastic arriving distribution (A_3);

$\varepsilon_k(z)$:The PGF of the random variable which is determined by A_1

$\vartheta_k(z)$:The PGF of the random variable which is determined by A_2

$\pi_k(z)$:The PGF of the random variable which is determined by A_3 ; and

$\beta_{k,n}$:The probability of Q_d spillbacks at time slot k of cycle n .

Under the equilibrium condition, the queue distributions at both the upstream and downstream intersections should become stable, indicating the existence of stationary distributions for $\delta_k(z)$, $\tau_{k,n}(z)$, and $\theta_k(z)$.

Note that due to the same computing complexity associated with their non-linear functions, this study also proposes an efficient numerical procedure to compute the time-varying queue distribution. Figure 4-7 shows the flowchart, similar to Figure 4-7, to generate the numerical solutions.

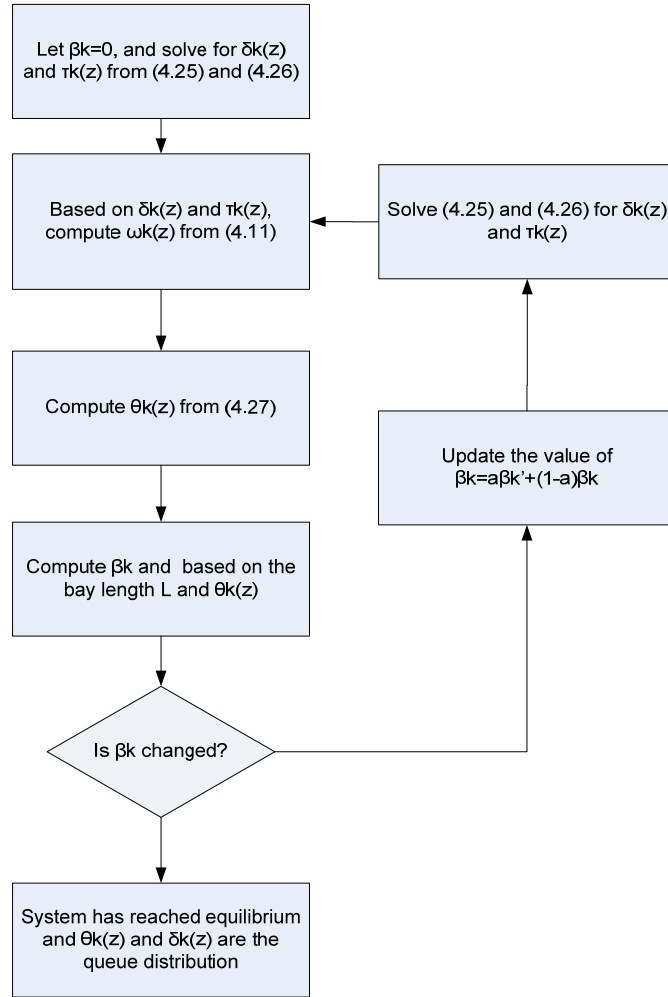


Figure 4-7: Flowchart for computing the stochastic through queues

The above flowchart comprises the following steps of computation:

Step-1: Initialization by setting all $\beta_{k,0} = 0$ for any k ;

Step-2: Compute $\delta_{k,n}(z)$ and $\tau_{k,n}(z)$, using Equations(4.25), (4.26), $\beta_{k,0}$, and $\mu_k(z)$;

Step-3: Compute time-dependent departure rate, $\omega_k(z)$, based on $\delta_{k,n}(z)$ and the platoon dispersion relation by Equation (4.11);

Step-4: Solve Equation (4.27) for $\theta_{k,n}(z)$;

Step-5: Check the convergence based on the difference between $\beta_{k,n}^{(i-1)}$ and $\beta_{k,n}^{(i)}$, and

terminate the iteration if the difference between $\beta_{k,n}^{(i-1)}$ and $\beta_{k,n}^{(i)}$ is less than a

specified threshold (τ); Otherwise, proceed to Step 6;

Step-6: Adjust the spillback probability (β) by setting $\beta_{k,0}^{(i+1)} = \alpha\beta_{k,n}^{(i)} + (1 - \alpha)\beta_{k,n}^{(i-1)}$

and return to Step (2); α is a parameter between 0 and 1.

4.5 Operational Analysis of DDI

This section illustrates how to apply the developed dynamic models to analyze traffic queue dynamics at a DDI design. As shown in Figure 4-8, the bridge segment in a DDI has the most complex traffic interaction. Both the through and left turning traffic from the arterial and the left turn vehicles from the freeway off-ramp will move onto the bridge segment alternatively, based on the signal phase at the ramp terminal intersection.

Let Q_w denote the through queues along the arterial and Q_r be the queues on the freeway off-ramp. Also, let Q_b represent the queues on the bridge; one can then estimate the arrival process, denoted as A_2 , at the end of Q_b with the two departure flows, D_1 and D_2 . Hence, one can also formulate its time-varying queue status as follows:

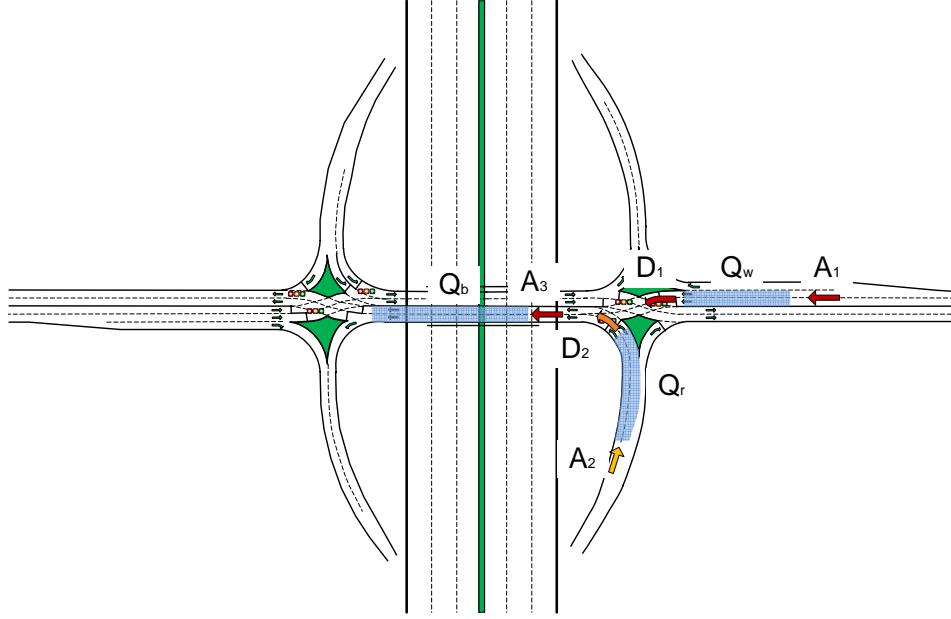


Figure 4-8: The distribution of queue locations at a DDI design

For Q_w

$$\left\{ \begin{array}{ll} \delta_{k+1,n}(z) = \delta_{k,n}(z)\mu_k(z) & k = 0,1 \dots, r-1 \\ \delta_{k+1,n}(z) = \left[\frac{\mu_k(z)}{z} (\delta_{k,n}(z) - \delta_{k,n}(0)) + \varepsilon_k(z)\delta_{k,n}(0) \right] (1 - \beta_{k,n}) \\ \quad + \mu_k(z)\delta_{k,n}(z)\beta_{k,n} & k = r, r+1 \dots, r+g \end{array} \right. \quad (4.28)$$

For Q_r

$$\left\{ \begin{array}{ll} \tau_{k+1,n}(z) = \tau_{k,n}(z)\gamma_k(z) & k = 0,1 \dots r-1 \\ \tau_{k+1,n}(z) = \left[\frac{\gamma_k(z)}{z} (\tau_{k,n}(z) - \delta_{k,n}(0)) + \vartheta_k(z)\tau_{k,n}(0) \right] (1 - \beta_{k,n}) \\ \quad + \gamma_k(z)\tau_{k,n}(z)\beta_{k,n} & k = r, r+1 \dots, r+g \end{array} \right. \quad (4.29)$$

For Q_b

$$\begin{cases} \theta_{k+1,n}(z) = \theta_{k,n}(z)\omega_k(z) & k = 0,1 \dots, r-1 \\ \theta_{k+1,n}(z) = \frac{\omega_k(z)}{z}(\theta_{k,n}(z) - \theta_{k,n}(0)) + \pi_k(z)\theta_{k,n}(0) & k = r, \dots, r+g-1 \end{cases} \quad (4.30)$$

where,

$\delta_{k,n}(z)$: The PGF of Q_w at time slot k of cycle n ;

$\tau_{k,n}(z)$: The PGF of Q_r at time slot k of cycle n ;

$\theta_{k,n}(z)$: The PGF of Q_b at time slot k of cycle n ;

$\mu_k(z)$: The PGF of the stochastic arriving distribution (A_1);

$\gamma_k(z)$: The PGF of the stochastic arriving distribution (A_2);

$\omega_k(z)$: The PGF of the stochastic arriving distribution (A_3);

$\varepsilon_k(z)$: The PGF of a random variable determined by A_1 ;

$\vartheta_k(z)$: The PGF of a random variable determined by A_2 ;

$\pi_k(z)$: The PGF of a random variable determined by A_3 ; and

$\beta_{k,n}$: The probability of Q_b incurs spillback to the end of the bridge at time slot k of cycle n .

The procedure to solve the above $\delta_{k,n}(z)$, $\tau_{k,n}(z)$ and $\theta_{k,n}(z)$ is identical to the flowchart for computing the through queues at a CFI (see Figure 4-7).

4.6 Closure

This chapter illustrates a set of dynamic operational models to analyze the time-varying queue patterns at the CFI and DDI designs. The developed models, despite its exploratory nature, are applicable to other unconventional intersections, because such designs generally comprise multiple closely-spaced signals where complex interactions take place between traffic streams from neighboring intersections. Using the PGF

modeling logic, the proposed models can realistically capture their complex queue dynamics within a link and between the downstream and upstream intersections.

To facilitate the application of the developed dynamic models, this study has also presented an efficient numerical solution process to circumvent the computing complexity for solving non-linear equations. With the proposed efficient procedures, users can perform the following operational analysis at a sufficiently reliable level:

- Delay estimation: Although the planning model can provide an estimate of the overall intersection control delay, the dynamic queue models presented in this chapter can offer the delay by movement which is more desirable for operational analysis.
- Effect of the bay length: Due to the right-of-way availability, some turning bays in a CFI or DDI design may not always meet the required lengths. One can therefore apply the dynamic queue models to estimate such impacts by taking into account some critical factors such as the distance between two neighboring signals, the queue spillback, and interdependence between upstream and downstream traffic patterns.
- Signal Optimization: The movement-based queues and delays estimated with the proposed dynamic models can serve as the basis for design and evaluation of the optimal signal plan proposed for a CFI or DDI design.

CHAPTER 5

SOFTWARE DEVELOPMENT FOR CFI AND DDI DESIGNS

5.1 Software Structure

This chapter illustrates the structure of MUID (Maryland Unconventional Intersection Design Tool), the computer program developed for designing CFIs and DDIs, including its operational data flows, principal system modules, and primary interface, as well as its output functions. MUID employs all queue and delay models developed in the previous chapters to guide users in evaluating a preliminary CFI or DDI design and in identifying potential deficiencies. The program can also serve as a training tool to educate traffic professionals.

The entire MUID program, at this development stage, comprises the following five main modules: (1) a main window for selection of the target design type and for input of essential information for analysis; (2) an input module for entering and editing both demand and geometry information about the target design using its interactive graphic interface; (3) a computing module to execute all requested computing functions based on those models presented in Chapters 2, and 3; and (4) a display module to present the estimated results and all related information needed by users.

Figure 5-1 presents the operational flow of the MUID system and the interrelations among its five principal modules. The main function of each key module is briefly illustrated below (see Figure 5-2).

Main window: This window allows users to select the design type for preliminary analysis. MUID currently offers analysis and evaluation for the following five types of unconventional intersection: CFI-T (Figure 5-3), two-leg CFI-A (Figure 5-4), two-leg CFI-B (Figure 5-5), full CFI (Figure 5-6), and DDI (Figure 5-7). The main window has four function zones: a design selection menu, a design illustration and description zone, an analysis information input zone, and a demand input zone. The demand input and editing functions are available in a separate window, as shown in Figure 5-8.

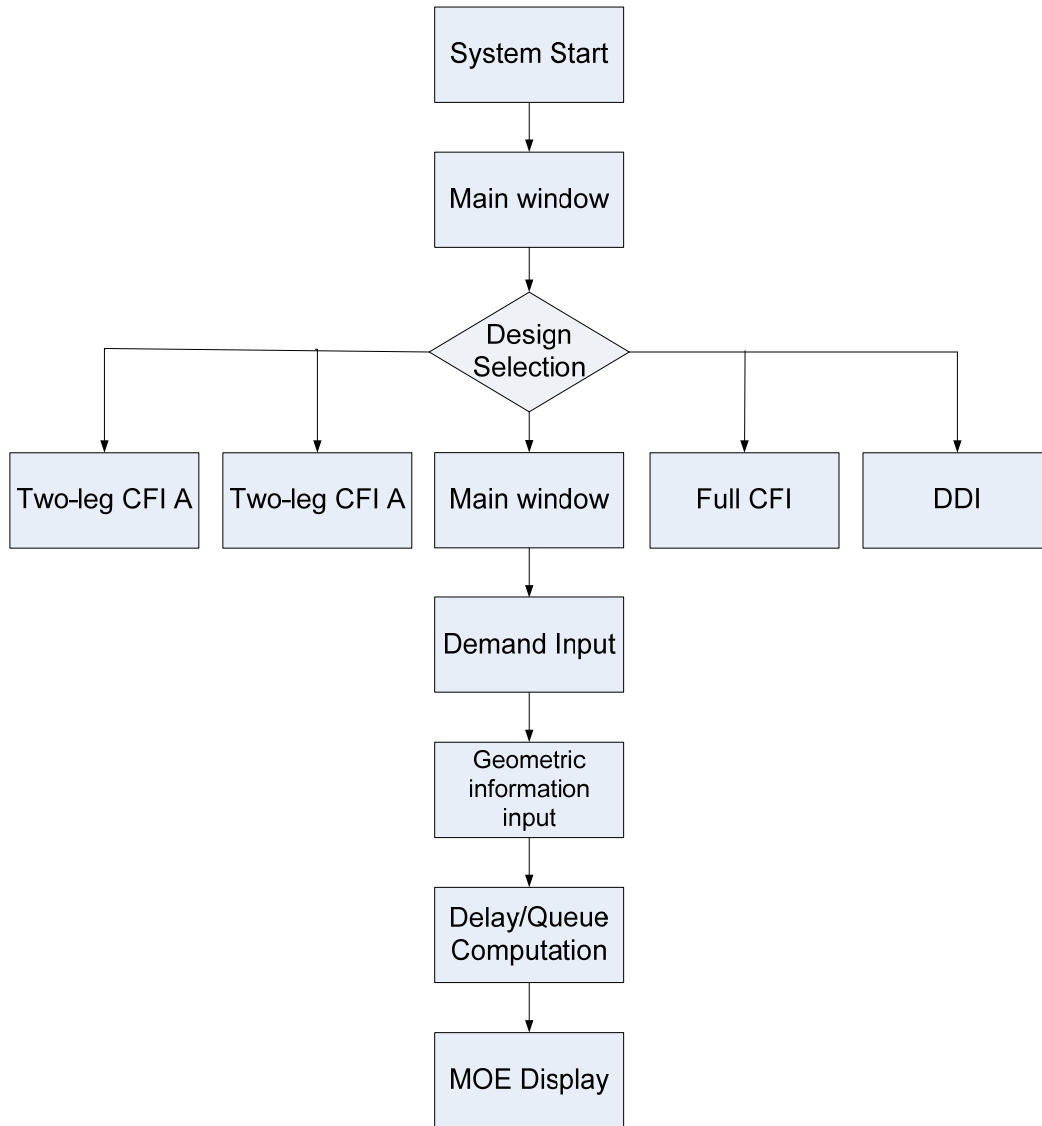


Figure 5-1: MUID operational flow chart



Figure 5-2: MUID starting menu

Main Window

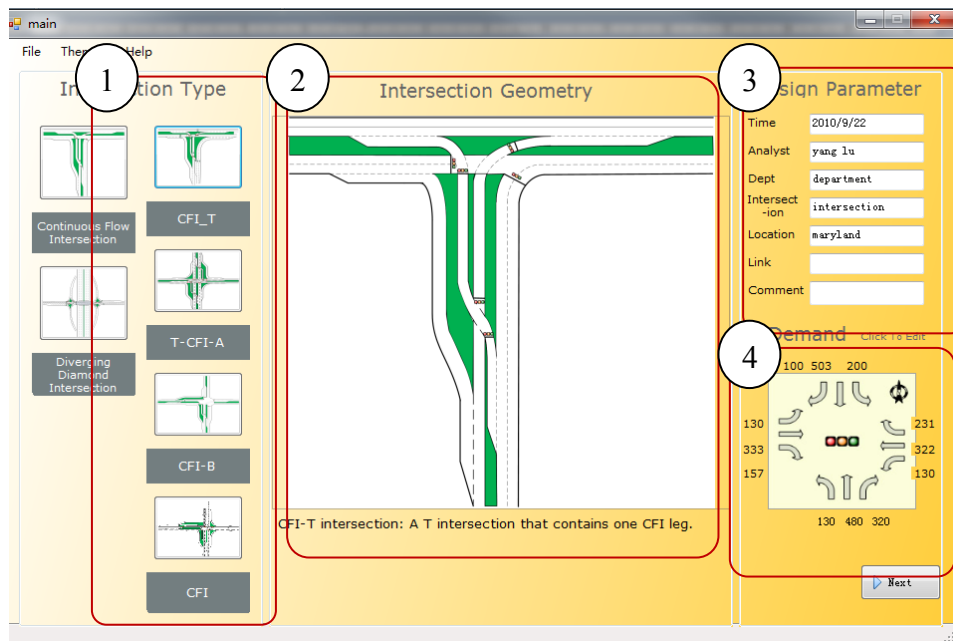


Figure 5-3: Main interface window showing its four zones

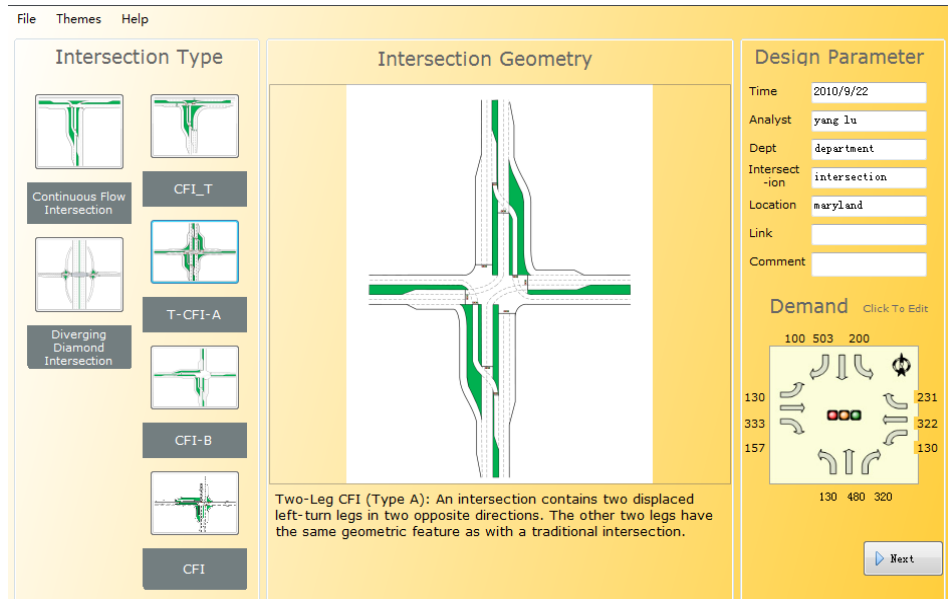


Figure 5-4: Design selection menu — two leg CFI-A

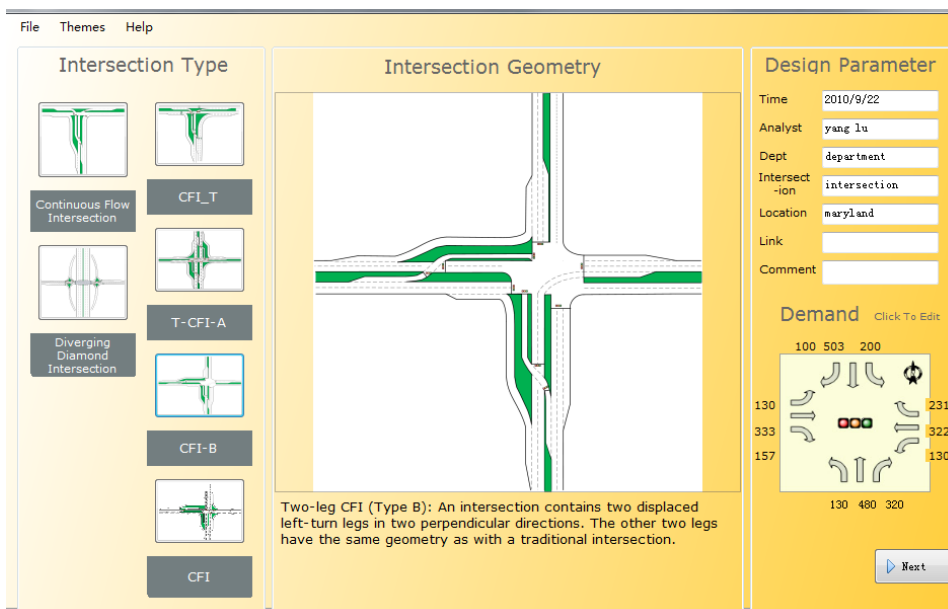


Figure 5-5: Design selection menu — two-leg CFI-B

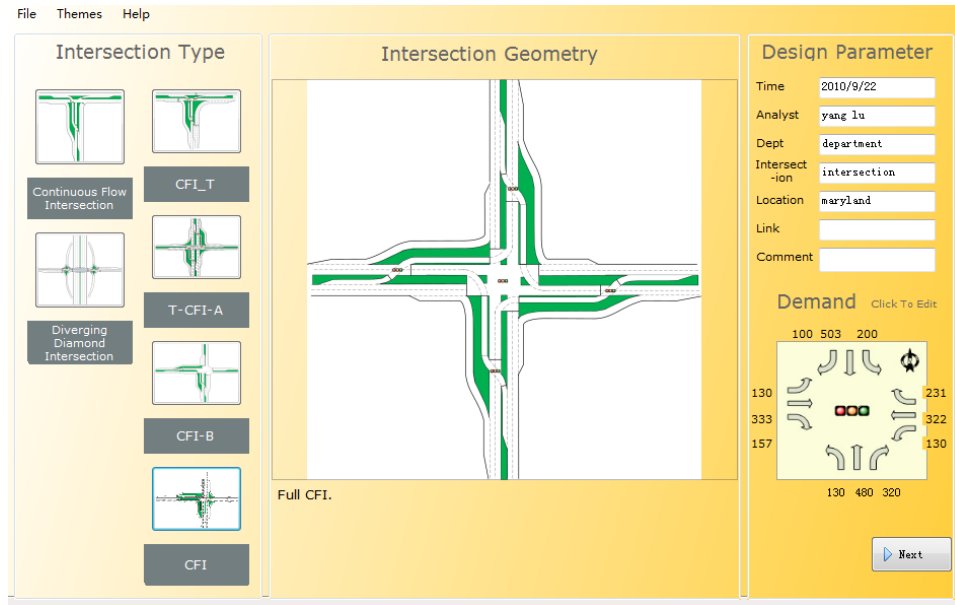


Figure 5-6: Design selection menu — full CFI

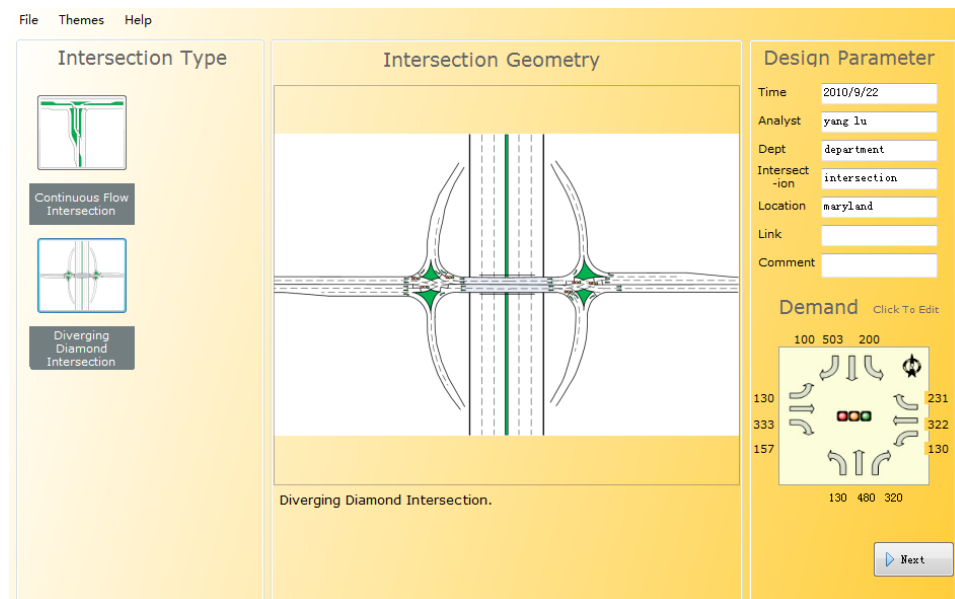


Figure 5-7: Design selection menu — DDI

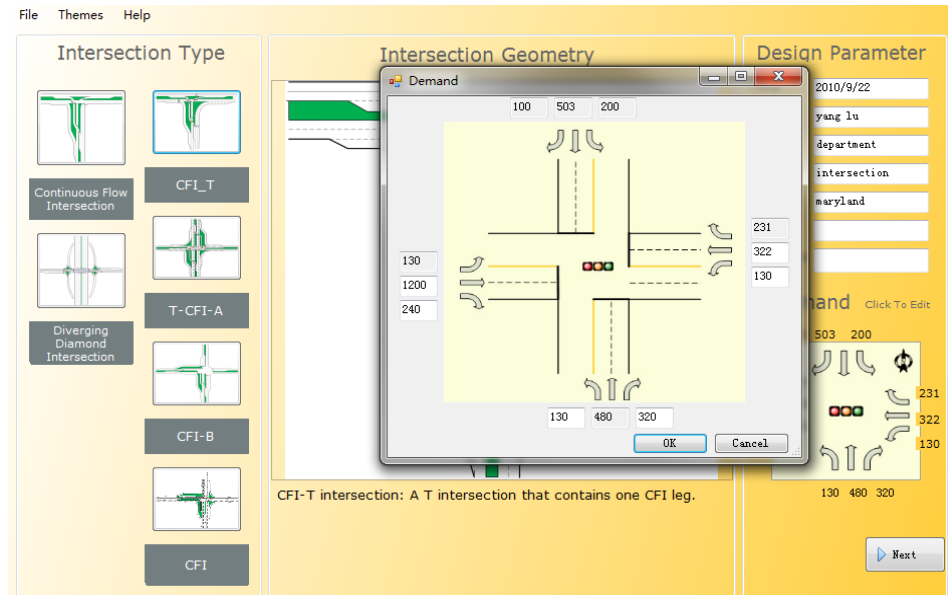


Figure 5-8: Demand input window

The design window comprises three functional sections: (1) a design illustration panel (Figure 5-9); (2) a zoom bar; and (3) a data display panel. Users can view the geometric features of the selected design in the illustration panel and can make any necessary changes to the lane configuration (Figure 5-10). The zoom bar, which lies underneath the illustration panel, can dynamically change the display scale of the design. Users can also use the data panel at the right side of the window to modify the design's bay length (Figure 5-11).

Design Evaluation Window

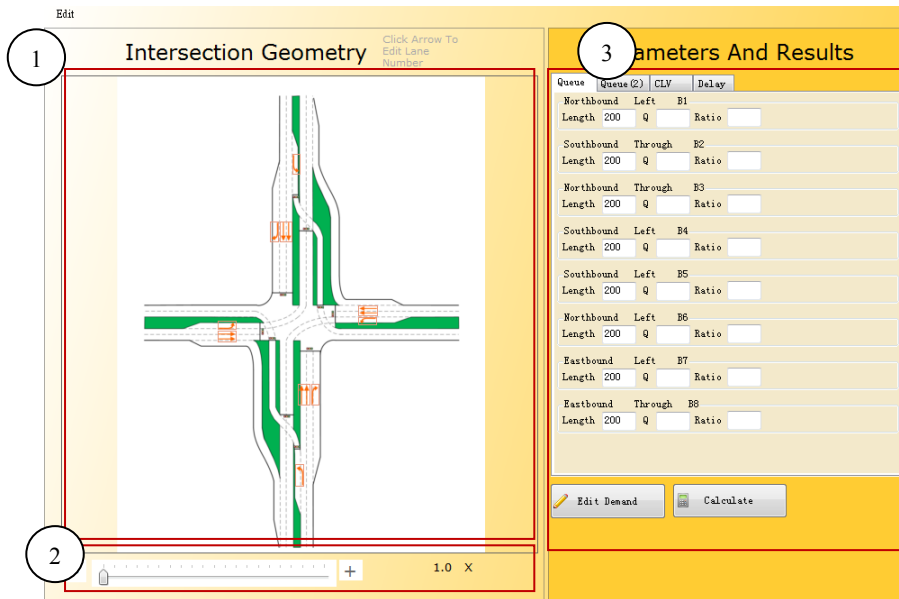


Figure 5-9: Design evaluation window

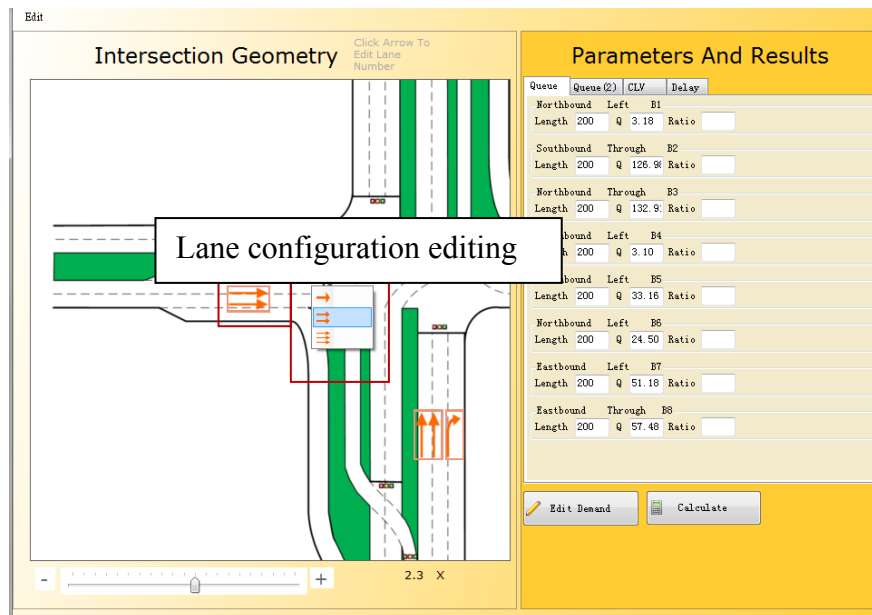


Figure 5-10: Illustration of the editing box for lane configuration

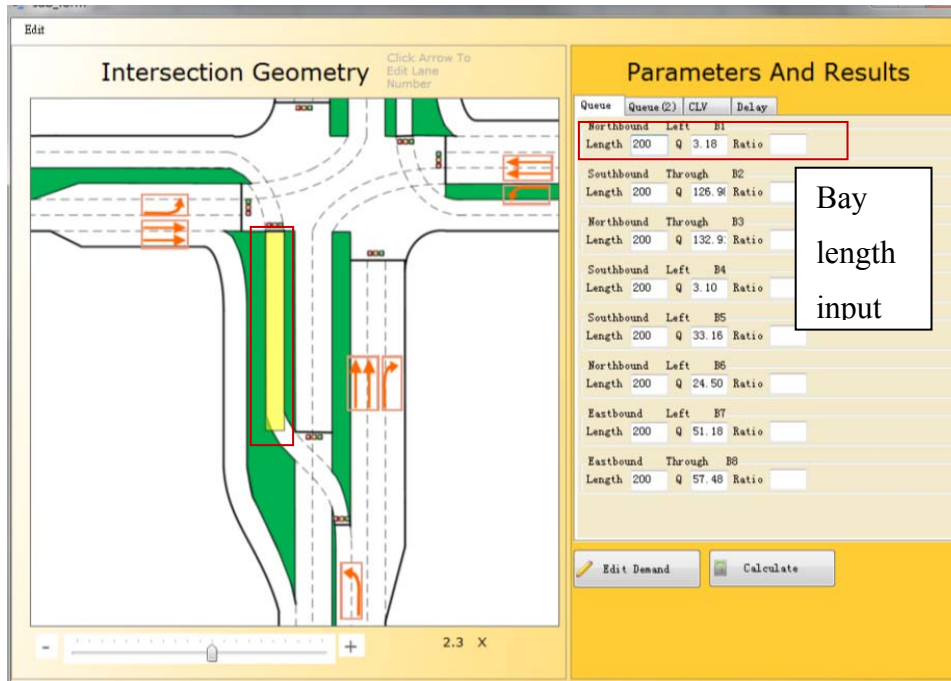


Figure 5-11: Illustration of the editing box for modifying bay length

Users can have MUID compute queues and delays for any of the five designs by clicking the “Calculate” button in the bottom right corner of the design window. Users can choose to display either the queue length at each bay location (Figure 5-12) or the total intersection delay (Figure 5-13) using their respective icons.

Queue and delay computation window

Intersection Geometry

Click Arrow To Edit Lane Number

Parameters And Results

Queue	Queue (2)	Queue (3)	CLV	Delay
B1	Length 200	Q 0.86	Ratio	
B2	Length 200	Q 445.21	Ratio	
B3	Length 200	Q 445.21	Ratio	
B4	Length 200	Q 0.86	Ratio	
B5	Length 200	Q 1.41	Ratio	
B6	Length 200	Q 188.31	Ratio	
B7	Length 200	Q 381.95	Ratio	
B8	Length 200	Q 0.86	Ratio	

Estimated Queue length

Calculation Button

Figure 5-12: Calculating all estimated queue lengths

Queue | Queue(2) | Delay

Average Delay (sec)
43.71

CLV Center
1400.00

CLV South
1050.00

CLV North
1050.00

label1

Calculate

Figure 5-13: Calculating the total estimated intersection delay

5.2 Illustrative Example

This section walks through the MUID application via the following example: a two-leg CFI preliminary design with the following the geometric features:

- The length of all left turn bays was set at 200 ft.
- The length of all right-turn bays was set at 200 ft.
- One lane for each left turn and right-turn bay, and two lanes for the through links.

Estimating the delays and queues for such a design involves the following steps:

Step 1: Select the target design from the main window (Figure 5-14).

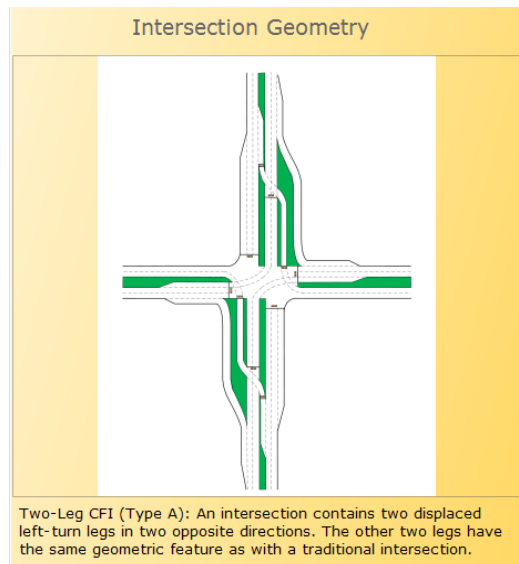


Figure 5-14: Geometry selection for the example two-leg CFI-A

Step 2: Input the volume data into the MUID window (Figure 5-15)

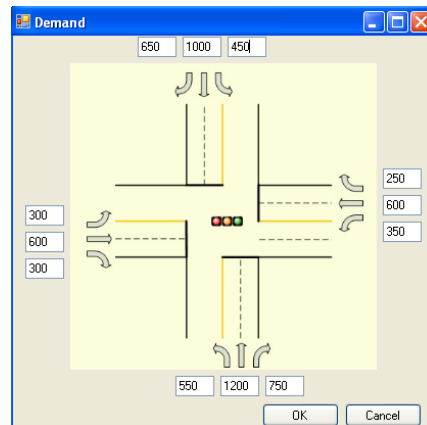


Figure 5-15: Interface window for traffic volume data

Step 3: Execute the computing module to display estimated queue length and the total intersection delay (Figures 5-16 and 5-13).

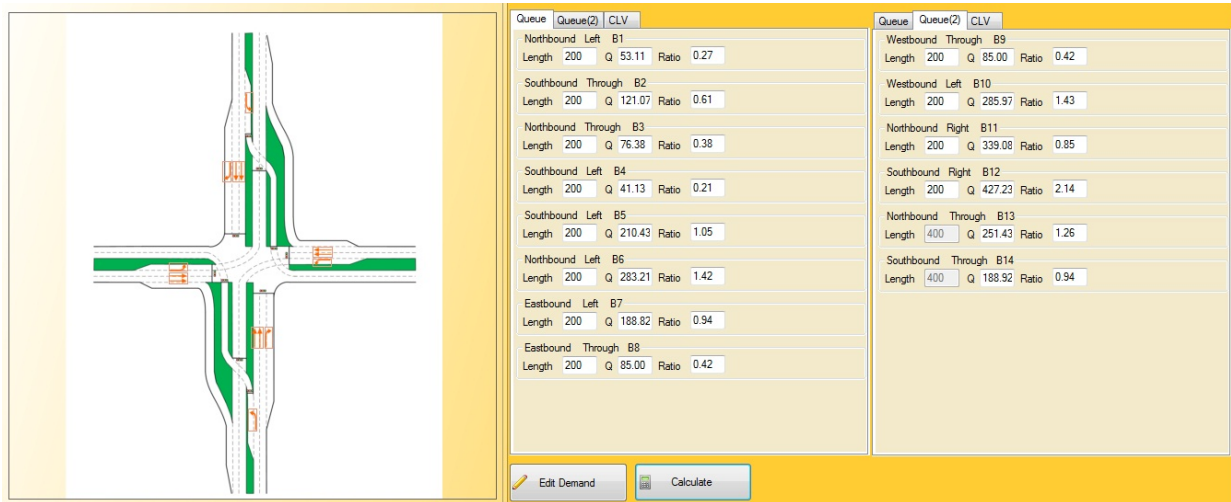


Figure 5-16: The window for computing and displaying the estimated queue lengths

Note that, rather than going through a time-consuming simulation process, SHA engineers and other potential users can use the above simple procedure to efficiently estimate the adequacy of each provided bay length at different volume levels, and to identify potential bottlenecks from traffic spillbacks at some turning bays — which, in turn, cause gridlock for the entire intersection. Such a tool also enables potential users to perform an efficient comparison between different candidate designs based on the spatial distribution of queue lengths and the resulting total intersection delay under different traffic patterns and volume levels. However, note that the MUID’s estimates of delays and queues are primarily intended for use at the preliminary planning stage; they are not for final design development, which must consider signal control strategies, spacing between intersections, and the time-varying distribution of traffic demand.

CHAPTER 6

CONCLUSION AND RECOMMENDATIONS

6.1 Conclusion

The emergence of unconventional intersections in the traffic community has been motivated by the notion of improving service quality with innovative control strategies, such as rerouting the turning movements or flipping the paths of two traffic streams to facilitate the high-volume flows, thus increasing an intersection's overall capacity. Extensive results from simulation-based studies and limited field data from the few existing unconventional intersections support the widespread belief that such intersections can (1) increase the capacity for primary traffic movements while reducing total delay; (2) decrease the number of conflict points in an intersection by rerouting turning movements and improve the safety performance; and (3) produce more cost-effective solutions than conventional grade-separation designs.

However, despite the growing interest in implementing unconventional intersection designs in recent years, the traffic community still lacks efficient and reliable tools to assist engineers in identifying potential design deficiencies. This study, responding to that need, has produced a beta version of software for planning and analyzing the CFI family and the DDI designs. Building on the results of extensive simulation statistical experiments, this software comprises 16 well-calibrated queue estimation models and four equations for computing total delay. Its user-friendly interface can facilitate the efficient performance of a preliminary evaluation of any CFI or DDI design. To create a foundation for the future development of its operational modules for the final design stage, this study also investigated several critical issues that may affect the precise estimate of a design's effectiveness, including the complex interrelationships between the spatial distribution of queue lengths at different bays; the effects of time-varying demand patterns on the resulting queues and delays; and the effects of intersection spacing, as well as signal control strategies, on the overall performance of a CFI or DDI design. Some important research findings are summarized below:

- For either CFI or DDI design, the average intersection delay depends significantly on two primary factors: the congestion level of each subintersection (represented by the CLV) and the ratio of the maximum queue length to the available bay length at each potential bottleneck location. Any queue spillback occurring at those critical bays may propagate the congestion across the entire intersection, causing gridlock. The vital role of the relationship between queue size and bay length on the overall intersection delay, as well as on the capacity, has not been well recognized in the literature.
- For a CFI-T design, the impacts of its six potential queue locations on the total intersection delay can be divided into three levels, where the first level — the through and left turn queues between the main intersection and the crossover subintersection — is the most critical, because any queue spillback in this zone will reduce the capacity of upstream intersections. The left turn queues at the main and crossover intersections belong to the second level; the third level, the right-turn and through queues at the main intersection, is the least critical.
- For a two-leg CFI-A (or -B) design, the impacts of its 14 potential queue locations on the total intersection delay can be sorted into four levels: (1) the through queue between the main and crossover intersections; (2) the left turn queue between the main and crossover intersection; (3) the left turn queue at each crossover intersection; and (4) the through and left turn queue on the conventional legs. The impact ratio between levels 1 and 4, based on the estimated parameters, is about 3 to 1, which indicates that facilitating the through movement between the main and crossover intersections ought to be the design priority when faced with resource constraints. Besides, among its subintersections, the congestion level of the central intersection (reflected by its CLV) has the largest impact on the total intersection delay.
- For a full CFI design, the formation of a queue at any of its 16 bay lengths will significantly affect the total intersection delay. However, based on the comparison of their relative impacts, one can also classify their contribution to the overall intersection delay into the following four levels: (1) all through queues between

- the main and crossover intersections; (2) all left turn queues between the main and crossover intersections; (3) all left turn queues at the crossover intersections; and (4) all through queues at the main intersection. The estimation results reveal that the relative impacts of these four levels on the total intersection delay can be expressed with the ratios of 5, 4, 3, and 2. Among all five intersections in a full CFI design, the congestion level of the central (main) intersection affects the overall delay the most — about 1.6 times more than each individual subintersection.
- For the DDI design, all six potential queue locations are critically correlated to the total intersection delay. One can classify them, based on their relative contribution to the total delay, into the following two levels: (1) the queue length between the two ramp terminals, and (2) the queue length at the remaining four locations. The statistical analysis of the simulation data indicates that the queue lengths developed by the through and left turn movements at the terminal intersections of the two ramps have the same effect on the total intersection delay. The similar impact of congestion levels at these two ramp terminal intersections on the overall DDI delay occurs because of the symmetry of the design.

6.2 Recommendations for Future Extension

Since this is a pioneering study toward the production of effective tools for evaluating and designing various unconventional intersections, much remains to be done along this line, including both theoretical development and field evaluation. Some priority areas needed to enhance the capability of MUID and to expand its scope of applications are summarized below:

- Extend the existing statistical models for the planning level application to the operational model that can precisely account for how detailed geometric features, signal controls, and traffic patterns between neighboring intersections affect total intersection delay and the spatial distribution of traffic queues.

- Convert the operational model, which is based on rigorous traffic flow theories, into a user-friendly computer program that can facilitate the final design evaluation and provide accurate cost-benefit analyses.
- Expand the MUID computer system to handle the evaluation of other increasingly popular unconventional intersections, such as Super Street and Mid-U-turn designs.
- Develop a comprehensive cost-benefit module to enable traffic engineers to compare, at the final design stage, the marginal construction costs of unconventional intersections with their marginal capacity increases.
- Construct a knowledge-based system to document the field operational experiences of existing unconventional intersections in the US and other countries, including any resulting efficiencies, such as in queues and delays, as well as their impacts on driving patterns and accident frequency.
- Design a computer-aided program, based on both research results from existing studies and lessons obtained from those who have designed or operated unconventional intersections, to train traffic engineers interested in enhancing their knowledge about this subject.

REFERENCES

1. Abate, J., 1995. Numerical inversion of Laplace transforms of probability distributions. *ORSA Journal on Computing*, 7 (1), pp.36-43.
2. Abramson, P., Bergren, C., and Goldblatt, R., 1995. Human Factors Study of the Continuous Flow Intersection at the Dowling College NAT Center. 4th Annual Symposium on Intermodal Transportation, Oakdale, N.Y.
3. Bared J. G., Edara, P .K., and Jagannathan, R., 2005. Design and Operational Performance of Double crossover Interchange and Diverging Diamond Interchange. *Transportation Research Record*, 1912, pp.31-38.
4. Broek, M. S. van den, Leeuwaarden, J. S. H, van, 2006. Bounds and Approximations for the Fixed-Cycle Traffic-Light Queue. *Transportation Science*, 40 (4), pp.484-486.
5. Cheong S., Rahwanji S., and Chang G.L., 2008. Comparison of Three Unconventional Arterial Intersection Designs: Continuous Flow Intersection, Parallel Flow Intersection, and Upstream Signalized Crossover. 11th International IEEE Conference.
6. Chlewicki, G., 2003. New Interchange and intersection Designs: The Synchronized Split-Phasing Intersection and the Diverging Diamond Interchange. Prepared for 2nd Urban Street Symposium, Anaheim, CA.
7. Cowan, R., 1981. An analysis of the fixed-cycle traffic-light problem. *Journal of Applied Probability*, 18, pp.672-683.
8. Darroch, J. N., 1964. On the traffic-light queue. *The Annals of Mathematical Statistics*, 35, pp.380-388.
9. Esawey, M.E., and Sayed, T., 2007. Comparison of Two Unconventional Intersection Schemes. *Transportation Research Record*, 2023, pp. 10-19.
10. FHWA, US Department of Transportation, 2010. Alternative Intersections/Interchanges: Information Report (AIIR).
11. Hildebrand, T. E., 2007. Unconventional Intersection Designs for Improving Through Traffic Along The Arterial Road. A Thesis Submitted to the Department of Civil and Environmental Engineering, the Florida State University.
12. Hummer, J.E., 1998. Unconventional Left turn Alternative for Urban and Suburban Arterials: Part One. *ITE Journal*, 68 (9), pp. 26-29.

13. Hummer, J.E., 1998. Unconventional Left turn Alternative for Urban and Suburban Arterials: Part Two. ITE Journal on the Web, pp. 101-106.
14. Inman, V. W., 2009. Evaluation of Signs and Markings for Partial Continuous Flow Intersection. Transportation Research Record, 2138, pp. 66-74.
15. Jagannathan, R., and Bared, J. G., 2004. Design and Operational Performance of Crossover Displaced Left turn Intersections. Transportation Research Record, 1981, pp.86-96.
16. Kim, M., Lai, X., Chang G. L., and Rahwanji, S., 2007. Unconventional Arterial Designs Initiatives. Presented at IEEE Conference on Intelligent Transportation Systems, Seattle.
17. Leeuwaarden, J. S. H., van, 2006. Delay Analysis for the Fixed-Cycle traffic light queue. Transportation Science, 40 (2), pp.189-199.
18. McNeill, D. R., 1968. A solution to the fixed-cycle traffic light problem for compound Poisson arrivals. Journal of Applied Probability, 5, pp.624–635.
19. Miller, A. J., 1963. Settings for fixed-cycle traffic signals. Operation Research, 14 (4), pp. 373–386.
20. Newell, G. F., 1965. Approximation methods for queues with applications to the fixed-cycle traffic light. SIAM Review, 7 (2), pp. 223-240.
21. Ohno, K., 1978. Computational Algorithm for a Fixed Cycle Traffic Signal and New Approximate Expressions for Average Delay. Transportation Science, 12, pp. 29-47.
22. Pitaksringkarn, J. P., 2005. Measures of Effectiveness for Continuous Flow Intersection: A Maryland Intersection Case Study. ITE 2005 Annual Meeting and Exhibit Compendium of Technical Papers.
23. Poorbaugh, J., Houston, B., 2006. Diverging Diamond Interchange. Institute of Transportation Engineers, Washington, DC.
24. Reid, J. D., Hummer, J. E., 1999. Analyzing System Travel Time in Arterial Corridors with Unconventional Designs Using Microscopic Simulation. Transportation Research Record, 1678, pp.208-215.
25. Reid, J. D., and Hummer, J. E., 2001. Travel Time Comparisons between Seven Unconventional Arterial Intersection Designs. Transportation Research Record, 1751, pp.55-56.
26. Reid, J., 2004. Unconventional Arterial Intersection Design, Management and Operations Strategies. Parsons Brinckerhoff.

27. Rouphail, N., Tarko, A., and Li, J., 1996. Traffic flows at signalized intersections. Traffic Flow Theory Monograph, Ch. 9.
28. Sadek, A. W., Smith, B. L., and Demetsky, M., 2001. A prototype case based reasoning system for real-time freeway traffic routing. Transportation Research Part C, 9, pp. 353-380.
29. Tarko, A. P., 2000. Random queues in signalized road networks. Transportation Science. 34 (4), pp.415-425.
30. Viti, F., Zuylen, and H.J. van, 2004. Modeling Queues at Signalized Intersection. Transportation Research Record, 1883, pp. 68-77.